Assessing the effect of cone ratio, feed solids concentration and viscosity on hydrocyclone performance

Prepared by: Pharaoh Muzanenhamo

Dissertation presented for the degree of ***Master of Science in Engineering***

Department of Chemical Engineering

University of Cape Town

DECLARATION

I know the meaning of plagiarism and declare that all the work in the document is my own. I have used the prescribed referencing system for citation and referencing. Each significant contribution to, and quotation in, this report from the work, or works, of other people has been attributed, and has been cited and referenced.

Signature of author:

PHARAOH KUDZAISHE MUZANENHAMO

Department of Chemical Engineering,

University of Cape Town,

South Africa

October 2014

ABSTRACT

In the mineral processing industry, comminution circuits contain slurries composed of a mixture of particles of varying degrees of liberation and size. Hydrocyclones are commonly used to classify these particles. If the classification stage is not efficient, both grinding and flotation cannot be optimised or operated efficiently. Ores that are mined in industry contain metals of varying specific gravity, which makes recovery of the desired metal challenging.

This study focussed on the effect of the hydrocyclone spigot to vortex finder diameter ratio, termed as the cone ratio, solids concentration and viscosity on the classification of two dual density ores. The rheological characteristic of the overflow was also evaluated. A UG2 ore (Upper Group), which consists mainly of silicates, and chromite, and an iron ore, containing mainly iron and silicates, were used as feed material. The UG2 test work was carried out on a University of Cape Town (UCT) 4 inch Multotec cyclone, while the iron ore test work was carried out on an Anglo-American 4 inch Krebs cyclone. The cyclone performance was assessed using the corrected cut size, water recovery to the underflow, sharpness of separation and feed throughput. The rheological characterisation of both the UG2 and iron ore were carried out using an AR (ARES-G2) 1000EX vane rheometer.

The results obtained indicated that the cyclone cone ratio, feed solids concentration and viscosity influence the cyclone performance. For the UG2 it was observed that as the cone ratio increased the cut size decreased and levelled off at a cone ratio of 1. However, for the iron ore it was observed that the cut size increased with an increase in the cone ratio, until it reached a peak at a cone ratio of approximately 0.68, before decreasing. The water recovery to the underflow increased with cone ratio and solids concentration and for both ore types. However it was observed that the water recovery was more sensitive to the cone ratio within the range of conditions investigated. The sharpness of separation for the UG2 ore increased with cone ratio for all solids concentrations investigated and reached a peak at a cone ratio of approximately 1 then decreased. The sharpness of separation for the iron ore illustrated different trends at different feed solids concentration. Between 10 and 20 wt. % feed solids concentration the sharpness of separation for iron ore was fairly constant, while at 50 wt. % solids concentration the sharpness of separation increased with cone ratio and then levelled off at a cone ratio of 0.67.

An increase in the volumetric throughput with cone ratio was observed for both ore types. Rheological characterization revealed Bingham plastic behavior for both ore types. An increase in the feed viscosity led to an increase in the cut size, water recovery and sharpness of separation for both UG2 and iron ore.

A comparison of the results with a semi mechanistic model revealed a good fit for the volumetric throughput, water recovery and viscosity. However, the sharpness of separation and cut size had more scatter. The standard error for the sharpness of separation model fit was 21% for UG2 and 23% for iron ore while the error for the cut size was 41 % for the UG2 ore and 43 % for the iron ore.

It was recommended that for future work, test work should be carried at a constant pressure in order to assess purely the effect of cone ratio. Furthermore, a coarser ore should be used in order to evaluate the effect of cone ratio and feed viscosity on the individual deportment of the prevalent components in the dual density ore types investigated by carrying out assays.

ACKNOWLEDGEMENTS

I would like to extend my gratitude to my supervisor Associate Professor Aubrey Mainza and Mr Jason Waters for their guidance and overwhelming support throughout the project. I would also like to acknowledge the following:

- Members of The Centre of Minerals Research for their assistance with various aspects of this work especially Tatenda Gota for his overwhelming support during the test work at the University of Cape Town.
- Members of the Anglo-American team for helping me carrying out my experiments on their pilot plant. Special mention to Dr Henrique Turrer for assisting with the communication barriers during the experimental programme.
- University of Rio de Janeiro with special mention to Yemcy Calcina allowing me to use their Mastersizer for the iron ore particle size distributions.
- Amira P9 group for the financial support during my master's programme.
- My parents Farrow and Thandazani Muzanenhamo for their never ending encouragement and support during the project duration.

Lastly but by no means the least, I thank the Father the Son and the Holy Spirit for instilling in the energy, focus and dedication to fulfil this thesis and for keeping me sane throughout the hardships.

TABLE OF CONTENTS

LIST OF TABLES

Chapter 1

Chapter 2

Chapter 3

Chapter 4

Chapter 5

Chapter 6

LIST OF FIGURES

Chapter 2

Chapter 3

Chapter 4

Chapter 5

Chapter 6

NOMENCLATURE

ρ_s	Solid density (kg/m^3)
ρ_p	Pulp density (kg/m^3)
ρ_L	Fluid density
E_a	Uncorrected cyclone efficiency or partition number
E_c	Corrected efficiency or partition number
E_i	Actual efficiency or partition number from Whitten Model
M_u	Mass flow rate of the underflow stream (kg/s)
M_f	Mass flow rate of the feed stream (kg/s)
α	Sharpness of separation
R_{LZVV}	Position of locus zero vertical velocity (mm)
R_C	Cyclone radius (m)
R_O	Vortex finder radius (m)
R_U	Spigot or apex radius (m)
d_{50}	Particle cut-size diameter (μm) corresponding to 50% efficiency
D_U	Inside diameter of the apex (m)
D_i	Inside diameter of the inlet (m)
D_O	Inside diameter of the vortex finder (m)
Q_f	Feed flow rate (m^3/hr.)
η	Fluid viscosity (Pa.s)

CHAPTER 1: INTRODUCTION

The intention of this thesis is to assess the effect of the hydrocyclone spigot to vortex finder ratio, termed as the cone ratio (Kilavuz & Gulsoy, 2011), feed solids concentration and viscosity on the overall cyclone performance when classifying two dual density ores.

Mineral beneficiation is a process by which valuable constituents of an ore are concentrated by means of physical and chemical separation processes. Comminution coupled with physical separation is the first stage in extracting the minerals from the ores. Comminution is energy intensive and inefficient (Wills & Napier-Munn, 2006). As a result comminution devices such as mills are placed in closed circuits with classifiers for size separation. The closed comminution circuit enables the coarser material to recirculate to the mill and the fine material is removed and sent for further processing (Mainza, et al., 2005). The most common classifiers in a mineral processing application include screens and hydrocyclones.

Hydrocyclones achieve classification by the use of centrifugal forces to separate particles according to size, density and shape, in a fluid that experiences essentially free vortex motion. Although the first hydrocyclone was patented in 1891 by Bretney in the United States of America, cyclones only became widely used after the World War II in the mining industry (Bretney, 1891 and Svarovsky, 2000). These devices play an important role in applications such as thickening, liquid-liquid separation and classification (Wills & Napier-Munn, 2006).

Cyclones have been shown to be the most widely used classifiers for particle sizes between 10 and 100 μm (Hesham & Batsh, 2013). In the mineral processing industry, cyclones have to a large extent replaced mechanical classifiers and are widely used owing to the following advantages summarized by Fuerstenau & Han (2003); Svarovsky (2000).

- they are adaptable as they can be used for liquid clarification, slurry thickening, degassing of liquids, separation of immiscible liquids and solid classification by size
- they can handle higher throughputs compared to other classifiers such as screens
- they have minimal space constraints as they are relatively small devices and require low capital investment and maintenance costs

- there is minimal agglomeration within the cyclone as a result of the high shear forces

Even though hydrocyclones have been installed in operations for over sixty years there still exists some uncertainty about the influence of some design and operating variables on their performance. The compactness of these devices makes internal observation very difficult. Once installed there are limited options for hydrocyclone performance optimization. The most viable option is to change both spigot (apex) and vortex finder size combinations as provision for this is made during hydrocyclone design and manufacture (Wills & Napier-Munn, 2006).

Cyclones in the minerals processing industry may treat ore types with a similar particle size but containing minerals with varying particle density and shape. These physical properties can influence the performance of the cyclone and its efficiency of desired mineral separation. Slurry rheology is also known to influence the transport and classification of the solid liquid mixture which forms the slurry (Shi, et al., 2010). The behaviour of these multicomponent particles in cyclone classification is poorly understood and unaccounted for in most experimental models available in literature (Narasimha, et al., 2012). Classification of multicomponent ores becomes problematic because the higher density components despite their size, will preferentially report to the hydrocyclone underflow and coarse low density particles will report to the cyclone overflow (Lynch and Rao, 1968). This phenomenon negatively affects the recovery of minerals during subsequent size sensitive processes such as flotation, as most of the valuable minerals will not be recovered if they are not liberated (Mainza, et al., 2005).

Due the problems encountered in the classification of multicomponent ore, this study was commissioned to assess the effect of the spigot to vortex finder ratio on ore types containing two different density components referred to as dual density ores. Table 1-1 provides a list of the two ores and their respective components and specific gravity that were investigated in this thesis.

Table 1-1: List of ores investigated and their respective components (Anglo-American (2013); Mainza, 2006)

Ore	Components	Relative Density
UG2 (Upper Group)	Silicates (Rich in PGM)	2.80
	Chromite	4.97
Iron Ore	Silicates	2.80
	Iron	4.19

1.1. Research Objectives

The principle objective of this work is to assess the influence of the cone ratio and feed solids concentrations on the hydrocyclone performance. A secondary objective was to characterise the rheological behaviour of the feed and overflow streams for a wide shear rate range (0-600/s) at different solids concentrations. This was achieved using a conventional AR 1500 vane rheometer.

1.2. Hypothesis

The following hypotheses were tested in this thesis:

- Changing the cyclone cone ratio will alter the cyclone performance. This is because the ratio of the spigot to the vortex finder shifts the locus of zero vertical velocity which influences the performance of the hydrocyclone by altering the cut size.
- Increasing the fluid viscosity will alter the cyclone performance. This is because as the fluid viscosity increases hindered settling and hindered discharge through the spigot is observed which results in a coarser cut size and high water recovery to the underflow.
- A flat bottom hydrocyclone will yield a coarser cut size, a more thickened underflow and less sharpness of separation. This is because the flat bottom hydrocyclone will produce "eddy currents" at the flat bottom part, causing both the coarser particles and the liquid media that were supposed to report to the underflow to end up reporting to the overflow.

1.3. Key Questions

The following key questions were formulated:

1. What is the effect of cone ratio on cyclone performance assessed by the three partition curve properties?
2. How does the cyclone performance differ between a conventional and flat bottom cyclone at similar operating conditions?
3. What is the effect of viscosity on the cyclone performance?
4. Is there a relationship between the feed and overflow rheological characteristics?

1.4. Thesis Structure

This thesis is divided into 8 main chapters and appendices. The details of the chapters are as follows:

Chapter 1: Introduction

In this chapter, background information leading to the research and the objectives of the research are outlined.

Chapter 2: Literature review

This chapter contains a review of literature related to the research. This includes articles on the effect of cone ratio and solids concentration on cyclone classification. An overview of slurry rheology is also presented.

Chapter 3: Experimental methodology

A description of the experimental methodology used to conduct the cyclone test work for both the UG2 are iron ore is provided. The sample preparation is also discussed. This chapter ends with the method used for the rheological characterisation of both UG2 and iron ore.

Chapter 4: Hydrocyclone results and discussion

This chapter provides results obtained from the cyclone tests. A discussion of the experimental results is also given alluding to literature.

Chapter 5: Rheology results and discussion

In this chapter the rheology characterisation results are analysed and discussed for both the feed and overflow at the operating conditions investigated.

Chapter 6: Model fitting of results

This chapter assesses the model fitting of the experimental data to a semi mechanistic hydrocyclone model.

Chapter 7: Conclusions and recommendations

Conclusions from significant findings in the research are summarized in this chapter and recommendations for further work are proposed.

CHAPTER 2: LITERATURE REVIEW

This section of the thesis reviews the literature discussing the effects of cone ratio, feed solids concentration and slurry viscosity on cyclone performance.

2.1. Hydrocyclone geometry

A picture and schematic of a typical conventional cyclone is illustrated in Figure 2-1. The device has a cylindrical section of diameter (D_C) which has a central tube mounted within termed the vortex finder of diameter (D_o). The inlet orifice (D_I) is located on the cone periphery and the underflow exits through the spigot of diameter (D_u). The cyclone has a length (L_C) and cone angle (θ). These dimensions are significant design variables that control the separation performance.

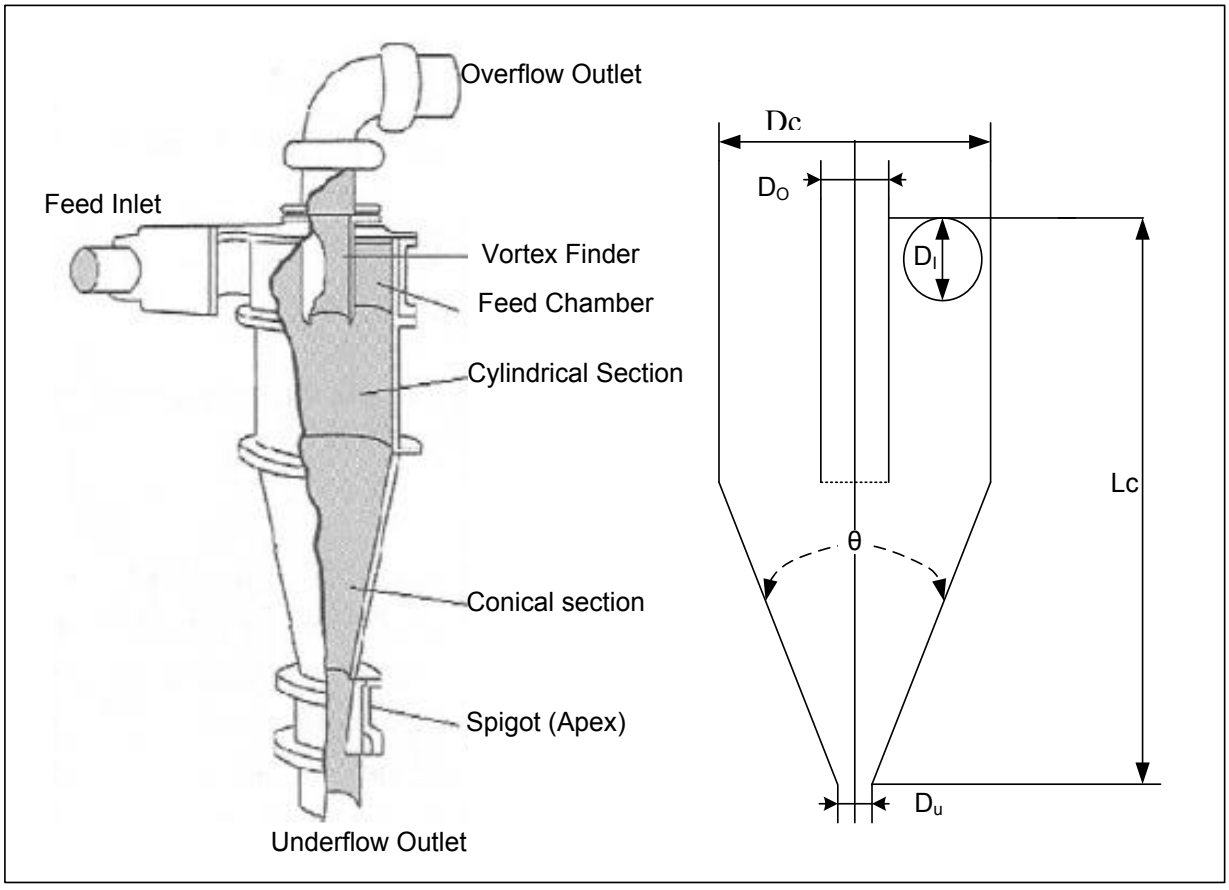

Figure 2-1: Hydrocyclone schematic and dimensions (Wills & Napier-Munn, 2006)

2.1.1. Feed inlet

The feed inlet pipe is close to the top of the cyclone; it is the part through which the slurry is introduced into the cyclone (Mainza, et al., 2005). The shape of the hydrocyclone inlet determines the magnitude of centrifugal forces, the initial angular momentum and the stabilization of flow field patterns (Marthinussen, 2011). At a constant feed pressure increasing the inlet size will increase the cyclone throughput. A number of correlations that relate the cyclone throughput to the inlet diameter have been proposed and they are of the following form:

$$Q_f = D_i^n$$

Where: Q_f is the feed volumetric throughput volumetric, Di the inlet diameter and n an experimental exponent.

The various quantities obtained for the exponent n from different authors are illustrated in Table 2-1. It is observed that the inlet has a significant effect on the throughput as the exponent value ranges 0.77 to 2.0.

Table 2-1: Summary of exponent n from various authors adapted from (Magwai & Bosman, 2008)

Bradley (1965)	0.9-2.0
Rao, Lynch and Nageswarao (1976)	0.85
Plitt (1976)	0.84
Svarovsky (1984)	0.85-0.94
Asomah and Napier-Munn (1997)	0.77

Furthermore, Huang et al., (2009) suggested that an inlet with a rectangular cross-section is normally preferred over a circular cross-section inlet, whenever larger flow rates and swirling forces are required. Similarly, the inlet design enhances production capacity, as it is related to the import shape, either formed as involute or conventional (Svarovsky, 2000). Current hydrocyclone manufacturers design inlets in involute form to reduce wear and turbulence, and for better performance (Marthinussen, 2011). Different types of single inlet configurations are illustrated in Figure 2-2.

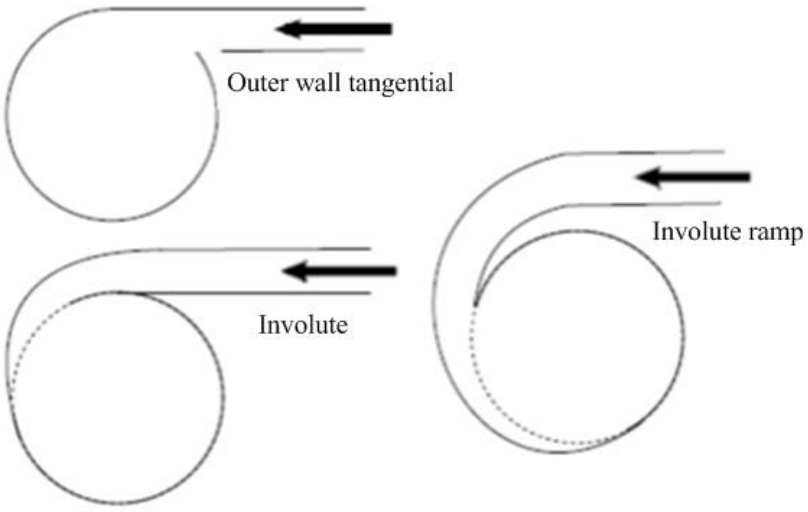

Figure 2-2: Design variations for single inlet hydrocyclones (Marthinussen, 2011)

2.1.2. Vortex finder

The hydrocyclone vortex finder is the overflow pipe that is located at the center of the cylindrical section and that extends into the cyclone body. The vortex finder extends below the feed entry to avoid the short-circuiting of material straight to the overflow, which would reduce the separation efficiency (Kelsall, 1952). Longer vortex finders are preferred to minimize the excessive by-pass into the overflow that is caused by density differences in dual density ores (Bradley, 1965) (Mainza, et al., 2005). However, vortex finder length was not investigated in this thesis.

2.1.3. Spigot or Apex

The underflow exits through the spigot, which is located at the bottom of the cone. The spigot diameter has a direct effect on the underflow-to-throughput ratio, and thus strongly influences the volumetric flow split, underflow density and cut size (Svarovsky, 2000). Manufacturers supply different sizes of both the vortex and the spigot to accommodate a wide range of separation (Wills & Napier-Munn, 2006).

2.1.4. Cylindrical and Conical section

The cylindrical section of the hydrocyclone is the upper section of the cyclone, in which the inlet discharges the material, while the vortex finder extends concentrically into its chamber (Mainza, 2006). As noted in Figure 2-3, the flat bottom cyclone has a longer cylindrical section.

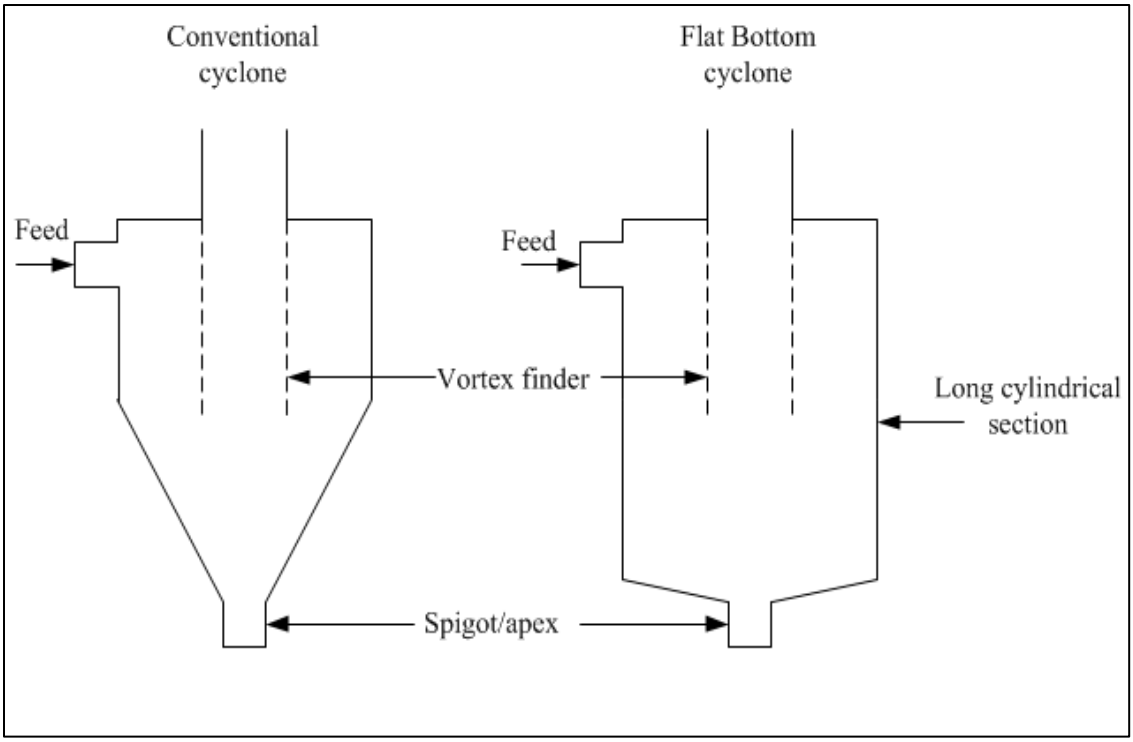

Figure 2-3: Diagram illustrating the differences between the conventional cyclone and the flat bottom cyclone adapted from (Mainza, et al., 2005)

It has been observed that cyclones with longer cylindrical sections tend to have a less sharp separation. Sharpness of separation is discussed in Section 2.5 of this document. The size of the cyclone is quoted using the internal diameter of the cylindrical section, D, as shown in Figure 1-1 (Mainza, 2006).

This work focuses mainly on classification using a conventional hydrocyclone. However, a comparison is also carried out with regard to the classification by means of a flat bottom cyclone, in an attempt to assess the differences in performance at similar operating conditions. A flat bottom cyclone is not actually flat but has a large cone angle >150 degrees. Both the conventional and flat bottom hydrocyclone classify the feed material into two products, namely the cyclone overflow and underflow (Mainza, et al., 2005). A schematic illustrating the conventional cyclone and the flat bottom cyclone is given in Figure 2-2.

The flat bottom cyclone has the same features as the conventional cyclone. The main difference lies in the long cylindrical section and the flat bowl-shaped bottom of the flat bottom cyclone. In most common flat bottom designs, the conical section is absent and has a central discharge,

which is termed the spigot or apex, as illustrated in Figure 2-1. Flat bottom cyclones have been shown to be widely applicable for purposes of sorting according to particle size and density (Svarovsky, 2000).

2.2. The hydrocyclone separation process

Hydrocyclones achieve solid-liquid or liquid-liquid separation using a centrifugal field. The separation phenomenon is illustrated in Figure 2-4. As the feed slurry is pumped tangentially into the upper feed chamber, it follows a circulating path with a net inward flow of fluid from the outside of the vortex finder. An air core is created on the axis, which extends from the spigot opening through the vortex finder to the top of the hydrocyclone (Dahlstrom, 1954) (Lilge , 1962) (Tarr, 1998). The air core is generated as a result of the high magnitude of the centrifugal force, which is several times the magnitude of gravitational force. Coarser particles move in a spiral towards the wall of the cyclone and discharge through the spigot. The cleaned liquid together with the finest particles leaves through the vortex finder, from where it is directed to further processing by the overflow pipe (Fuerstenau & Han, 2003). The particle migration is shown in Figure 2-4. The blue arrows indicate the path taken by the coarser particles, whereas the red arrows indicate the path taken by the finer particles. As the feed slurry is tangentially fed into the hydrocyclone, the linear velocity is resolved into three components, namely radial, vertical and tangential. The velocity profiles of hydrocyclones were first measured by Kelsall, (1953), he found that the tangential velocity increased to a maximum from hydrocyclone wall towards the centre, and then decreased rapidly (Rietema, 1960) (Svarovsky, 2000).

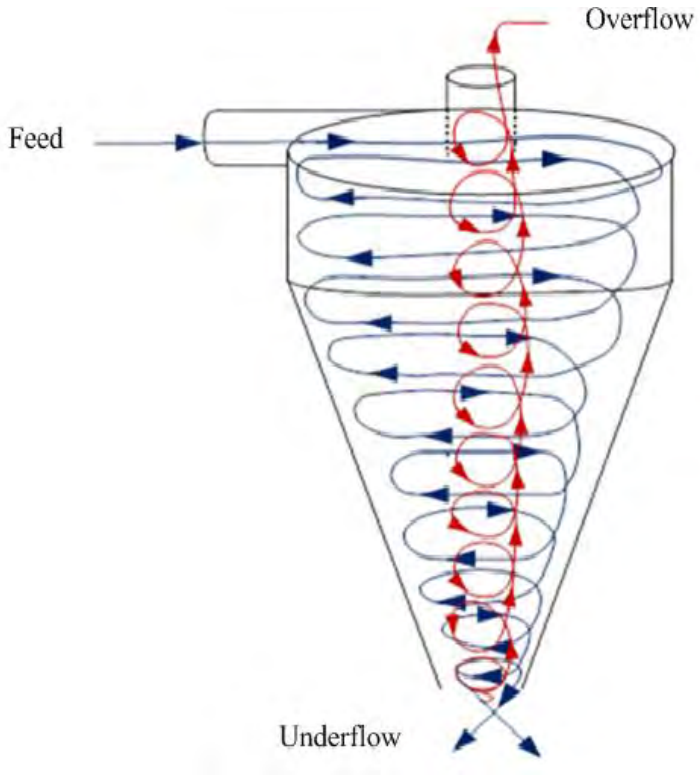

Figure 2-4: Schematic of separation phenomenon in the hydrocyclone (Bradley, 1995)

2.2.1. Tangential motion

The air core, which is defined as a cylindrical air envelope in the centre of the hydrocyclone, is where the fluid experiences a maximum tangential velocity. The tangential velocities of the fluid (v_t) increase with decreasing radius until a maximum velocity is reached at a radius smaller than the exit radius of the vortex finder (Rietema, 1960) (Svarovsky, 2000). As a result, the effect of changing the vortex finder diameter can be deduced from a relationship between the radius and vertical velocity, as described by Equation 2-1.

$$v_t r^n = C \qquad \textbf{2-1}$$

Where C is a constant with n values normally ranging from 0.6 to 0.9

According to the equilibrium orbit theory, which is discussed in Section 2.3.1, the solid particles at any given size and fluid medium will attain the same velocities at any point in the core (Plitt, 1976). This suggests that Equation 2-1 means that the tangential velocity is independent of the vertical position, although it can be influenced by wall effects. This agrees with Elsayed (2010), who stated that the maximum tangential velocity profiles have planes of envelopes as cylinders

coaxially within the cyclone, where radial forces on solid particles are greater than the centrifugal force, thus causing finer particles to report to the overflow. The tangential velocity distribution in a hydrocyclone as a function of cyclone sectional radius is illustrated in Figure 2-5.

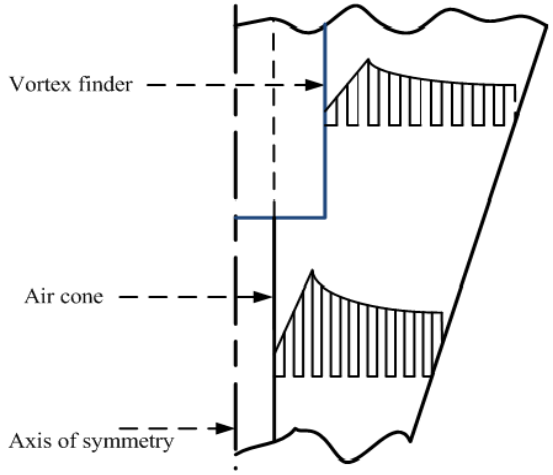

Figure 2-5: Tangential velocity distribution within a hydrocyclone (Svarovsky, 2000)

2.2.2. Vertical motion

Within the cyclone, the downward motion is counterbalanced by an upward flow in the core region (Rietema, 1960) (Svarovsky, 2000). A locus of points where particles have zero vertical velocity is expected, since both upward and downward motion exist. Figure 2-6 illustrates this locus of zero vertical velocity (LZVV). There is a strong downward flow along the outer wall of both the cylindrical and conical portions. This results in the separation of the coarser particles to the underflow orifice.

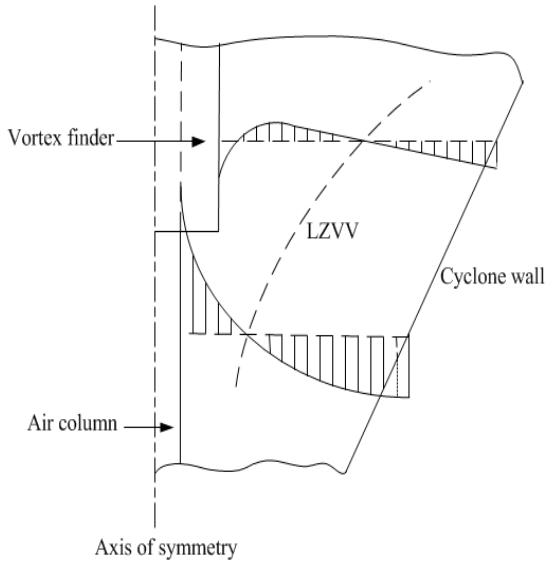

Figure 2-6: Vertical velocity distribution in a hydrocyclone showing locus of zero vertical velocity LZVV adapted from (Svarovsky, 2000)

2.2.3. Radial motion

The radial velocity is much smaller than the vertical and tangential velocity. The classical theory of hydrocyclone action is that particles within the flow pattern are subjected to two opposing forces – an outward centrifugal force (F_C) and an inwardly acting drag force (F_D) (Wills & Napier-Munn, 2006). Figure 2-7 illustrates the forces acting on the orbiting particle. Equations 2-2 and 2-3 illustrate that the radial velocity of particles differ as a result of the centrifugal force. This shows that radial velocities vary with the size, specific gravity and shape of the particle.

The centrifugal and drag forces are represented by Equations 2-2 and 2-3 respectively:

$$F_C = \frac{\pi d_p^3 \omega^2 r}{6}(\rho_s - \rho) \qquad \textbf{2-2}$$

$$F_D = 3\pi d_p \mu v_r \qquad \textbf{2-3}$$

Where d_p is the particle diameter (m), ω is the angular velocity (rad/s), r is the radius of orbit of the solid particle (m), ρ_s is the solid density (kg/m^3), ρ is the fluid density (kg/m^3) and v_r is the relative radial velocity between the liquid and solid particles (m/s).

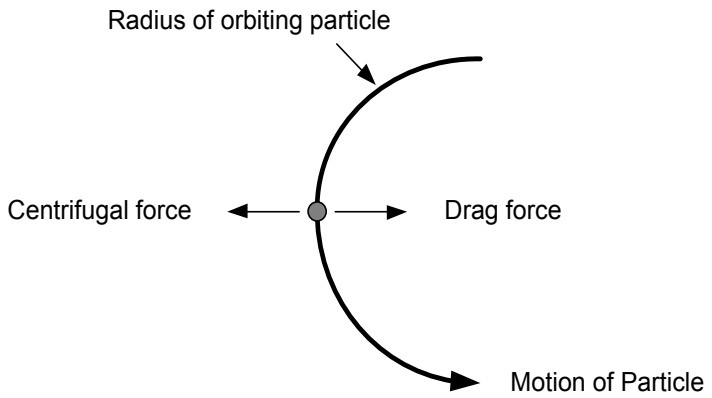

Figure 2-7: Forces experienced by a particle orbiting with the hydrocyclone (Wills & Napier-Munn, 2006)

2.3. Hydrocyclone classification theories

There have been many theories developed to explain the separation process that occurs within hydrocyclones. Some of these theories are based on actual physical models derived from first principles, while others are models derived as empirical equations from linear regression analysis (Tongsiri, 2007). The most common models used are the equilibrium orbit theory and the crowding theory.

2.3.1. Equilibrium orbit theory

The equilibrium orbit theory was first proposed by Criner (1950) and Driessen (1951); it is based on the concept of the equilibrium radius (Asomah, 1996). Various researchers such as Yokioka and Hotta (1995), Lilge (1962), Bradley (1958,1965), Smith and Coghin (1984), Pericleous et al., (1984), Kawatra et al., (1996) describe this theory as that which best predicts cyclone performance. The theory assumes that each particle within a cyclone is in equilibrium under the effect of two opposing forces. These are an outward acting centrifugal force due to the tangential flow within the cyclone and an inward acting drag force that is due to radial, inward velocity. Particles of different size will therefore have different equilibrium orbit radii. Particles near the inner wall of the cyclone report to the apex whilst particles close to the axis of the cyclone report to the vortex finder. This suggests that the vertical velocities of these particles are opposite to each other. Therefore, at some point within the cyclone there exists a plane where the vertical velocity of particles is zero. This plane is called the envelope of zero velocity (Kawatra et al.,

1996). A particle at the envelope of zero velocity therefore has an equal probability of reporting to the spigot or vortex finder. The particle size at the envelope of zero velocity is referred to as the cut size. This theory assumes that flow conditions within the cyclone are laminar (Trawinski, 1972).

At equilibrium, the particle size is assumed to be the cut size (d_{50}) (Plitt, 1976). Equating Equations 2-2 and 2-3 will yield the following expression:

$$d_{50} = \left(\frac{18\mu v_r r}{(\rho_s - \rho)\omega^2}\right) \qquad \textbf{2-4}$$

According to Bradley (1965), the position of the LZVV can be estimated by using Equation 2-5:

$$R_{LZVV} = \frac{R_c}{1 + \frac{D_u}{D_o}} \qquad \textbf{2-5}$$

Where R_{LZVV} is the radius of locus of zero vertical velocity (mm), Rc is the cyclone diameter (mm), Du is the spigot diameter and Do is the vortex finder.

The ratio of the spigot diameter and vortex finder diameter in the denominator of Equation 2-5 is defined as the cone ratio (Kilavuz & Gulsoy, 2011). The change of cone ratio affects the LZVV, which in turn affects the cut size (Bradley, 1965). An increase in the cone ratio results in a decreased LZVV, causing the cut size to decrease. The decreased LZVV implies that there is a probability of finding finer particles closer to the air core, thus a finer separation is expected (Plitt, 1976). This can be visualized from the schematic showing the changes in the radius of the locus of zero vertical velocity (R_{LZVV}) with increasing cone ratio in Figure 2-8.

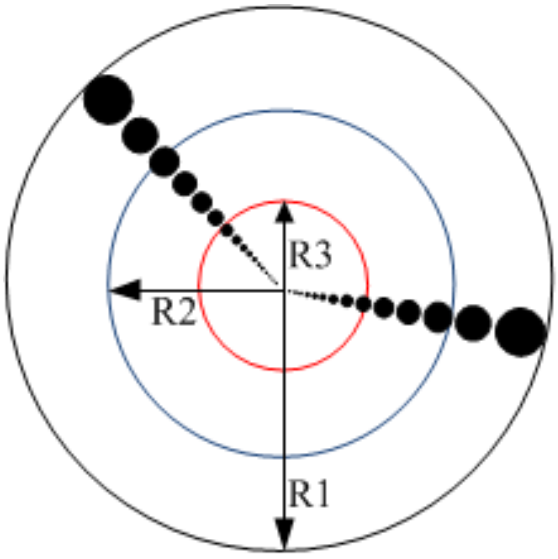

Figure 2-8 : Top view schematic representing the changes in cut size with increasing cone ratio. The 2nd circle inwards is the initial locus, whereas the inner circle is the locus after increasing cone ratio. The black dots represent the ore particles according to particle size.

The air core is the result of rotating fluid as an axial core of low pressure that induces a free liquid surface, and that communicates directly with the atmosphere at either of the outlets (Bradley, 1965). The formation of an air core determines the vortex stability, thus influencing the overall separation of finer particles from coarser particles.

2.3.2. Crowding theory

The crowding theory was first proposed by Fahlstrom (1960, 1963). This theory suggests that the classification performance is primarily a function of the capacity of the underflow spigot and the particle size distribution of the feed particles. Fahlstrom suggested that the separation is not only due to the hindered settling of particles within the cyclone, but also due to the hindered discharge through the spigot. According to Fahlstrom, if the spigot is restricted, under the influence of centrifugal force, the probability of a given particle passing through the spigot is determined by its mass (Asomah, 1996). He proposed that the underflow discharge condition and any cut size (d_{50}) within the feed size distribution could be predicted by Equation 2-6 below. This theory emphasises the effect of the spigot size on the cyclone separation. The crowding effect can be observed in practice by reducing the spigot diameter. The crowding theory is more applicable to

inclined cyclones, however, as they tend to produce thickened underflows (Magwai & Bosman, 2008).

$$d_{50} = K_o(1 - g_u)^{1/n} \qquad \textbf{2-6}$$

Where K_o is the maximum feed particle size on a sieve analysis plot/data, g_u is the solids recovery in the underflow and n is the gradient of the sieve analysis plot of feed solids.

2.4. Representation of hydrocyclone separation efficiency

The imperfection in the performance of any real separator can be characterized by separation efficiency (Svarovsky, 2000). Operating conditions as well as dimensions contribute to the cyclone's performance. A partition curve (actual or uncorrected efficiency curve) is the most common method of presenting hydrocyclone performance. This curve describes the relationship between the fraction or percentage of each feed particle size that reports to the underflow and the the particle's size. Partition curves are usually S-shaped, and the closer the curve is to the vertical, the higher the separation efficiency. At any point on the curve, where the weight fractions of the given size material in the underflow and feed ore streams are du and df respectively, then the actual efficiency at that point is given by Equation 2-7:

$$\mathrm{E_a} = \frac{\mathrm{M_u . d_u}}{\mathrm{M_f . d_f}} = \frac{\mathrm{f_i - o_i}}{\mathrm{u_i - o_i}} \cdot \frac{\mathrm{u_i}}{\mathrm{f_i}} \qquad \textbf{2-7}$$

Where E_a = actual efficiency, M_u = mass flow rate of the underflow stream, M_f = mass flow rate of the feed stream, f_i = feed solid weight fraction, u_i = underflow solid weight fraction and o_i = overflow solid weight fraction.

During the cyclone separation process, a portion of the feed solids short-circuits to the underflow. It is assumed that the same fraction of feed water (R_f) also short-circuits to the underflow. As a result, the actual partition curve does not pass through the origin. A correction thus has to be made to describe the classification alone (Kelsall, 1953). The corrected partition curve E_c is referred to as the corrected partition or corrected efficiency curve. It is given by Equation 2-8:

$$E_c = \frac{E_a - R_f}{1 - R_f} \qquad \textbf{2-8}$$

Where E_c = corrected efficiency, E_a = actual efficiency, and R_f = water recovery to underflow.

The following are the performance characteristics of a hydrocyclone classifier, which are required to describe its performance: corrected cut size(d_{50}), sharpness of separation (α), and water recovery to underflow (R_f). Figure 2-9 illustrates the partition curve as well as the corrected partition curve, noting the important points on the curves.

Cut size (d_{50}) and dmax

The cut size is often used to measure the efficiency of a hydrocyclone. The cut size is defined as the size that has a 50% chance of reporting to the overflow or underflow streams. The d_{50c} is the cut size that corresponds to the particle size that has a 50% probability of reporting to both the overflow and underflow for the corrected partition curve.

The limit of separation, which is the largest particle size remaining in the overflow after separation (viz. the particle size above which the grade efficiency is 100% for all particle sizes), is referred to as d_{max}.

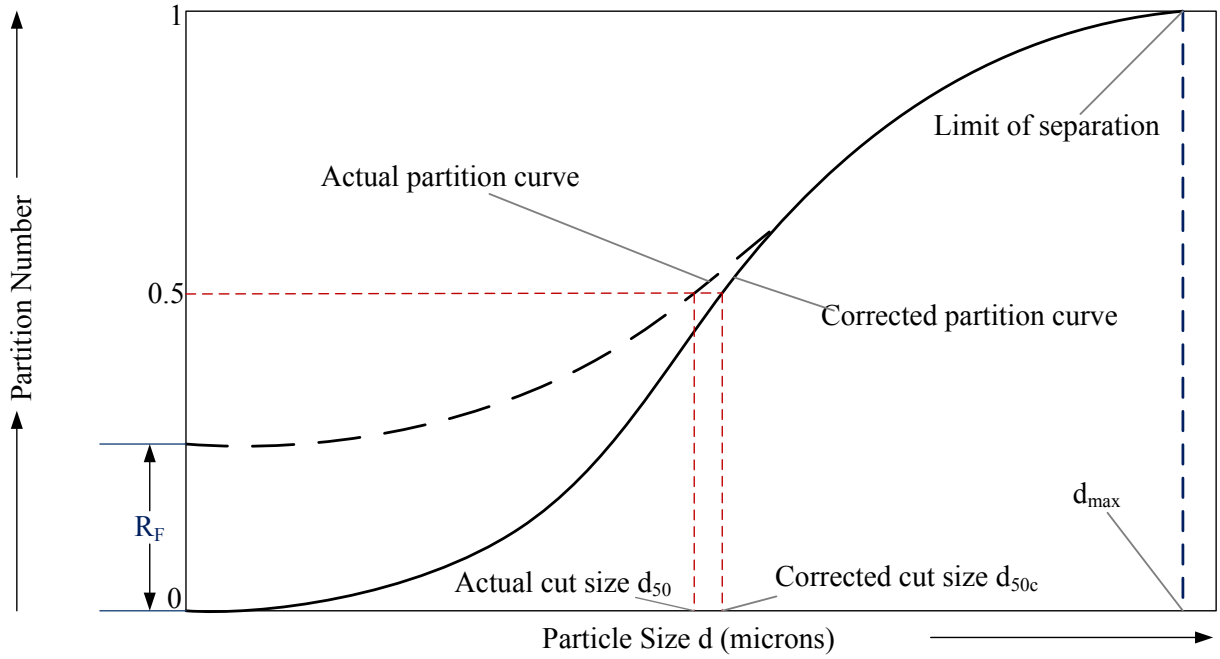

Figure 2-9: Hydrocyclone partition curve (Svarovsky, 2000)

Sharpness of separation (α)

Sharpness of separation (α) is a measure of the quantity of misplaced particles in the underflow and overflow streams (Majumder, et al., 2007). During classification, it is desirable to minimize the amount of misplaced material; a sharper cut means that less material is misplaced (Mainza, et al., 2005). The sharpness of the cut is related to the general slope of the grade-efficiency curve. For an ideally sharp separation, the grade-efficiency curve would be a vertical line at the cut size.

Water Recovery (R_f)

Water recovery is defined as the ratio of the volumetric water flow rates of the underflow to the feed streams (Kilavuz & Gulsoy, 2011). The water recovery is an important indicator especially for classification, which involves further processing before valuable minerals are recovered (Lusinga, et al., 2009). A high water recovery to the underflow correlates to a decrease in the separation efficiency of the hydrocyclone, as finer particles become entrained in the underflow. As a result of bypassing, it is generally desirable to limit the water recovery to underflow to about 40%. A summary of water recoveries is given in Table 2-2.

Table 2-2: Summary of effects of water recovery (Svarovsky, 2000)

Rf (%)	Efficiency
>50%	very poor
40-50%	poor
30-40%	reasonable
20-30%	good
10-20%	subject to underflow density and roping
<10%	product for conveying or stockpiling

2.4.1. Hydrocyclone performance analysis models

In some cases the water recovery to the underflow is not a fundamentally accurate method for obtaining the equivalent fraction of feed solids that are by-passing (Cilliers, 1994). An example of such a scenario is when a cyclone is clarifying slurry with a low solids concentration, when assumption becomes a poor estimate. In such a case, it is necessary to use models that take into account scenarios such as complex ore properties, dual density nature and particle shape irregularities. These models can then be regressed to obtain the cyclone performance parameters (Plitt, 1976). Table 2-3 summarises the most common models for analysing hydrocyclone performance.

Table 2-3: Models and methods of prediction of parameters of corrected efficiency curves

Model	Equation	Prediction method
Harris	$E_c = \left[1 - \left(\frac{d}{d_{max}}\right)^m\right]^r$	Non-linear regression & graphical
Reid–Plitt	$E_c = 1 - e^{[-0.6931\left(\frac{d}{d_{50c}}\right)^m]}$	Simple linear regression & graphical
Whiten	$E_{oa} = C.\frac{e^{\propto\left(\frac{d}{d_{50c}}\right)-1}}{e^{\propto\left(\frac{d}{d_{50c}}\right)+e^{\propto}-2}}$	Non-linear regression

In this thesis, the Whiten model will be used to model the cyclone performance. This is because its parameters are independent of operating conditions and as such, the model becomes more helpful in optimising operating conditions (Irannajad et al., 2009). Sometimes the performance analysis of size classification devices tends to show a 'fish-hook effect' on efficiency curves. Nageswararao (2000) defined this 'fish-hook' as an inflection in the efficiency curve, depicting a dip at sub-sieve sizes, but it is rarely reported in the literature. Wills & Napier-Munn (2006), however, argued that the fish-hook effect is generally observed only if sub-sieve sizing is

performed and that its significance on the precision of measurements of the actual efficiency of the cyclone is negligible. Nevertheless, modified Whiten and Plitt-Reid models are regarded as the best modelling function to fit efficiency curves of hydrocyclones with fish-hook behaviour at fine sizes (Lynch & Rao, 1968) (Irannajad et al., 2009).

2.5. Effect of design variables investigated in thesis

2.5.1 Effect of vortex finder

The vortex finder size is an especially important dimension, which significantly affects the cyclone performance, as its size plays a critical role in defining the flow field inside the cyclone, including the pattern of the outer and inner spiral flows (Elsayed & Lacor, 2010). The work done by Plitt (1976) illustrated that the diameter of the vortex finder was related to cut size, as shown by Equation 2-9:

$$d_{50} \alpha\, D_o^n \qquad \textbf{2-9}$$

Where n=1.21, d_{50} is the cut size (microns) and D_o is the vortex diameter in (cm).

Equation 2-9 shows that the cut size increases with an increasing vortex finder diameter. However, for larger vortex finder diameters (Do>>0.167Dc), some feed material may bypass classification and be diverted to the overflow (Rietema, 1960) (Lilge, 1962). Conversely, a small vortex finder (Do<0.167Dc) created an undesirable circulating load of ore particles within the cone (Lilge, 1962). As a result, it was concluded that it is preferable to have the vortex finder almost equal to 0.167Dc to ensure the most effective classification. A log-log plot of the vortex finder against the weight percentage of solids reporting to the overflow produced a straight line, confirming the power relationship indicated in Equation 2-10 (Fahlstrom, 1963; Marais and Hoffman, 1962):

$$\varphi_s = D_o^{0.9} \qquad \textbf{2-10}$$

Where: D_o is the vortex finder diameter (cm) and φ is the solids fraction (%).

Referring back to Section 2.3.1, it can be noted that increasing the vortex finder diameter results in a decrease in the cone ratio. This increases the R_{LZVV}, thereby increasing the cut size, as the

two have an inverse relationship. This confirms the relationship proposed by Plitt (1976), viz. that cut size increases with increasing vortex finder diameter.

The work done by Lusinga et al., (2009) using water only and silica slurry indicated that, as the vortex finder diameter increased, the water recovery to the underflow increased. This was attributed to the fact that, as the vortex finder diameter increased, the air core diameter increased too, thus pushing more liquid to the cyclone wall and as a result reporting to the underflow. This is in agreement with the work done by Kilavuz et al., (2011).

2.5.2 Effect of spigot diameter

It has been observed that an increase in spigot diameter results in an exponential increase in water split (Banerjee et al., 2013; Lusinga et al., 2009; Svarovsky, 2000). The exponential relationship trend of water split to overflow with varied spigot diameters can be estimated by Equation 2-11 below, as proposed by Banerjee et al., (2013):

$$R_{of} = kD_u^n \qquad \textbf{2-11}$$

Where k is the proportionality constant determined experimentally, and the exponential value of n ranges from -0.10 to -0.175. The negative sign indicates the effect of spigot diameter on the percentage of water split to the overflow.

Furthermore, although a large spigot size increases product capacity, it reduces the cut size (Tarr, 1985). For smaller sizes, the probability of all the particles reporting to the underflow is reduced due to the reduced air core forcing some coarser particles to report to the overflow. With an increased spigot diameter and all other parameters being held constant, the probability of finer and lighter particles crossing the line of zero vertical velocity increases, resulting in a decreased cut size (d_{50}). The relationship between the cut size and the spigot diameters can be estimated from the experimental correlations developed by Lynch and Rao (1966), as shown by Equation 2-11 below.

$$\log d_{50} \propto 0.29 D_u \qquad \textbf{2-12}$$

The validity of Equation 2-12 is limited if the 'hindered settling' effect is experienced (Asomah, 1996). Hence, cut size depends on spigot diameter, density differences of the ore and particle

size distribution of the feed. Work done by Mainza (2006) on UG2 ore showed that the cut size increased with a decrease in the spigot diameter. This was also observed by Lusinga et al., (2009), who carried out tests on a 100mm cyclone using silica.

When selecting the spigot size, it is important to maximize the underflow density and to ensure that it can withstand the amount of solids (Mainza, et al., 2005). The solid content in the underflow increases with increased feed concentration and feed rate. The different types of sprays that can occur at the spigot are given in Figure 2-10. Fanning (flaring) and roping are undesirable, as they are an indicator of poor classification. Fanning is observed when the feed solid concentration is too dilute and the feed pressure is too high (Napier-Munn, et al., 2005). As the solid concentration increases, the spigot spray diameter decreases, until a critical value of solids concentration is reached. At the critical value of solids concentration, the air core collapses, and the discharge emerges as a very high density discharge (more than 50% solids by volume), resulting in roping (Wills & Napier-Munn, 2006).

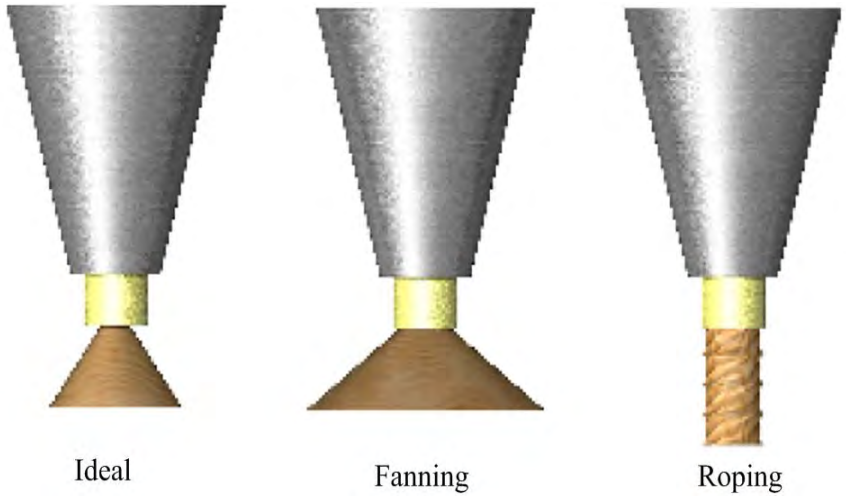

Figure 2-10: Types of underflow discharges, adapted from (Wills & Napier-Munn, 2006)

2.5.3. Effect of cone ratio on hydrocyclone performance

An experimental study by Lusinga et al., (2009) using silica showed that the cut size decreased linearly with an increase in the cone ratio for a particular vortex finder. Furthermore, the cut size of adjusting the cone ratio was higher for relatively coarser particles, than it was for the finer particles. They explained this phenomenon by referring to Equation 2-5 of the equilibrium orbit

theory, which states that, when the cone ratio increases, the position of L_{ZVV} shifts towards the air core, thus causing the fine particles to have a high probability of reporting to the overflow stream (Bradley, 1965). These findings are moreover in agreement with the findings of (Kilavuz & Gulsoy, 2011) that carried out tests using 25.4 mm and 50.8 mm diameter cyclones at varying cone ratios and pressures. The cut size increased linearly with increasing cone ratio as well as increasing pressure. They attributed this to the fact that, at higher pressures, the centrifugal force on the particles increased and the finer particles were first dragged toward the cyclone wall and then to the underflow, thus reducing the cut size.

Increasing the cone ratio has been found to increase the flow rate of water to the underflow (Lusinga et al., 2009; Plitt, 1976; Wills & Napier-Munn, 2006). A correlation was found between the pulp recovery to the underflow and the cone ratio, as defined by Equations 2-13 and 2-14 (Kilavuz & Gulsoy, 2011) for a 25.4 mm and 50.8 mm cyclone respectively.

$$R_f \, \alpha \, (D_o/D_u)^{-1438} \qquad \textbf{2-13}$$

$$R_f \, \alpha \, (D_o/D_u)^{-1948} \qquad \textbf{2-14}$$

Where R_f is the volumetric recovery of feed slurry to the underflow %, Do is the vortex finder diameter and Du is the spigot diameter.

High water recovery to the underflow entrains finer particles and consequently dilutes the underflow stream, which is typically a recycled feed to the mills in a closed loop grinding circuit. Thus, too high water recoveries to the underflow reduce both the hydrocyclone and ball milling performance (Tarr, 1985), (Wills & Napier-Munn, 2006)

The effects of design variables are crudely summarized by Svarovsky (1984) as illustrated by Table 2-4.

Table 2-4: Effects of design variables in hydrocyclones (Svarovsky, 1984)

Increase capacity	**Reduce cut size**	**Improve sharpness of separation**	**Increase flow ratio**
Increase cyclone diameter	Reduce cyclone diameter	Increase outlet diameter	Increase underflow diameter
Increase inlet diameter	Reduce inlet diameter	Increase cone angle	Reduce overflow diameter
Increase outlet diameter	Reduce outlet diameter		Increase body length
Increase body length	Reduce cone angle		Reduce vortex finder length
Reduce vortex finder length	Reduce vortex finder length		
	Increase body length		

2.6. Slurry rheology

Rheology is the science of flow and the deformation of matter (Barnes, et al., 1998). It describes the deformation of a phase under the influence of stress. Shear stress (τ) and shear rate (γ) are used to express different types of laminar deformations. Slurry rheology is known to have an influence on the performance of wet comminution devices, such as ball mills, and on wet classifiers, such as hydrocyclones (Shi, et al., 2010).

There are two types of flow curves, namely Newtonian and non-Newtonian. Most slurries in a comminution circuit exhibit non-Newtonian behaviour at solids concentrations above 15% volume for a base metal with a 20% fines content passing 38μm (Shi & Napier, 1996). The different flow curves are illustrated in Figure 2-11. The rheological behavior of slurries can be classified as being either time dependent or time independent. Time dependent behavior is characterized by the viscosity of the fluid changing with time under constant shear conditions. When a material becomes more fluid with increasing time of flow under steady state conditions, it is called thixotropic, while rheopexic behavior results in a fluid becoming more resistant to flow with increasing time under steady state conditions. Most industrial grinding operations are continuous; the rheology involved is denoted as time independent slurry behavior (Klimpel, 1997).

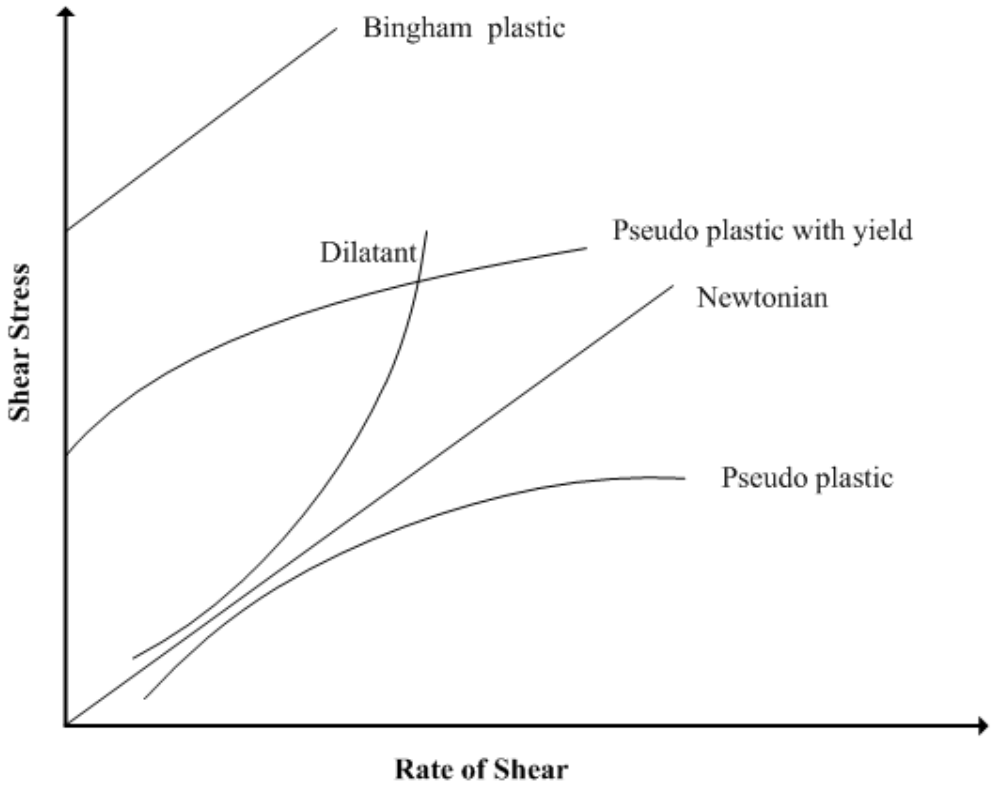

Figure 2-11: Graph illustrating shear stress vs. shear rate for time -independent slurries (Wills & Napier-Munn, 2006)

A fluid's resistance to shear is represented by its viscosity. Viscosity of fluid is a measure of its resistance to gradual deformation by shear stress; it plays a significant role in hydrocyclone classification. This is because slurry viscosity alters the particle settling velocities and the slurry velocities within the hydrocyclone, thus affecting its performance (Tavares, et al., 2002). The apparent viscosity is defined as the ratio of shear stress to shear rate. It is the slope of the flow curve from the origin to a particular point on the flow curve (Van Wazer et al., 1963). The viscosity for Newtonian liquids is constant and is represented by Equation 2-14 as defined by Muster & Prestidge (1995). However, for non-Newtonian fluids, the viscosity varies.

$$\eta = \frac{\text{Shear stress } (\tau)}{\text{Rate of shear strain } (\gamma)} \qquad \textbf{2-15}$$

The intercept at the shear stress axis on a rheogram is the apparent yield stress. Most ores at high solid concentrations will not flow if the shear stress does not exceed a certain value, which is called the yield stress (Mingzhao, 2005). Plastic viscosity is another property used to

characterize the rheological behavior of non-Newtonian fluids. At high shear rates, the pseudo plastic fluids behave like Bingham plastics, in that there is a near linear relationship between shear rate and shear stress (Gao and Forssberg, 1993; Govier et al., 1957; Napier-Munn, 1983).

2.6.1. Key variables that affect slurry rheology

Hydrocyclones are subjected to feed slurries of various solids concentrations, ranging from almost clean liquids to slurries containing up to 60% solids. As a result, the slurries become either coarse fast-settling or slow-settling (Tavares , et al., 2002). Coarse fast-settling slurries contain large particles of high specific gravity that are prone to settle when introduced to liquid, whereas slow-settling slurries contain particles of low specific gravity that tend not to settle when introduced to a liquid media. Slurry viscosity affects classification performance and thus the overall energy efficiency of a grinding circuit (Mingzhao, et al., 2004), Waters (2012).

Fluid viscosity can change as a result of alterations in size distribution, solid percentage, and temperature (Kawatra, 1996). When the viscosity of the slurry increases to a point where the frictional drag of the cyclone wall stops the rotary motion, roping is initiated (Lynch & Rowland, 2005) (Lynch & Rowland , 2005). This initiation occurs mainly as a result of the formation of a solid bed in the apex region of the cyclone. Work done by Dyakowski (1995) showed that the excess fluid viscosity decays the tangential velocity and consequently the rotational motion at the underflow.

There are three key factors that influence slurry rheology, and these are:

1. solids concentration
2. particle size
3. temperature

2.6.1.1. Solids concentration

The influence of solids concentration on slurry rheology is significant, since the range of solids concentrations can lead to different types of flows (Mingzhao, 2005). The effect is more pronounced at high solids concentrations, where small changes in solids concentrations result in large shifts in viscosity (Kawatra and Eisele, 1988). These large shifts occur at the inflection point. The inflection point is when the viscosity of the slurry starts to increase exponentially with

a small change in the solids concentration. Beyond this point, the suspension flow characteristics are less predictable and more difficult to control (Becker, et al., 2013).

The rheological characterisation done by Becker, et al., (2013) on two Southern African platinum ores, Great Dyke and UG2 ore is illustrated in Figure 2-12. The analysis was done on the flotation feed, concentrate and tailings of the respective ores. At low solid concentrations, the viscosity increases linearly with increasing solids concentrations. These findings are in agreement with what was observed by He, et al., (2004). As the solids concentration increases, the rheological behaviour of the slurries become more non-Newtonian. He, et al., (2006) conducted rheological investigations using limestone slurry. They observed that an increase in solids concentration transformed slurry rheological behavior from a weakly dilatant (shear thickening) to a pseudo plastic (shear thinning) one, with yield stress at solids concentration ranging from 60wt% (35.71vol%) to 78.5wt% (57.49vol%). At solids concentrations less than 65wt% (40.75 volume %), the slurry showed a weakly dilatant behavior. This was attributed to large inter-particle distances between particles, which resulted in weak van der Waals forces. At low shear rates, particles are able to slip over each other, whereas at higher shear rates, the movement of particles is restricted.

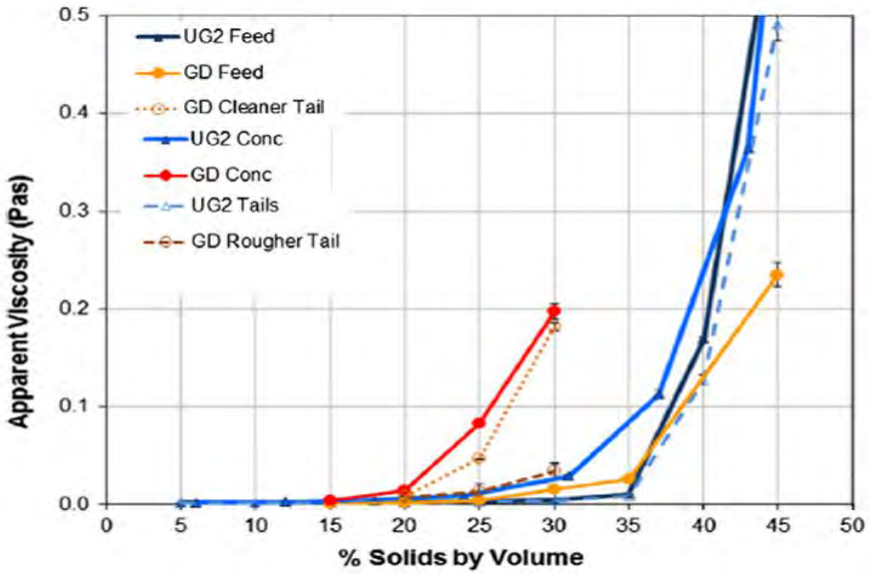

Figure 2-12: Viscosity at various solids concentrations for UG2 ore and Great Dyke ore from Becker, et al., (2013)

2.6.1.2. Particle size

The particle size as well as their distribution has a significant influence on the slurry viscosity. The finer the particle size, the higher the probability of agglomeration and aggregation, which affects the movement of slurries (He, et al., 2004). The d_{50}'s for the work done by Becker, et al., (2013) are summarised in Table 2-5.

Table 2-5: d_{50} from analyses done by Becker, et al., (2013) on Great Dyke and UG2 ores

	UG2 (µm)	Great Dyke (µm)
Feed	18	110
Concentrate	7	13
Tailings	17	128

From Figure 2-12, it can be seen that for both the Great Dyke and UG2 samples, the flotation concentrate has an inflection point at a lower solids concentration than those of the tailings and the feed. This illustrates that the finer samples are more rheologically complex than the coarser samples (Becker, et al., 2013). These findings are in agreement with what was found by Mangesana et al., (2011), Kawatra and Eisele (1988), who observed that, at constant solids concentration, a reduction in particle size would result in an increase in the slurry viscosity. This was attributed to an increased particle surface area. As a result, the amount of free fluid is reduced, thus increasing the effective solids concentration. However, the work of Clarke (1997 and De Bruijn (1951) contradicts the findings of Becker, et al., 2013 and Kawatra and Eisele, 1988. Clarke found that the slurry viscosity increased with particle diameter. This was attributed to inertial effects, which resulted in additional energy dissipation.

2.6.1.3. Temperature

The viscosity of slurries is also a function of the absolute temperature. Various authors have reported that the viscosity of a slurry increases with a decrease in the temperature (Baguley, 1988; Kawatra and Eisele, 1988). The temperature dependence of viscosity can be represented in terms of an Arrhenius type of equation for a range of temperatures. This can be represented by Equation 2-15:

$$\eta = Ae^{\frac{Ea}{RT}} \qquad \textbf{2- 16}$$

Where η is the relative viscosity at a particular shear rate, Ea is the fluid-flow activation energy, T is the temperature in Kelvin, R is the universal gas constant and A is the fitting parameter.

2.6.2. Effect of viscosity on hydrocyclone performance

Since the viscosity determines the flow of slurry, it has a significant impact on the hydrocyclone performance. As a result, the importance of the viscosity has been recognized by many authors: Bradley (1965), Agar and Herbst (1966), Napier-Munn (1980) Kawatra et al., (1987), and Svarovsky (2000). Based on Equations 2-3 and 2-3, researchers have proposed a relationship, which is given by Equation 2-17

$$d_{50} \alpha \, \eta^{\beta} \qquad \textbf{2- 17}$$

Where η is the viscosity and β has a theoretical value between 0.5 and 0.6

The exponent 0.50 is usually used; it assumes that the settling of particles takes place in a laminar regime (Asomah, 1996). Some exponents reported in literature are reported in in Table 2-6.

Table 2-6: Powers on viscosity terms in d_{50} equations adapted from (Asomah, 1996)

Authors	Viscosity Power
Yoshioka and Hotta (1955)	0.5
Bradley and Pulling (1956)	0.5
Lilge (1962)	0.5
Svarovsky (2000)	0.5
Agar and Herbst (1966)	0.58*
Castro (1990)	0.6465#
Williamson et al/ (1983)	0.48*

Studies done by Kawatra et al., (1988), Horsley and Allen (1987) and Castro (1990) have concluded the following impact of slurry viscosity on the hydrocyclone performance:

- increasing the slurry viscosity will lead to an increase in the separation cut size
- the sharpness of separation decreases with an increasing slurry viscosity

- an increase in the feed viscosity will result in a higher underflow to throughput ratio
- an increase in the feed viscosity will result in an increase in the amount of fines recovered in the underflow

These findings were confirmed by Shi, et al., (2010) who did a study on a 50.8 cm hydrocyclone treating copper ore. It was observed that both the cut size and water recovery to the underflow increased with feed viscosity, as shown in Figure 2-13.

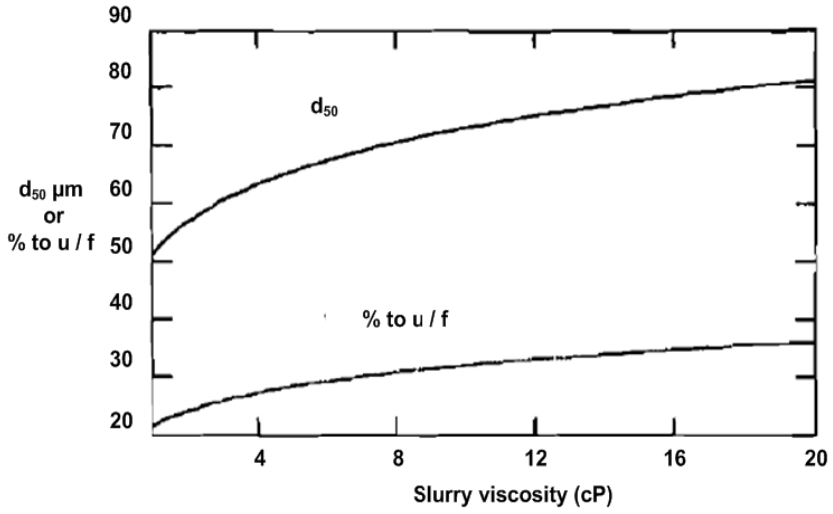

Figure 2-13: Effect of slurry viscosity on cut size and water recovery to underflow (Shi, et al., 2010)

2.7. Rheology models

Different models have been used to describe the flow of slurry. The models describe the mathematical relationship between shear stress and shear rate. A summary of the rheological models found in the literature is given in Table 2-7. The models commonly used to describe Newtonian slurry behavior are the Newton and Bingham models. Non-Newtonian slurry behavior is commonly described using the two-parameter Ostwald/de Waele power law, the Bingham plastic, the Casson and the three-parameter Herschel-Buckley and Sisko models (He, et al., 2007). For this thesis, the Bingham plastic model was used.

Table 2-7: Summary of rheology models (Mangesana, 2011)

Model	Equation	Interpretation of equations
Newton *(Bartos,1992)*	$\tau = \eta\gamma$	Shear stress is directly proportional to shear rate
Ostwald/de Waele (*Atzeni, et al., 1985)*	$\tau = C\gamma^P$	Applied to shear thinning or thickening fluids with no yield stress, P>1: Shear Thickening, P<1: Shear Thinning, P=1: Newtonian Fluid
Bingham model *(Tattersall, 1976)*	$\tau = \tau_B + \eta_B\gamma$	Approximates yield point, does not take into account shear thinning or shear thickening behaviour
Herschel/Buckley *(Atzeni, et al., 1985)*	$\tau = \tau_{HB} + C\gamma^P$	Similar to the Bingham model but it gives an indication of shear thinning or shear thickening ,P>1: Shear Thickening , P<1: Shear Thinning, P=1: Newtonian Fluid
Sisko *(He, et al., 2004)*	$\tau = \pi_\infty\gamma + m\gamma^n$	Combines low and intermediate shear power law with high shear Newtonian limiting behaviour

2.8 Ores investigated in this thesis

The two ore types investigated in this thesis are UG2 and iron. These ores are dual density in nature. This means they have two dominant minerals with different densities, as shown in Table 2-8.

Table 2-8 : List of ores investigated and their respective components (Anglo-American (2013); Mainza, 2006)

Ore	Components	Relative Density
UG2 (Upper Group)	Silicates (Rich in PGM)	2.80
	Chromite	4.97
Iron Ore	Silicates	2.80
	Iron	4.19

As a result of the dual density nature of these ore types, there is usually a misplacement of fine high-density particles to the underflow and coarse low-density particles to the overflow in hydrocyclone separations (Lynch and Rao, 1966). In UG2 ore, the phenomenon negatively affects the recovery of silicates during subsequent size-sensitive processes, such as flotation (Mainza et al., 2004).

Mainza (2006) investigated classification of UG2 ore with a three product cyclone in an attempt see whether this type of cyclone could overcome the dual density classification problem. The three product hydrocyclone is similar to the conventional hydrocyclone; instead of one overflow, however, it has two overflow streams, as illustrated in Figure 2-14.

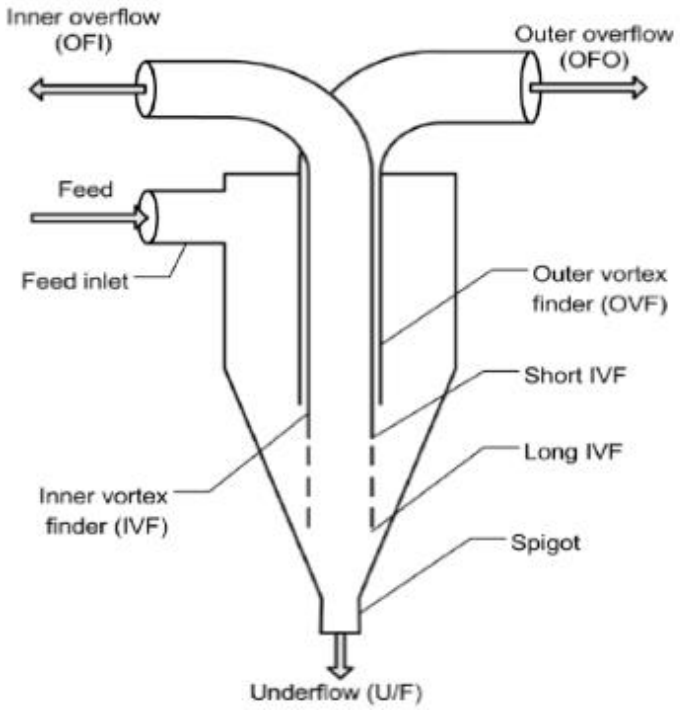

Figure 2-14: A schematic illustrating the main components of a three product hydrocyclone (Mainza, et al., 2005)

The conventional vortex finder is termed the outer vortex finder (OVF) and the additional vortex finder is termed the inner vortex finder (IVF) (Mainza, et al., 2005). The three product cyclone makes use of particle crowding and a decrease in the vertical path travelled by particles in the upward central current to concentrate the fine and/or coarse dense minerals selectively in a second overflow (Obeng & Morrell, 2003). Mainza et al., (2004) observed that the utilization of the three product cyclone resulted in mid-sized silica and fine chromite reporting to separate vortex finders at a selected vortex finder arrangement.

2.9. Cyclone Models

Most of the hydrocyclone models that are used describe the hydrocyclone performance assume a single average mineral density. However, this is not true, as the density differences in some industrial comminution circuits may have distinct density differences, as shown in Table 2-5. The most commonly used models are Lynch and Rao (1975), Plitt (1997) and Nageswararao (1978). The short coming of these empirical models is that they cannot be used outside the range of conditions under which they were developed (Narasimha, et al., 2014).

2.9.1. Rao and Lynch model

The Lynch and Rao (1975) model was the first widely used empirical model with its origins in the early 1960s. The model equations were structured to reflect the strong correlations observed between performance criteria such as cut size and the cyclone geometry. The hydrocyclone performance criteria were given by the following formula:

$$\mathbf{log_{10}d_{50c}} = K_1 D_o - K_2 D_u + K_3 D_i + K_4 C_w - K_5 Q_f + K_6 \quad \textbf{2-18}$$

$$\mathbf{Q_f} = K D_o^{0.73} D_i^{0.86} P^{0.42} \quad \textbf{2-19}$$

$$\mathbf{R_f} = K_1 \frac{D_u}{WF} - \frac{K_2}{WF} + K_3 \quad \textbf{2-20}$$

Where D_o is the cyclone vortex finder diameter (cm), D_u spigot diameter, D_i Inlet diameter, C_w solids weight % in feed, Q_f feed flow rat, K1-K6 are empirical constants, WF mass flow rate of water in feed (t/hr.)

2.9.2. Plitt model

The Plitt model is a semi-empirical model that is based on a large experimental database complied by Plitt, Lynch and Rao (Plitt, 1976).The equations for the performance criteria are given by Equations 2-21 to 2-24.

$$\mathbf{d_{50_c}} = \frac{F_1 39.7 D_c^{0.46} D_i^{0.6} D_o^{1.21} \eta^{0.5} \exp(0.063 C_v)}{D_u^{0.71} h^{0.38} Q_f^{0.45} \left(\frac{\rho_s - 1}{1.6}\right)^k} \quad \textbf{2-21}$$

$$\mathbf{m} = F_2 1.94 \left(-\left(\frac{1.58\,S}{1+S}\right)\left(\frac{D_c h}{Q_f}\right)^{0.15}\right) \quad \textbf{2-22}$$

$$\mathbf{P} = \frac{F_3 1.88 Q_f^{1.8} \exp(0.0055 C_v)}{D_c^{0.37} D_i^{0.94} h^{0.28} Q_f^{0.45} (D_u^2 + D_o^2)^{0.87}} \quad \textbf{2-23}$$

$$\mathbf{S} = \frac{F_4 \rho_p^{0.24} \left(\frac{D_u}{D_0}\right)^{3.31} h^{0.54} (D_u^2 + D_o^2)^{0.036} \exp(0.0054 C_v)}{D_c^{1.11} p^{0.24}} \quad \textbf{2-24}$$

Where D_c is the cyclone diameter (cm), η liquid viscosity (cP), C_v feed solids volume concentration (%), h distance between spigot and end of vortex finder (cm), k hydrodynamic exponent, which is estimated from data (default value for laminar flow 0.5), m efficiency exponent in efficiency curve, S is ratio of volumetric flow in the underflow to overflow, $Q_{u,o}$ flow rate in underflow and overflow respectively, ρ_p feed slurry density (g/cm^3) and F_1-F_4 are empirical constants to be estimated from data (default values =1).

2.9.3. Nageswararao model

The Nageswararao model was developed by Nageswararao under the supervision of A.J Lynch and L. Elber (Nageswararao, 1978). This model comprises empirical equations for the main cyclone performance criteria. It incorporates exponents derived from data sets obtained by Nageswararao (1978) and Rao (1975) from experimental tests which were carried out predominately using limestone on a Krebs hydrocyclone between 102-381mm. The equations for the performance criteria are given by Equations 2-25 to 2-29.

$$\frac{\mathbf{d_{50_c}}}{\mathbf{D_c}} = K_{D1} \left(\frac{D_o}{D_c}\right)^{0.52} \left(\frac{D_u}{D_c}\right)^{-0.47} \lambda^{0.93} \left(\frac{P}{\rho_p g D_c}\right)^{-0.22} \left(\frac{D_i}{D_c}\right)^{-0.5} \left(\frac{L_c}{D_c}\right)^{0.2} \theta^{0.15} \quad \textbf{2-25}$$

$$\mathbf{Q_f} = K_{D1} D_c^2 \left(\frac{P_1}{\rho_p}\right)^{0.5} \left(\frac{D_o}{D_c}\right)^{0.68} \left(\frac{D_i}{D_c}\right)^{0.45} \theta^{-0.1} \left(\frac{L_c}{D_c}\right)^{0.2} \quad \textbf{2-26}$$

$$\mathbf{R_f} = \mathrm{K_{W1}}\left(\frac{\mathrm{D_o}}{\mathrm{D_c}}\right)^{-1.19}\left(\frac{\mathrm{D_u}}{\mathrm{D_c}}\right)^{2.40}\left(\frac{\mathrm{D_i}}{\mathrm{D_c}}\right)^{0.45}\left(\frac{\mathrm{P}}{\rho_\mathrm{p}\mathrm{gD_c}}\right)^{-0.53}\lambda^{0.27}\left(\frac{\mathrm{D_i}}{\mathrm{D_c}}\right)^{-0.5}\theta^{-0.24}\left(\frac{\mathrm{L_c}}{\mathrm{D_c}}\right)^{0.22} \quad \textbf{2-27}$$

$$\mathbf{R_v} = \mathrm{K_{V1}}\left(\frac{\mathrm{D_o}}{\mathrm{D_c}}\right)^{-0.94}\left(\frac{\mathrm{D_u}}{\mathrm{D_c}}\right)^{1.83}\left(\frac{\mathrm{D_i}}{\mathrm{D_c}}\right)^{-0.25}\left(\frac{\mathrm{P}}{\rho_\mathrm{p}\mathrm{gD_c}}\right)^{-0.31}\theta^{-0.24}\left(\frac{\mathrm{L_c}}{\mathrm{D_c}}\right)^{0.22} \quad \textbf{2-28}$$

Where D_i is the inlet diameter (m) D_o vortex finder diameter (m), D_u underflow diameter (m), D_c cyclone cylinder diameter (m) Lc length of cylindrical section (m), θ cone angle (degrees), P feed pressure at inlet (kPa), ρ_p feed slurry density (t/m^3), g acceleration due to gravity (m/s^2), Q_f flow rate (m^3/h), R_f recovery of water to the underflow(%), R_v volumetric recovery of feed slurry to underflow(%), K constant to be estimated from data, λ hindered settling correction term, C_v volumetric fraction of solids in feed slurry.

2.9.4. Narasimha et al., Model

A semi-mechanistic model for hydrocyclones performance was developed by Narasimha et al., (2014). The model was developed using a dimensionless approach based on both fluid mechanics concepts from Computational Fluid Dynamics (CFD) and a wide range of industrial cyclone performance data. This model is advantageous because it can be used outside the range of conditions that it was developed. The model consists of equations for the water recovery (R_f), reduced cut size (d_{50c}), throughput (Q) and sharpness of separation (α).

$$\frac{\mathbf{d_{50_c}}}{\mathbf{D_c}} = \mathrm{K_D}\left(\frac{\mathrm{D_o}}{\mathrm{D_c}}\right)^{1.093}\left(\frac{\mathrm{D_u}}{\mathrm{D_c}}\right)^{-1.00}\left(\frac{(1-\mathrm{fv})^2}{10^{1.82*fv}}\right)^{-0.703}(Re)^{-0.436}\left(\frac{\mathrm{D_i}}{\mathrm{D_c}}\right)^{-0.936}\left(\frac{\mathrm{L_c}}{\mathrm{D_c}}\right)^{0.187} \quad \textbf{2-29}$$

$$\left(\frac{1}{Tan\,(\theta)}\right)^{-0.1988}\left(cos\left(\frac{i}{2}\right)\right)^{-1.034}\left(\frac{\rho_\mathrm{s}-\rho_\mathrm{f}}{\rho_\mathrm{f}}\right)^{-0.217}$$

$$\mathbf{Q_f} = \mathrm{K_{QO}}\left(\frac{\mathrm{D_i}}{\mathrm{D_c}}\right)^{0.45} D_c^2\sqrt{\frac{P}{\rho_\mathrm{p}}}\left(\frac{\mathrm{D_o}}{\mathrm{D_c}}\right)^{1.099}\left(\frac{\mathrm{D_u}}{\mathrm{D_c}}\right)^{0.037}\left(\frac{1}{Tan\left(\frac{\theta}{2}\right)}\right)^{0.405}\left(\frac{\mathrm{L_c}}{\mathrm{D_c}}\right)^{0.3} \quad \textbf{2-30}$$

$$\left(\frac{V_h}{V_t}\right)^{-0.048}\left(cos\left(\frac{i}{2}\right)\right)^{-0.092}$$

$$\mathbf{R_f} = K_W\left(\frac{D_o}{D_c}\right)^{-1.06787}\left(\frac{D_u}{D_c}\right)^{2.2062}\left(\frac{v_i^2}{R_{gmax}}\right)^{-0.20472}\left(\frac{1}{Tan\left(\frac{\theta}{2}\right)}\right)^{0.829}\left(\frac{\mu_m}{\mu_w}\right)^{-0.7118} \quad \textbf{2-31}$$

$$\left(\frac{L_c}{D_c}\right)^{2.424}\left(\frac{V_h}{V_t}\right)^{-0.8843}\left(\frac{\rho_s-\rho_f}{\rho_f}\right)^{0.523}\left(cos\left(\frac{i}{2}\right)\right)^{1.793\cdot}$$

$$\boldsymbol{\alpha} = K_\alpha\frac{\left(\frac{D_o}{D_c}\right)^{-1.06787}\left(\frac{v_i^2}{R_{gmax}}\right)^{-0.20472}\left(cos\left(\frac{i}{2}\right)\right)^{0.868}\left(\frac{(1-fv)^2}{10^{1.82*fv}}\right)^{0.72}}{\left(\frac{D_u}{D_c}\right)^{0.567}\left(\frac{\rho_s-\rho_p}{\rho_s}\right)^{1.837}\left(\frac{\mu_m}{\mu_w}\right)^{0.127}\left(\frac{1}{Tan\left(\frac{\theta}{2}\right)}\right)^{0.182}\left(\frac{L_c}{D_c}\right)^{0.2}} \quad \textbf{2-32}$$

CHAPTER 3: EXPERIMENTAL METHODOLOGY

3.1. Introduction

This chapter describes the experimental setups and procedures used to conduct both hydrocyclone and rheology test work. The cyclone tests were carried out at the University of Cape Town Centre for Minerals Research (CMR) laboratory and Anglo American Conceição de Mato Dentro (CMD) pilot plant, Brazil. The ores tested in the hydrocyclone work in this thesis are iron and Upper Group 2 (UG2) ore. These ores were chosen because of their dual density nature. UG2 obtained from a Lonmin concentrator in South Africa consists dominantly of silicates with a specific gravity of 2.8 which are rich in platinum group metal (PGM) and chromite, barren of the PGM with a specific gravity of 4.79 (Mainza et al., 2005). Iron ore consists of mainly silica of specific gravity 2.8 and iron of specific gravity 5.1. The Iron ore was sourced from an Anglo American CMD mine.

The chapter begins with a test rig description of the Anglo American CMD and UCT test rigs. Following an explanation of the feed preparation of both ores and the experimental matrix used. The experimental procedure including measurements taken is then described. This is then followed by the section which describes the rheology experiments on the iron and UG2 ore. These experiments were carried out at the University of Cape Town analytical laboratory using a AR1500EX TA vane rheometer manufactured by Thermal Analysis Germany. The description of the apparatus used for rheology measurements is given. This is followed by the feed preparation procedure to ensure homogeneous mixture for all samples. The methodology applied is then presented. Finally, a summary of the chapter is given.

3.2. Experimental apparatus

3.2.1. Anglo American experimental test rig setup

The Anglo-American CMD pilot plant facility is located at Minas Rio. It had a cyclone test rig comprising a 100 litre sump equipped with a 5.5 kW weir rubber lined centrifugal pump and variable distributor. The slurry from the sump was either pumped to the 4 inch hydrocyclone or recycled to the sump through a by-pass line. A schematic and picture of the test rig is shown in Figures 3-1and 3-2 respectively.

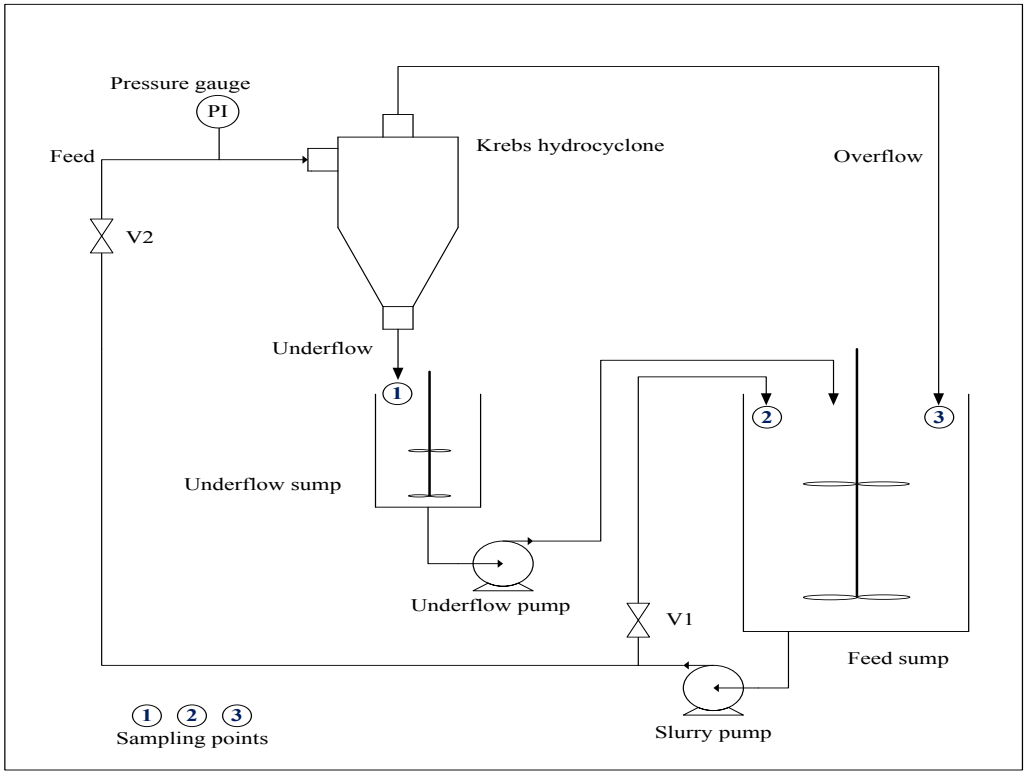

Figure 3-1: Schematic of the Anglo American hydrocyclone test rig

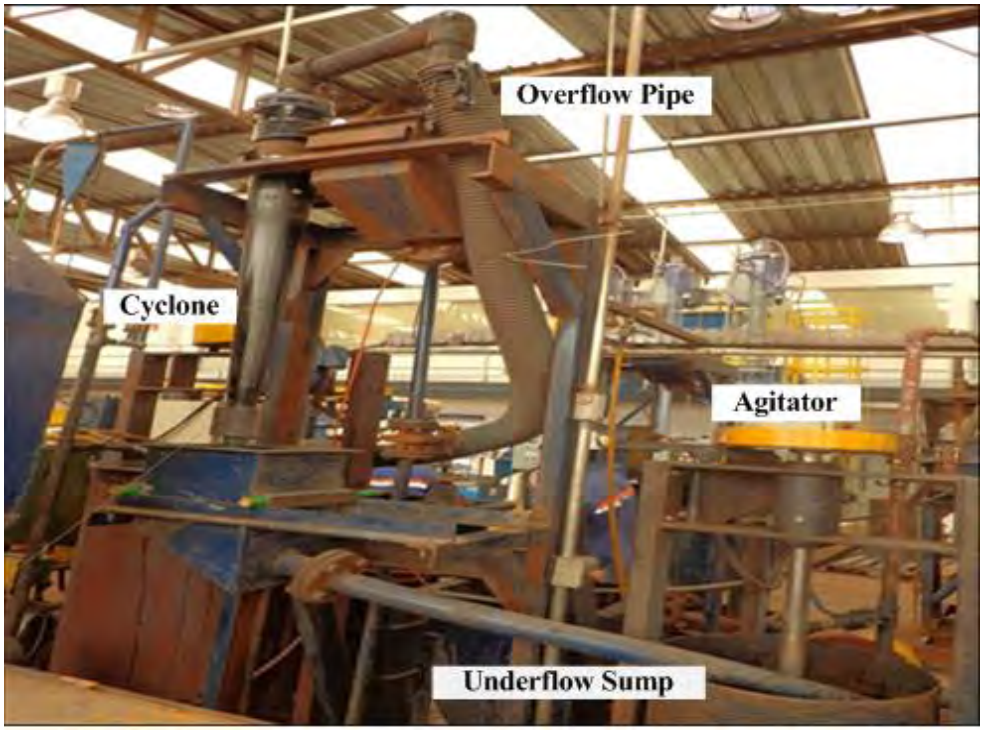

Figure 3-2: Picture showing the Anglo American hydrocyclone rig

The bypass line was used when taking the cyclone feed sample or to bypass the cyclone by directing the flow to the sump while changing the spigot or vortex finder. This was important because it allowed tests with different spigots and vortex finders to be carried out without encountering problems of slurry settling, which is usually the case if the system is shut down to facilitate these changes. If slurry is allowed to settle in the tanks and pipes it takes a long time to start up the rig after un-choking operations. In this experimental setup the hydrocyclone underflow stream feeds into a separate sump located underneath the hydrocyclone prior to being pumped to the feed sump, while the overflow is discharged directly in the feed sump. The specifications for the 4 inch Krebs cyclone used in the test work are given in Table 3-1.

Table 3-1: Dimensions of the Anglo American hydrocyclone test rig

Cyclone diameter, D_c (m)	0.1
Inlet diameter, D_i (m)	0.012
Vortex finder diameter , D_o (m)	0.025,0.032 and 0.040
Spigot diameter, D_u (m)	0.016 and 0.022
Cylindrical length, L (m)	0.34
Cone angle, θ (degrees)	15

3.2.2. UCT experimental test rig setup

A schematic and photograph of the hydrocyclone test rig at UCT is shown in Figures 3-3 and 3-4 respectively. The cyclone test rig is comprised of a 100 litre sump equipped with a 5.5 kW Weir Envirotech rubber lined centrifugal pump and Powerflex70 variable distributor. The pressure drop across the cyclone was measured for each test with a standard pressure gauge (maximum pressure 900 kPa) which was mounted on the cyclone feed inlet. The material from the sump was either pumped to a 4 inch Multotec cyclone or recycled to the sump through a by-pass line as shown in Figures 3-5 and 3-6. The function of the bypass line is exactly the same as for the cyclone test rig at CMD; namely to collect the feed sample or to allow easy change of the vortex finder and spigot components. An agitator was used to ensure complete suspension of solids in the sump. The hydrocyclone dimensions for the test work performed at UCT are given in Table 3-2.

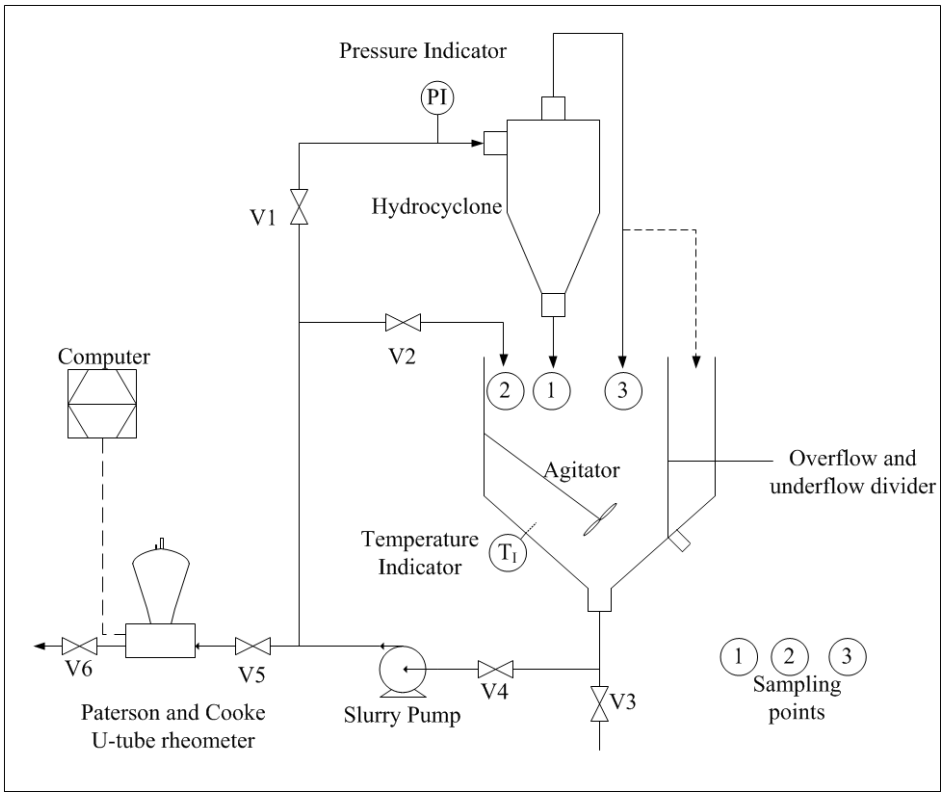

Figure 3-3: Schematic of the UCT hydrocyclone test rig

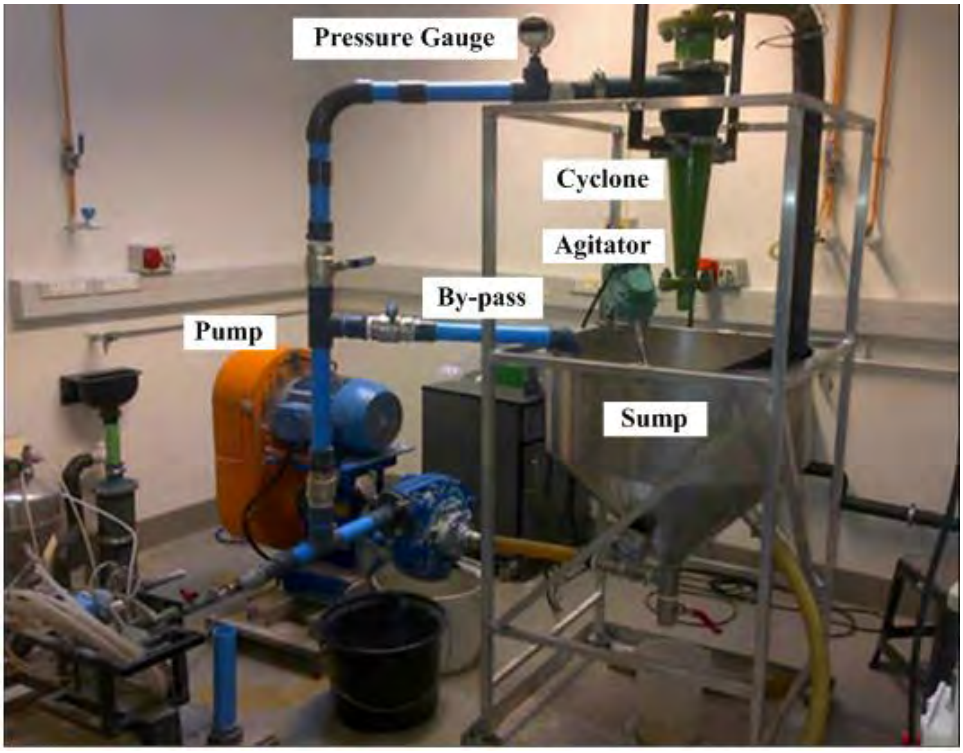

Figure 3-4: Picture showing UCT hydrocyclone test rig

Table 3-2: Dimensions of the Multotec hydrocyclone for the test work performed at UCT

Cyclone diameter, D_c (m)	0.1
Inlet diameter, D_i (m)	0.030
Vortex finder diameter , D_o (m)	0.041, 0.0340 and 0.026
Spigot diameter, D_u (m)	0.018, 0.023 and 0.030
Cylindrical length, L (m)	0.28
Cone angle θ, (degrees)	15

3.3. Feed preparation

3.3.1. Cyclone feed preparation for iron ore

The iron ore feed was obtained from the cyclone overflow of the ball mill discharge. The ore was stored in 50 litre agitated tanks to maintain homogeneity. The iron ore specific gravity was measured using a lab pycnometer and was found to be 3.67. During test work the agitated feed was pumped to the feed tank and the solids concentration was varied by either adding water or a thicker feed paste.

3.3.2. Cyclone feed preparation UG2 ore

The primary ball mill discharge (95 % wt. solids) from a Lonmin concentrator was used for the hydrocyclone tests. The UG2 ore was dried and thoroughly mixed and then split into 70 kg lots using a rotary splitter. The UG2 ore had a solids specific gravity of 3.60, which was determined using a UCT lab pycnometer.

The feed particle size distribution of both the UG2 and iron ore was measured using a Laser Mastersizer 2000 manufactured by Micromeritics. All the samples which were measured on the Laser Mastersizer where split (dry) into 1 gram samples using a rotary splitter. This was done to achieve a homogenous size distribution. The particle size distributions of these two ores are given in Figure 3-5. It is observed from Figure 3-5 that the iron ore has a finer size distribution in comparison to the UG2 ore. The iron ore has a d_{50} of 65 μm and a top size of 360 μm while the UG2 ore has a d_{50} of 140 μm and a top size of 1200 μm

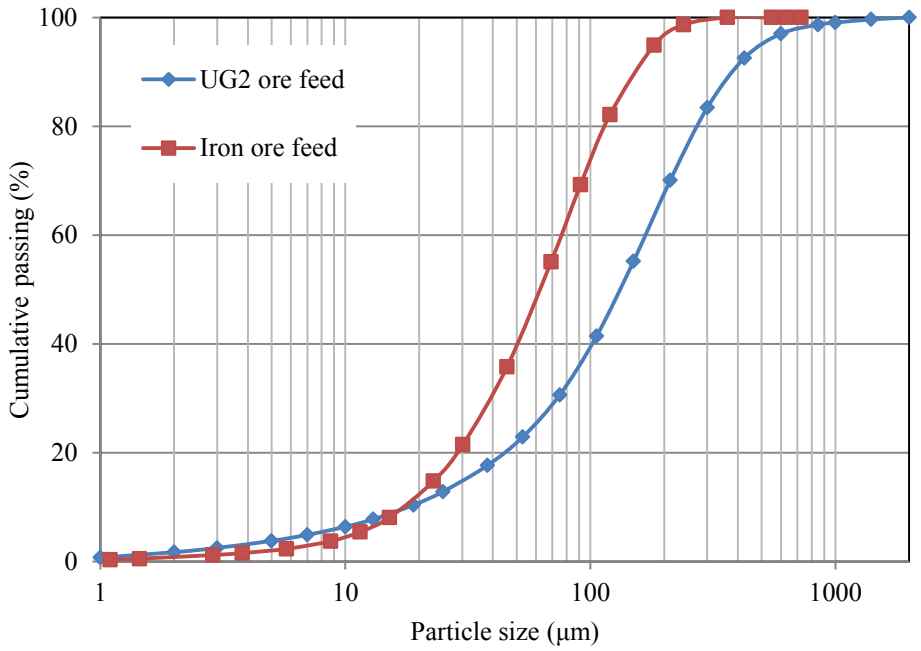

Figure 3-5: Particle size distribution for UG2 and iron ore feed

3.4. Experimental procedure

3.4.1. Experimental matrix and procedure for iron ore tests

The test matrix shown in Table 3-3 was designed for the experimental procedure. General factorial design was used in Design-Expert® software. This design was setup to analyze the influence of the test variables namely: cut-size (d_{50}), water recovery (R_f) and separation efficiency (α).

Table 3-3: Experimental matrix for tests performed with iron ore

Vortex finder diameter (m)	Spigot diameter (m)	Cone ratio (-)	Feed solids concentration (wt. %)				
			10%	13%	20%	40%	50%
0.040	0.016	0.4	√√√	√√	√√	√√	√√√
0.040	0.022	0.55	√	√√	√√	√√	√√
0.025	0.016	0.64	√	√√	√	√√	√√
0.032	0.022	0.69	√	√	√	√√	√√

Some tests were carried out in duplicate or triplicate in order to assess the repeatability of the data obtained. The operating conditions for each test performed are given in Appendix A. The

tests were done for a range of solid concentrations from 10-50 wt. % and pressures between 27 kPa and 103 kPa. These solid concentrations where chosen as they are within the range of concentrations for a typical iron ore concentrator. Furthermore, higher concentrations above 50wt. % would lead to roping.. The pressure conditions were subject to the operating pressure just before the onset of roping.

Test Procedure

At the beginning of each experiment, the slurry was placed in an agitated feed sump and water was added until the target solids concentration was reached. During this preparatory stage a Marcy scale was used to monitor the solids concentration. When the required solids concentration was attained, the feed by-pass line indicated by 2 in Figure 3-1 was opened and the feed sample was taken. The by-pass valve was then closed and slurry pumped through the hydrocyclone. During this period the cyclone pressure was adjusted until the cyclone was adjudged to be operating optimally from visual inspection of the cyclone underflow. The criterion was to operate the cyclone just before the onset of roping. Figure 3-6 shows photographs of the cyclone operating under roping condition and what was considered to be the near-rope condition. No sampling was performed under roping conditions. The feed pressure was adjusted using the variable speed drive at the feed pump .The test rig was allowed to run for 15 minutes to stabilize before taking samples of the overflow and underflow stream.

Figure 3-6: Left, roping phenomena. Right, desired spray for hydrocyclone condition

Flow rate measurements of the underflow and overflow streams were taken from the position indicated by 1 and 3 in Figure 3-1 respectively. This was done by discharging slurry into a 20 litre bucket and recording the time taken to fill the bucket to the 20 litre mark for each stream. The feed flow rate was then determined as the sum of underflow and overflow stream flow rates. Marcy scale readings of both the overflow and underflow were recorded during the test and these were compared with the values from the wet and dry masses. The underflow and overflow samples for analysis were taken by pulling the flexible rubber pipes and directing the stream into two separate buckets. Each stream was cut 5 times in 5 minute intervals. For each sample an 'A' sample for processing and a 'B 'sample for backup was collected. For each sample the wet mass was measured and recorded.

After recording the mass, the sample was filtered and the resulting solid wet cake was placed in an 80°C oven to dry. The mass of the dry sample was then recorded. This was done to enable the calculation of the solid content of each of the samples which were compared to the results obtained from Marcy scale measurements. The backup sample was stored to be processed only when problems were encountered with the A sample during analysis of results. Finally, the dried samples were packaged and sent to the Federal University of Rio de Janeiro (UFRJ) LTM laboratory for laser sizing using a Malvern Mastersizer 2000 to obtain the particle size distributions. An example of the data recorded for each test is shown in Table 3-4, only summarized data is appended. During shut down, the frequency on the variable distributor was decreased gradually. The pump was then switched off while simultaneously closing valve V2 shown in Figure 3-1, this was done to avoid slurry clogging up and drying in the pump internals. The feed sump agitators were kept running until the slurry was completely drained out of the sump.

Table 3-4: Example of raw data recorded for experimental programme

Test No.	Test 10wt % Run 1		
Spigot/Vortex	22/40		
Pressure (kPa)	15		
	Feed	**Underflow**	**Overflow**
Solids, TPH	0.59	0.4	0.19
Solids conc (wt. %)	10.5	14.6	2.05
Marcy scale (wt. %)	13	15	3
Size (µm)	**Feed**	**Underflow**	**Overflow**
240	100	100	100
182	98.4	98.5	100
120	94	93.7	100
90	79.6	77.9	99.1
70	65.5	62.7	96.9
45	50.4	46.7	92.7
30	30.6	26.3	82
23	16.8	13	66.1
15	10.8	7.6	54
11.5	5.4	3.2	36.4
8.7	3.6	1.9	26.5
5.7	2.5	1.3	18.8
3.8	1.6	1	11
1.5	0.9	0.7	4.5
1	0.4	0.3	1.7

3.4.2. Experimental matrix and procedure for UG2 ore tests

The test matrix shown in Table 3-5 was designed for the test work. General factorial design using Design-Expert® was implemented. This design was used to analyze the cut-size (d_{50}), water recovery (R_f) and separation efficiency (α). Tests were carried out in duplicate and triplicate in order to assess reproducibility. The operating conditions for each test performed are given in Appendix A. Like the tests performed at the CMD on iron ore, the work on the UG2 ore involved varying the solids concentration and cone ratio.

Table 3-5: Experimental matrix for UG2 ore test work

Vortex Finder (m)	Spigot Diameter (m)	Cone ratio (-)	Feed solids concentration (wt. %)			
			50	40	30	20
0.041	0.018	0.439	√√√	√√√	√√	√√√
0.034	0.018	0.529	√√√	√√	√√√	√√√
0.026	0.018	0.692	√√√	√√√	√√	√√
0.041	0.023	0.561	√√	√√√	√√√	√√√
0.034	0.023	0.676	√√√	√√√	√√√	√√√
0.026	0.023	0.885	√√√	√√	√√	√√
0.041	0.030	0.732	√√	√√√	√√√	√√√
0.034	0.030	0.882	√√√	√√	√√	√√√
0.026	0.030	1.154	√√√	√√√	√√√	√√√

Test procedure

The slurry for the tests was made up in the sump, and a Marcy specific gravity balance was used to calibrate the percentage of solids by weight in the slurry. Upon attaining the desired feed concentration, valve V4 and V2 in Figure 3-5 where opened. The 5.5 kW Weir rubber lined centrifugal pump drew suction from the bottom of the tank and the slurry exited from the by-pass stream. The by-pass stream labelled sample point 2 was used to take the feed sample. After taking the feed the valve labelled V1 in Figure 3-5 was opened and V2 closed to allow slurry to flow to the hydrocyclone. The Powerflex70 variable distributor was then adjusted to attain the desired conditions. The desired pressure was attained just before the onset of roping.

After the desired conditions where attained, the test rig was allowed to run for 15 minutes to reach steady state. During the test, flow rate measurements of the underflow and overflow were taken by directing the whole stream into a 20 litre bucket and measuring the time taken to fill the bucket. The feed flow rate was then calculated by adding the underflow and overflow stream flow rates. The underflow and overflow samples were taken using a custom made pelican cutter illustrated in Figure 3-7.

Each stream was cut 5 times in 4 minute intervals. For each sample the A sample for processing and the B sample for backup were obtained. The mass of the wet samples and dry samples was then measured and recorded. This was done to enable the calculation of the solid content of each

of the samples. The dried samples were then packaged and sent for laser sizing using a Malvern Mastersizer 2000 to obtain the particle size distributions.

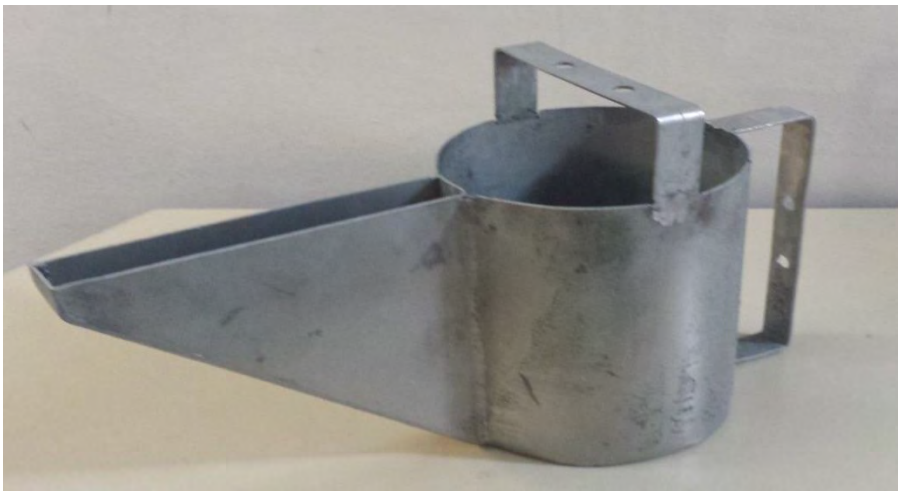

Figure 3-7: Custom made pelican cutter used for sampling

During shut down, the frequency on the variable distributor was decreased. The pump was switched off while simultaneously closing the valve labelled V4 in Figure 3-5, this was done to avoid slurry clogging up and drying in the pump internals. The feed tank was then drained through the valve labelled V3. Water was added to the feed tank again for cleanup. This was done to avoid blockages and scaling in the pipes and equipment when the rig was started up again.

3.4.3. Flat bottom cyclone test

In order to compare the performance between the flat bottom and conventional hydrocyclone, tests at similar operating conditions were carried out on a 4 inch flat bottom cyclone. The cyclone used was designed by Multotec. A similar procedure used for the UG2 test work with the conventional cyclone was followed for the flat bottom hydrocyclone.

Table 3-6: Operating condition for flat bottom and conventional cyclone

Feed Solids wt. %	Operating Pressure (Bar)	Cone Ratio (-)
20	0.75	0.732
30	0.75	0.732
40	0.75	0.732
50	0.56	0.732

3.5. Rheology experiments

The particle size distributions of the samples were measured using a Malvern Mastersizer and the distributions are illustrated in Figure 3-8 and 3-9 for the UG2 ore and iron ore respectively. This section of the chapter begins with the description of the feed rheology measurement setup. This is followed by the experimental procedure and sampling method. The second section of this chapter is the description of the apparatus used for the overflow and different size class samples. This is accompanied by the experimental procedure followed to obtain the rheograms.

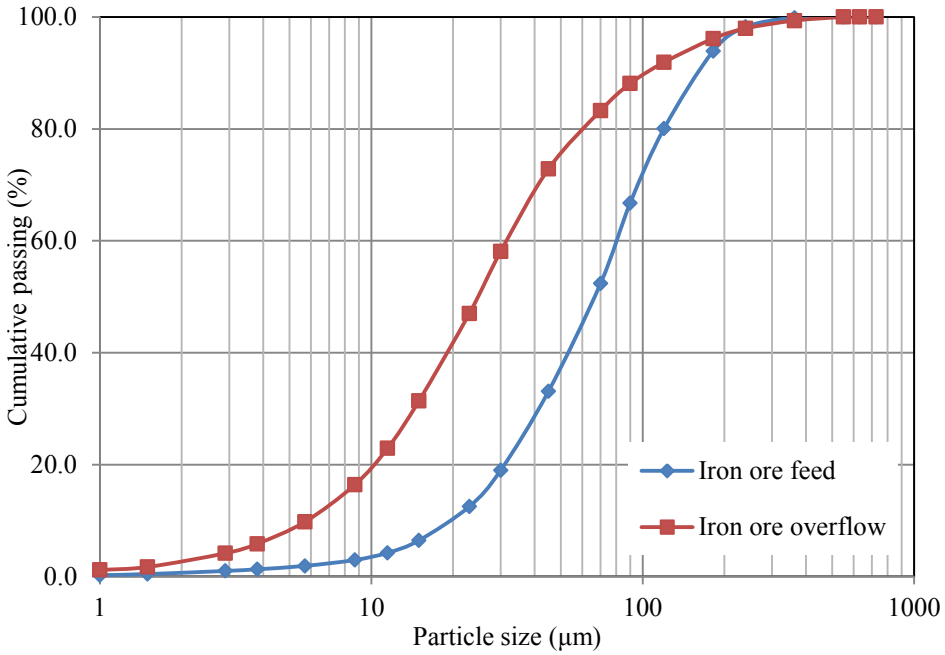

Figure 3-8: Particle size distributions for the feed and overflow for iron ore rheology analysis

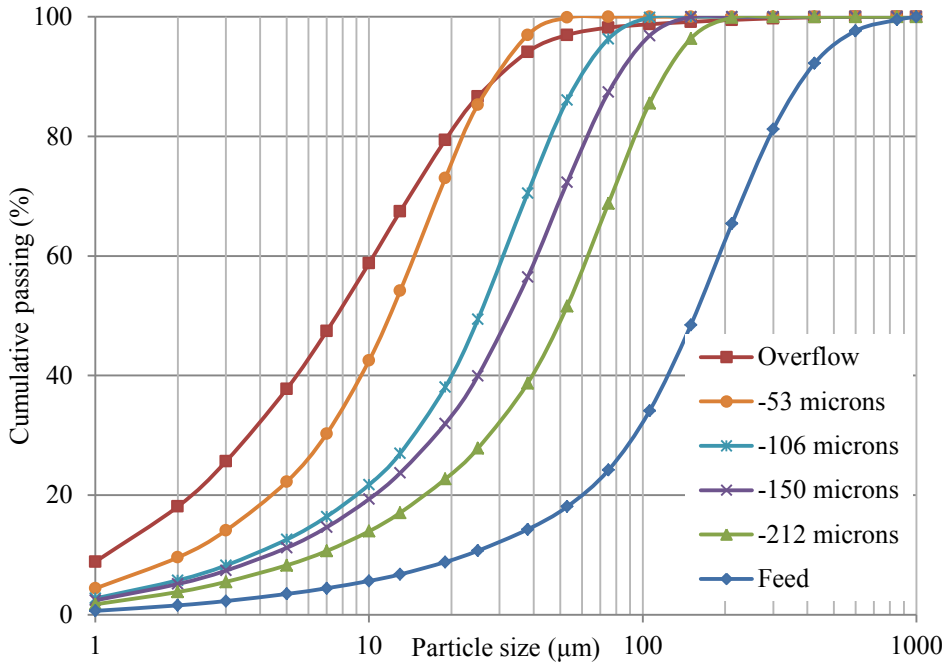

Figure 3-9: Particle size distributions for the feed, overflow and the different size classes investigated for UG2 ore rheology analysis

3.5.1. Apparatus description for feed rheology measurements

The setup of the AR1500EX vane rheometer which was used to characterize the UG2 and iron ore samples is illustrated in Figure 3-10.

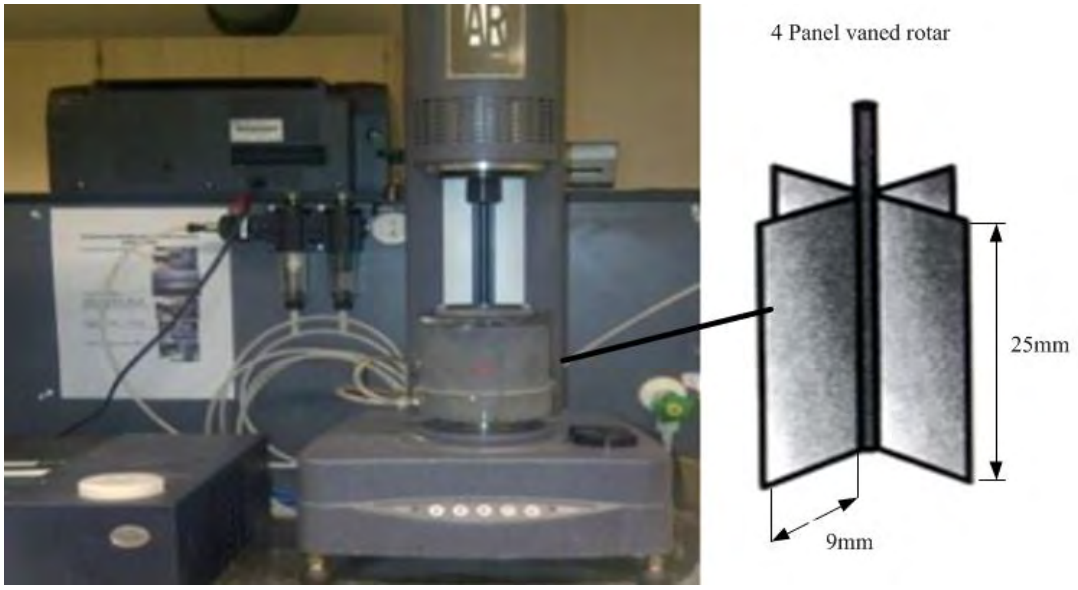

Figure 3-10: Rheometer setup to characterize UG2 and iron ore samples

The rheometer has standard 4 panel vaned rotor geometry which is more suitable for the analysis of suspensions within the minerals processing industry as it is less susceptible to artefacts arising from large particle sizes (Ndlovu, 2013). The rheometer was connected to the AR1500EX software on a computer desktop which served as the interface to view the results.

3.5.2. Experimental programme

The concentrations investigated for both the UG2 and iron ore rheology tests are given in Table 3-7. The solid concentration ranged from 10 wt. % to 70 wt. % for the feed samples and 10 wt. % to 60 wt. % for the overflow samples. The overflow samples could not be prepared beyond this concentration as they became too thick (viscous) and as a result, they could not be placed in the rheometer for processing. Temperature and particle size distributions were kept constant throughout all the runs to minimize their effect as they affect slurry rheology (Shi, et al., 2010). The temperature was monitored using the industrial thermometer attached to the sump while the size distribution was kept constant by assuring that the sample used was split using a rotary splitter to attain a homogenous distribution.

Table 3-7: Solid concentrations (wt. %) for UG2 and iron ore rheology assessment

	Concentration (wt. %)						
Cyclone O/F UG2 and iron ore	10	20	30	40	50	60	-
Cyclone Feed UG2 and iron ore	10	20	30	40	50	60	70
Feed at different size classes	10	30	50	60	70	-	-

3.5.3. Sampling procedure for cyclone overflow and feed at different size classes

The slurry for rheology tests at different solids concentrations were made up and placed in 50 ml sub samples which is the required quantity for measurement in the AR1500EX rheometer. Homogeneity of the particle size distribution was attained by using a rotary splitter on the dry sample when each sample was prepared. The AR1500EX sample collector was cleaned thoroughly and dried before introducing the sample. Upon introduction of the sample to the rheometer, the agitator was inserted and lowered to the designated height.

The sample temperature on the rheometer was then set to 23˚C before preconditioning for 10 seconds at a shear rate of $400s^{-1}$. The measurements were then taken and recorded by the software. The rate of shear stress and shear rate obtained for same was plotted to see the type of

rheogram obtained from the measurement. Temperature was kept constant at 23˚C throughout all the experiments using the built-in thermal regulator in the AR1500EX vane rheometer. Three measurements were taken for each sample to assess if the results were reproducible.

CHAPTER 4: HYDROCYCLONE TEST RESULTS AND DISCUSSION

4.1. Introduction

This chapter discusses the results of the various hydrocyclone tests carried out with regard to UG2 ore and iron ore. The separation performance of hydrocyclones was assessed and modelled using efficiency curves (partition curves). Such partition curves describe particle separation across the whole size distribution, while incorporating mass flow rates in the assessment (Mainza, 2006).

The experimental data obtained from the cyclone tests is always subject to error from sampling and uncertainties introduced by unavoidable variations in operating conditions (Mainza, 2006). To assess the consistency and integrity of the data, mass balancing was performed using Mbal, the mass balancing engine in JKSimet simulating software, as well as Microsoft Excel. After performing the mass balance, the data sets were found to be self-consistent; they were thus used to assess the performance of the cyclones for the various cone ratios at different feed solid concentration levels.

The chapter begins with a discussion of the results obtained from the water only tests, using a 4-inch cyclone manufactured by Multotec. Thereafter, the results obtained from using UG2 and iron ore are presented. All the results are presented with the 95% confidence limits indicated. However, in some cases, the confidence limit bars are of the same size or smaller than the data markers, so they are not very visible in the plots. The chapter concludes with a performance comparison of the flat bottom and conventional cyclone.

4.2. Water only tests

This section of the report focuses on the independent influence of the vortex and spigot diameters as well as the cone ratio on the water recovery to the underflow. The water only tests were performed at a pressure of 70 kPa on a 4-inch cyclone manufactured by Multotec. This was done to characterize cyclone operation without introducing the complexity of the ore, and to determine the fluid dynamics of the slurry (Tavares et al., 2002).

4.2.1. Independent effect of vortex and spigot diameter on R_f

The relationship between the water recovery to the underflow as a function of the spigot and vortex finder diameter is presented in Figure 4-1. It was observed that the water recovery decreases with an increase in the vortex finder diameter, but rises with an increase in the spigot diameter.

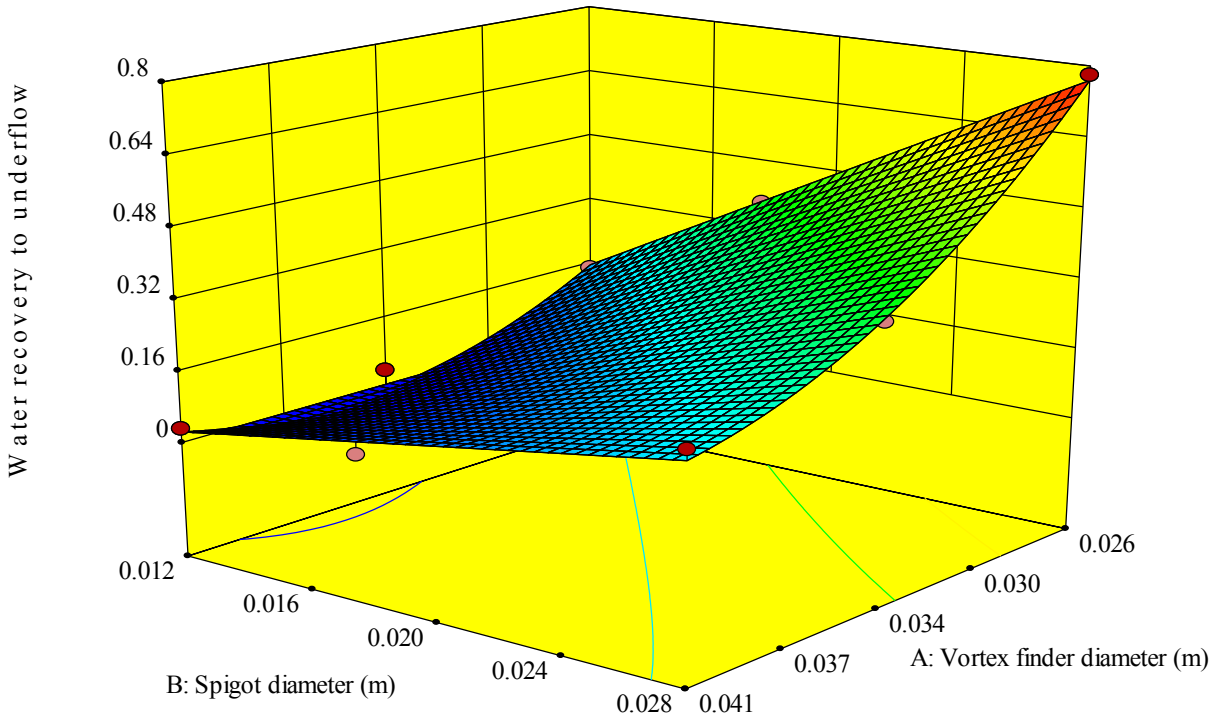

Figure 4-1:3D surface plot for water recovery as a function of vortex finder and spigot diameter

The decrease in water recovery with an increase in vortex finder diameter could be attributed to the decrease in resistance to flow in and around the vortex finder, hence allowing more water to pass through the cyclone overflow. An increase in the water recovery to the cyclone underflow, with an increase in the spigot diameter, could be attributed to the fact that, at larger spigot diameter openings, the air core generated within the cyclone is larger in diameter. This results in more fluid being pushed to the cyclone wall and, as a result, in more water reporting to the underflow. These results are in conformity the observations of Lusinga et al., (2009).

4.2.2. Effect of cone ratio on water recovery to underflow

The relationship obtained between the cone ratio, which was defined as the ratio of the spigot to the vortex finder diameter (Kilavuz & Gulsoy, 2011), and the water recovery to the underflow at 70 kPa for the water only tests, is shown in Figure 4-2. It can be seen that, irrespective of the diameter of the vortex finder and that of the spigot, the water recovery increases with the cone ratio. This phenomenon could be attributed to the fact that at smaller spigot diameters relative to the vortex finder diameters, the water is forced to the vortex opening due to the lower resistance to flow in that region. This is in accordance with the observations of Kilavuz et al., (2011), who carried out tests on 25.4 mm and 50.8 mm diameter cyclones.

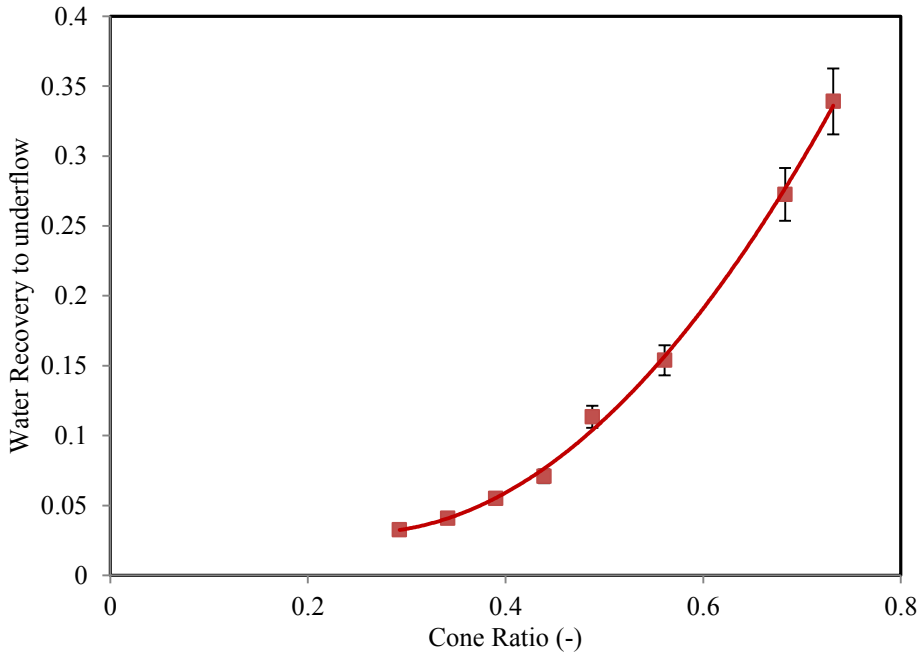

Figure 4-2: Effect of cone ratio on water recovery to underflow at 70 kPa

4.3. Interpretation of data

This section of the report analyses the particle size distribution data that was obtained from the Malvern Mastersizer for the different conditions investigated during the test work. The particle size distributions of the three hydrocyclone streams (feed, overflow and underflow), together with the respective flow rates and solids concentrations, were used to determine the partition curves and thus the cyclone performance.

4.3.1. Particle size distributions

The particle size distribution graphs for tests performed at different solids concentrations at the same cone ratio were plotted for both UG2 and iron ore. The results are presented in Figures 4-3 and 4-4 respectively, with the corresponding underflow and overflow mass splits presented in Tables 4-1 and 4-2 for the UG2 and iron ore respectively. It was observed that the mass split to the cyclone underflow decreases with an increase in the feed solids concentration for both ore types at the conditions investigated. The particle size distribution from tests performed at solids concentrations ranging from 20 to 50 wt. % for the UG2 ore at a cone ratio of 0.53 presents a similar graph as for iron ore at a cone ratio of 0.55. In the case of UG2 ore, it can be seen that, for the underflow streams, the 50 wt. % is coarser than the other streams, with the 20 wt. % having the finest distribution. The 30 wt. % and 40 wt. % are fairly similar. Analysis of the overflow streams shows that the 50 wt. % is the coarsest, with the weight percentages fairly closely to each other. In the case of the iron ore, it is observed that the underflow particle size distributions are fairly similar; however, the overflow particle size distribution becomes progressively coarser with an increase in feed solids concentration. The other particle size distributions are presented in Appendix A.

Table 4-1: Mass splits for tests performed at different feed solids concentration for the hydrocyclone operated with a cone ratio of 0.53 using UG2 ore

	Feed wt.%			
	20	**30**	**40**	**50**
Mass split to O/F %	4.8	12.8	11.7	12.8
Mass split to U/F %	95.2	87.2	88.3	87.2

Table 4-2: Mass splits for tests performed at different feed solids concentration for the hydrocyclone operated with a cone ratio of 0.55 using iron ore

	Feed wt.%			
	10	**20**	**40**	**55**
Mass split to O/F %	3.6	4.5	4.4	6.6
Mass split to U/F %	96.4	95.5	95.6	93.4

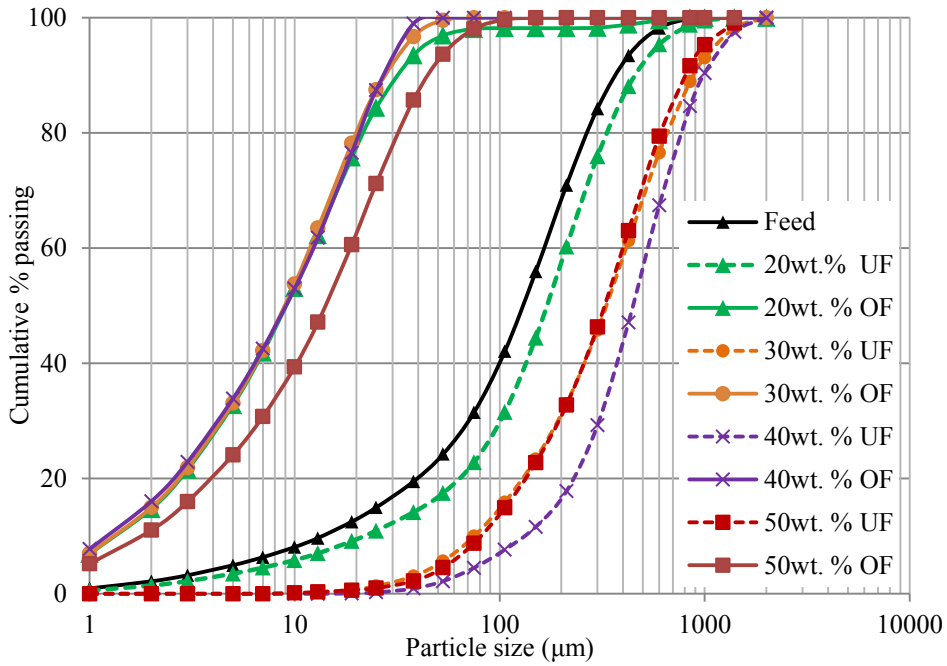

Figure 4-3: Comparison of UG2 overflow and underflow stream for tests performed at different feed solids concentration for the hydrocyclone operated with a cone ratio of 0.53

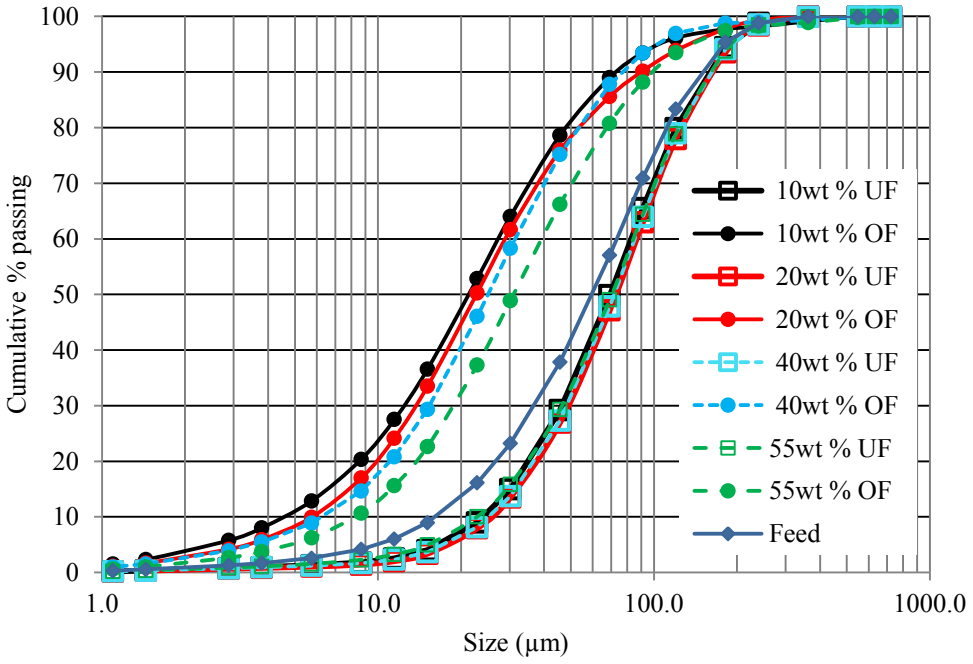

Figure 4-4: Comparison of iron ore overflow and underflow stream for tests performed at different feed solids concentration for the hydrocyclone operated with a cone ratio of 0.55

4.3.2. Efficiency curves

In order to assess the hydrocyclone performance, partition curves were modelled using the Whiten efficiency curve, and regression equations were obtained for the following curve parameters: corrected cut size (d_{50c}), sharpness of separation (α) and water recovery to underflow (R_f). These parameters, as well as the volumetric flow rate at the various cone ratios investigated, were used to assess the cyclone performance.

The partition curves were plotted for the UG2 and iron ore at different feed solids concentration for each cone ratio. Figures 4-5 and 4-6 illustrate the trends observed for UG2 and iron ore respectively.

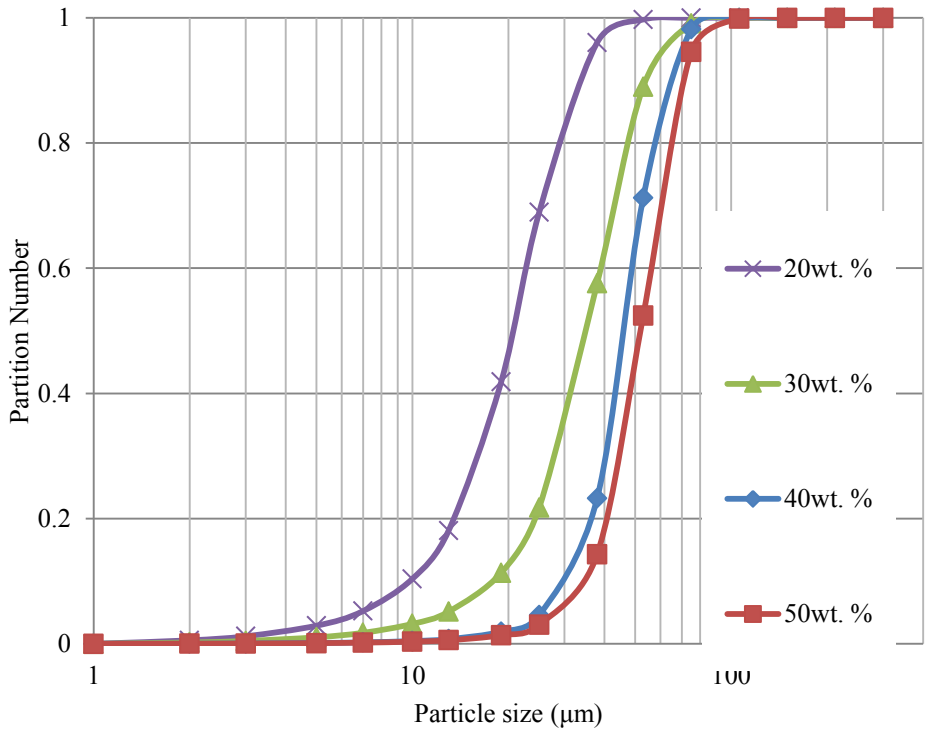

Figure 4-5: Efficiency curve for UG2 ore cone ratio of 0.55 at a range of feed solids concentration

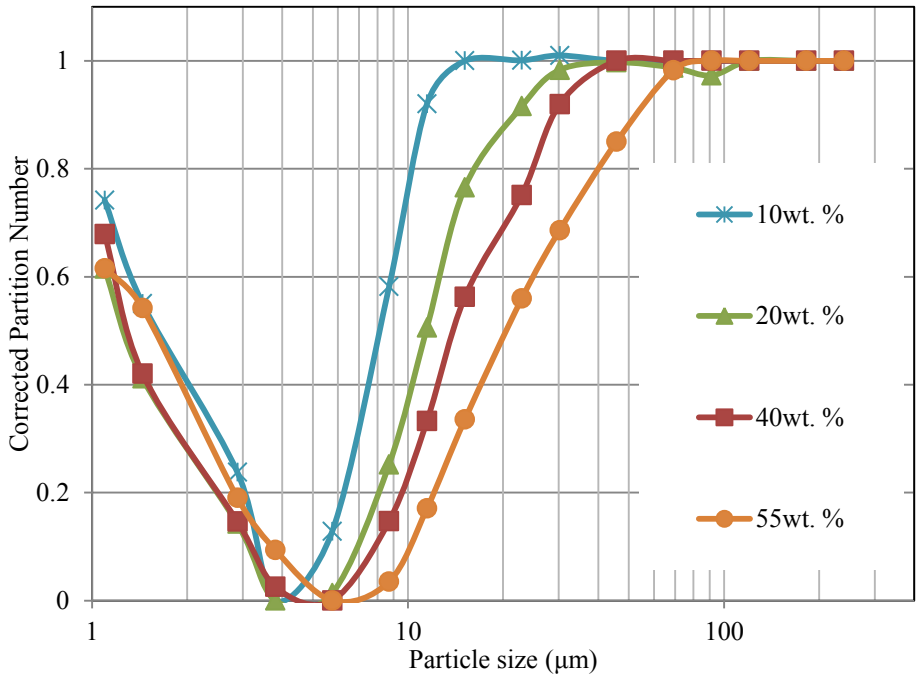

Figure 4-6: Efficiency curve for iron ore cone ratio of 0.55 at a range of feed solids concentration

It can be seen that, for both the UG2 and the iron ore, the partition curves shifted from lower to higher cut size with an increase in feed solids concentration for the same cone ratio. Similar trends are noted in the other efficiency curves, which are appended (see Appendix A). This indicates that the feed solids concentration has a significant influence on the cut size for both ore types. The UG2 ore gives a standard S partition curve, while the iron ore exhibits a highly exaggerated fishhook at particle sizes just below 10 microns for all tests. This phenomenon has been observed in cyclones operated in plants treating ores with density differences. However, this is not observed in the UG2 ore, which could be attributed to the fact that the UG2 ore feed was coarser and that it had a lower fraction of particles sub 10 microns.

4.4. Independent effect of vortex and spigot diameter

In order to assess the independent effect of the spigot and the vortex finder on the cyclone performance, tests were conducted at constant vortex finder diameter, while varying the spigot diameter and vice versa. This analysis was not conducted using iron, as there were limited spigot and vortex finder combinations on the site where the iron ore tests were conducted.

4.4.1. Effect of spigot and vortex diameter on corrected cut size

The effect of the vortex finder diameter on the corrected cut size for three different spigot diameters for tests performed using UG2 ore at feed solids concentration of 50 wt. % is summarised in Figure 4-7.

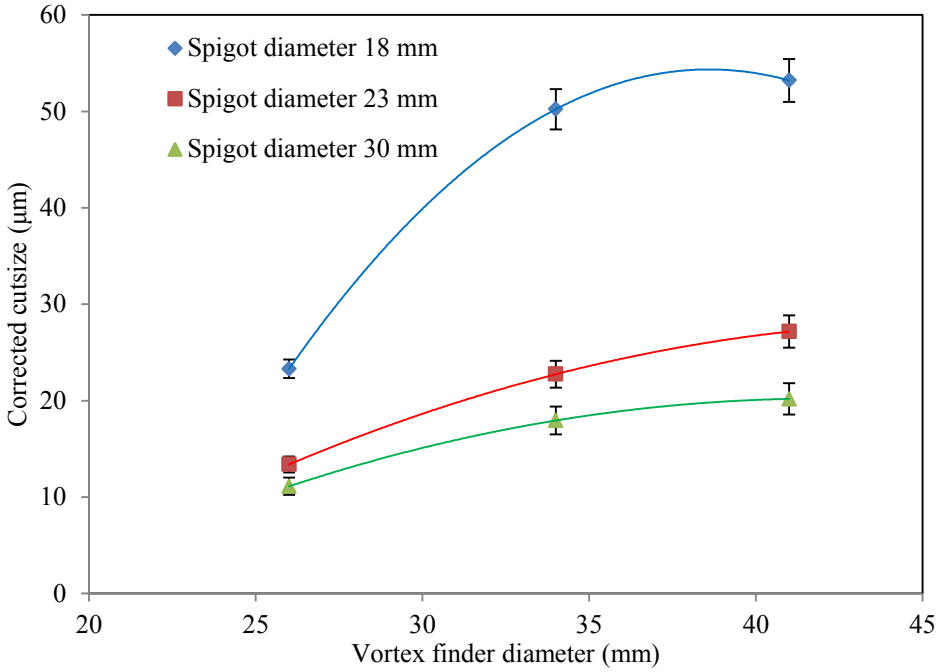

Figure 4-7: Effect of spigot and vortex finder diameter on corrected cut size for UG2 ore at 50 wt. % feed concentration

It was observed that increasing the vortex finder diameter leads to an increase in the corrected cut size for the spigot sizes tested. However, the increase in cut size was more pronounced for the spigot diameter of 18 mm than it was for 23 and 30 mm. This in agreement with the observations made by Mainza (2006) and Lusinga et al., (2009) with regard to the experiments performed using UG2 ore and silica, respectively. Plitt (1976) also postulated that the cut size was higher for cyclones with larger vortex finders for the same spigot diameter.

4.4.2. Effect of vortex and spigot diameter on water recovery

The effect of the vortex finder on water recovery to the hydrocyclone underflow using UG2 ore at 50 wt. % solids concentration is illustrated in Figure 4-8. It was observed that increasing the vortex finder led to a decrease in the water recovery for all spigot diameters investigated. Water recoveries above 40% are associated with poor operation of the hydrocyclone (Napier-Munn et

al., 1996) and thus tests with the smallest vortex finder at the two smallest spigot sizes would not be ideal. Conversely, a water recovery below 20% may introduce roping conditions (although this did not occur), as in the case of tests using the smallest spigot at the larger vortex finder sizes.

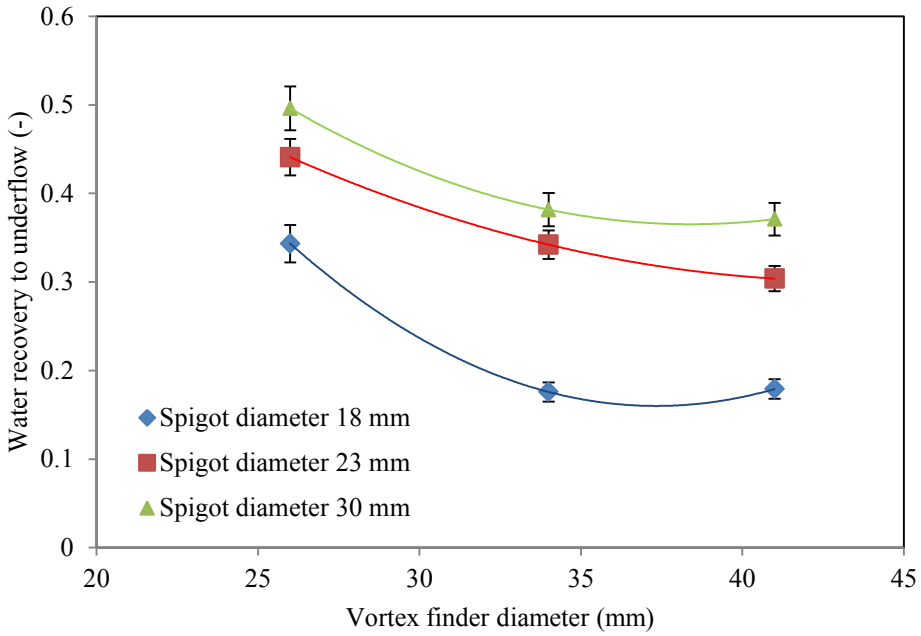

Figure 4-8: Effect of spigot and vortex finder diameter on water recovery to underflow for UG2 ore at 50 wt. % feed concentration

4.4.3. Effect of vortex and spigot diameter on sharpness of separation

Figure 4-9 shows the effect of the vortex finder diameter on the sharpness of separation at three different spigot diameters. In the range of vortex finder diameters investigated, it was observed that sharpness of separation decreased slightly with an increase in the vortex finder diameter for spigot diameters of 30 and 23 mm. However, at a spigot diameter of 18 mm, the sharpness of separation increases slightly, before declining. This phenomenon could be attributed to the fact that at a small spigot diameter and vortex finder diameter, there tend to be more restricted flow within the hydrocyclone (Kilavuz & Gulsoy, 2011). This results in the misplacement of coarser particles to the overflow resulting in a less sharp separation as indicated by a vortex finder of 26 mm and spigot of 18 mm.

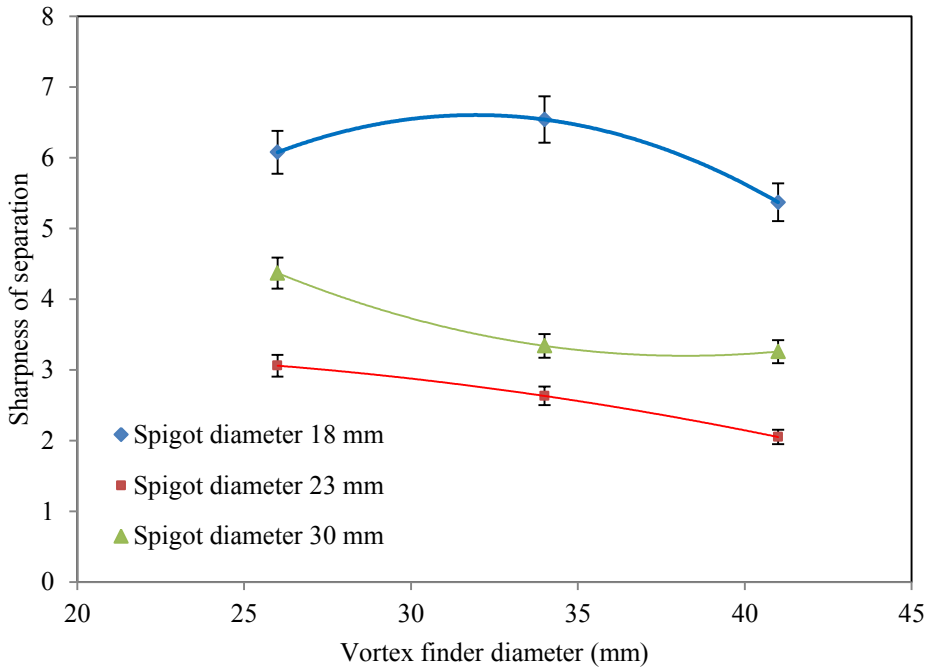

Figure 4-9: Effect of vortex on the sharpness of separation

4.4.4. Effect of vortex and spigot diameter on volumetric throughput

In order to assess the effect of the vortex finder diameter and the spigot diameter on the volumetric throughput of the cyclone, Figures 4-10 and 4-11 were plotted. Figure 4-10 shows that as the vortex finder diameter increases, the volumetric feed decreases for all spigot diameters investigated. This means that, for the conditions investigated, as the vortex finder diameter increased, there was more constriction within the cyclone, which led to a decrease in the throughput before the onset of roping. Even though it has been reported that the volumetric throughput is directly proportional to vortex finder diameter, this phenomenon was not observed. This behavior has been quantified by a number of authors, namely Plitt (1976), Lynch and Rao (1968) and Asomah (1997). Furthermore, Concha et al., (1996) reported that roping tends to occur more readily at larger vortex finder sizes.

From Figure 4-11, it can be observed that, as the spigot diameter increases, the feed throughput increases linearly for all the vortex finder diameters investigated. This means that, at the larger spigot diameters, there is less resistance to flow within the cyclone. These results are in conformity with the observations of Fahlstrom (1963), Mull and Jull (1978) and Tarr (1998).

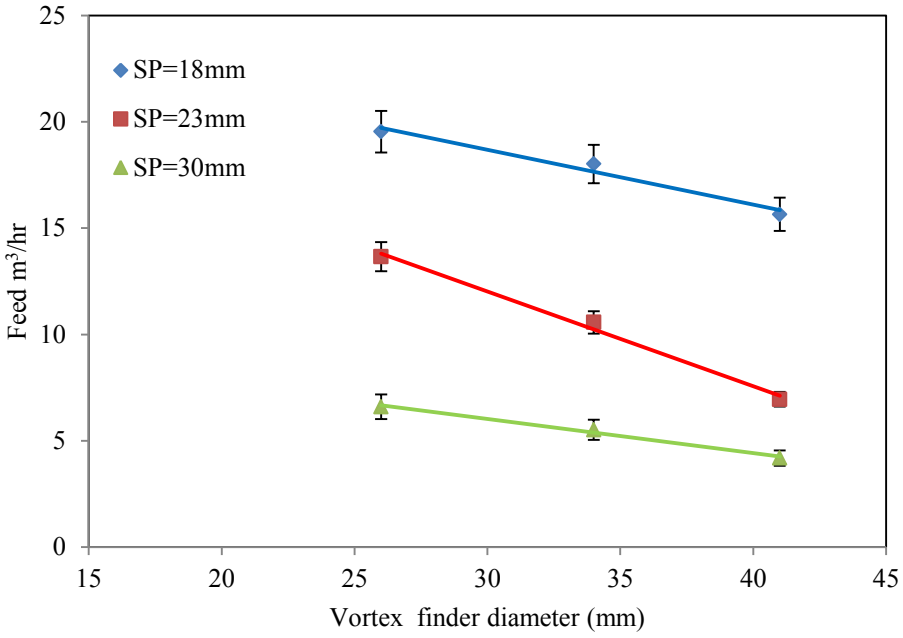

Figure 4-10: Effect of vortex on the volumetric throughput

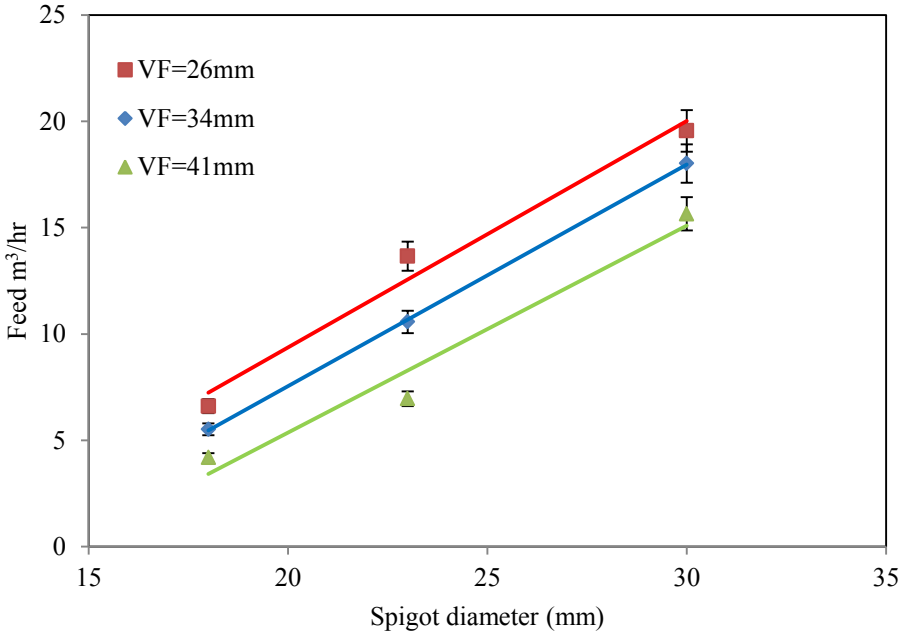

Figure 4-11: Effect of spigot diameter on volumetric throughput

4.5. Effect of cone ratio hydrocyclone performance

The hydrocyclone cone ratio, which is defined as the ratio of the spigot diameter to the vortex finder diameter (Kilavuz & Gulsoy, 2011) is commonly used to alter the performance of the cyclone. This is because it is one of the easiest geometries to alter once a cyclone has been setup up. This section of the report analyses the results of the effect of the cone ratio on the cyclone performance with regard to both the UG2 and iron ore.

4.5.1. Effect of cone ratio on cut size

The effect of the cone ratio on the corrected cut size for UG2 and iron ore is illustrated in Figures 4-12 and 4-16 respectively. For the UG2 ore, it was observed that, as the cone ratio decreases, a coarser cut size is achieved. This however does not mean that the largest cone ratio will result in the most efficient operation, as there is a trade-off between cut size and water recovery. The trend is consistent for all concentrations. A large increment in the cut size is noted between cone ratios of 0.68 and 0.52, with the difference more exaggerated for solid concentrations above 30 wt. %.

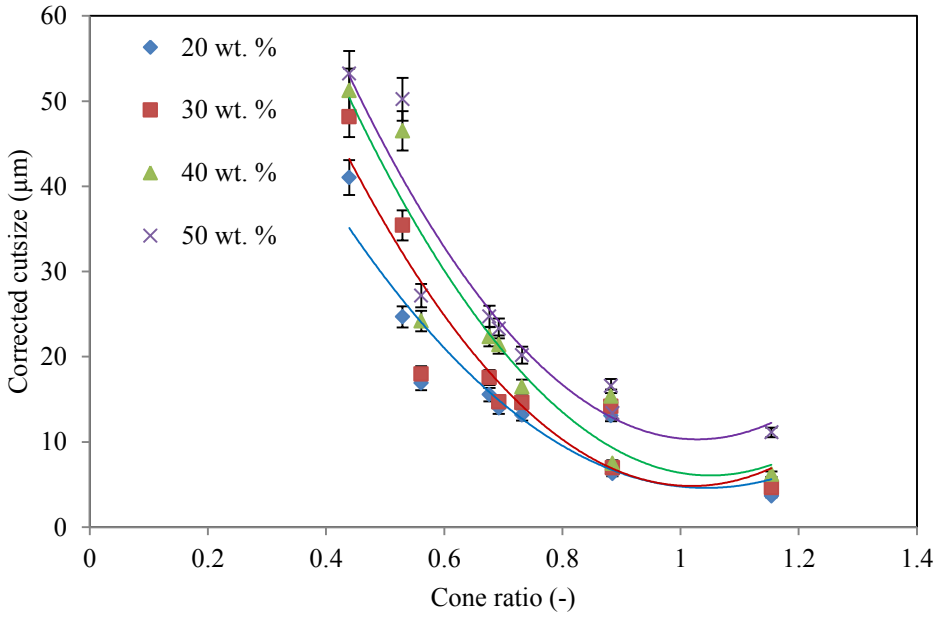

Figure 4-12: Effect of cone ratio and solids concentration on cut size for UG2 ore

The increase in the cut size with a decrease in the cone ratio for UG2 ore can be explained by the equilibrium orbital theory. This assumes that particles are distributed from the cyclone wall to its center according to particle size, with the coarsest size found near the cyclone wall and the finest particle size found towards the air core. Bradley (1996) showed that the existence of upward and downward velocity within the cyclone sets up a locus, where the velocity is zero. This is termed the locus of zero vertical velocity (LZVV), and the cut size lies along this region (Bradley, 1965). The radius of the LZVV is represented by the following formula:

$$R_{LZVV} = \frac{R_c}{1 + \frac{D_U}{D_O}} \qquad \textbf{5- 1}$$

Where: R_c is the radius of the cyclone and D_u/D_o is the cone ratio

The change of the radius of LZVV along the length of the cyclone is illustrated in Figure 5-13.

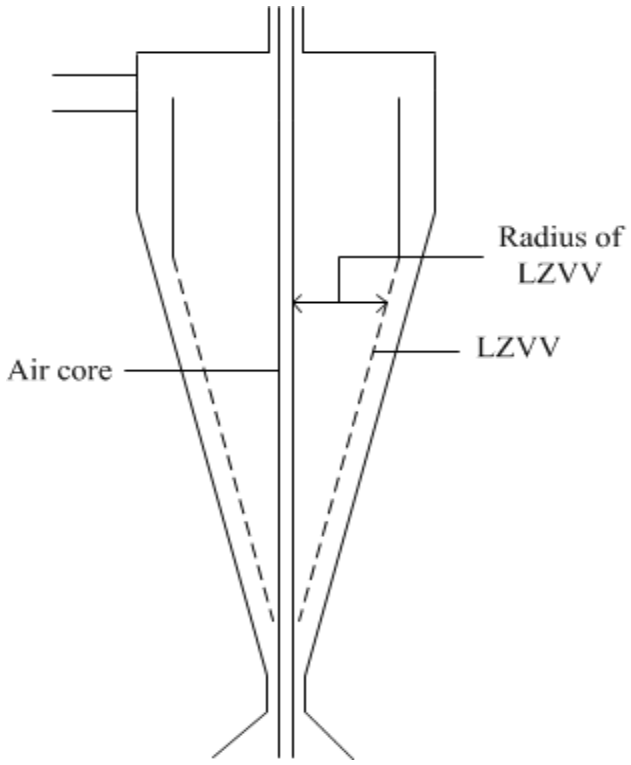

Figure 4-13: Change of the LZVV along the cyclone length adapted from (Bradley, 1965)

The theory suggests that the cut size lies on the LZVV described by Bradley (1965). As the cone ratio increases, the LZVV decreases, causing the cut size to decrease. This results in a finer separation. This can be visualized from the schematic showing the changes in the radius of the LZVV with increasing cone ratio at a particular cross-section of the cyclone, shown in Figure 4-14. R1, R2 and R3 are different radii of the LZVV at different cone ratios at a particular cross-section of the hydrocyclone.

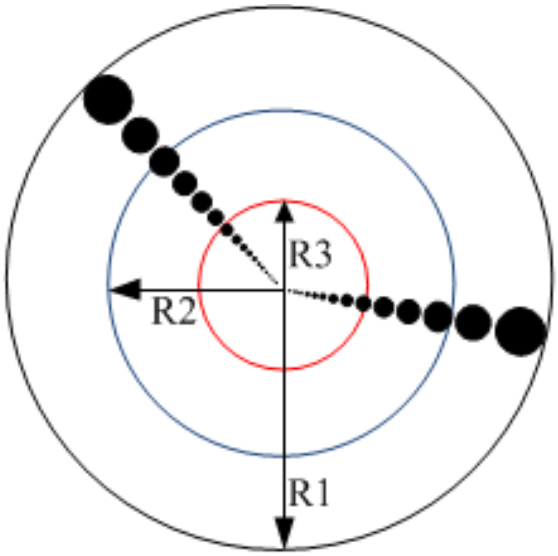

Figure 4-14: Top view schematic representing the changes in cut size with increasing cone ratio. The 2nd circle inwards is the initial locus, and the inner circle is the locus after increasing cone ratio. The black dots represent the ore particles according to particle size.

In an attempt to validate this theory, a graph illustrating the effect of the R_{LZVV} on the cut size for the UG2 ore was plotted and is represented in Figure 4-15 for different feed solids concentrations. It was observed that the R_{LZVV} increases with cut size for all the conditions investigated, which is in agreement with the postulations of Bradley (1965). Not all of the data points fell on the trend line. This could have been attributed to the fact that the equilibrium orbit theory assumes a linear size distribution from the cyclone wall and in practice this phenomenon is not always observed. The standard error was calculated using triplicate results and the error bars indicate the associated error.

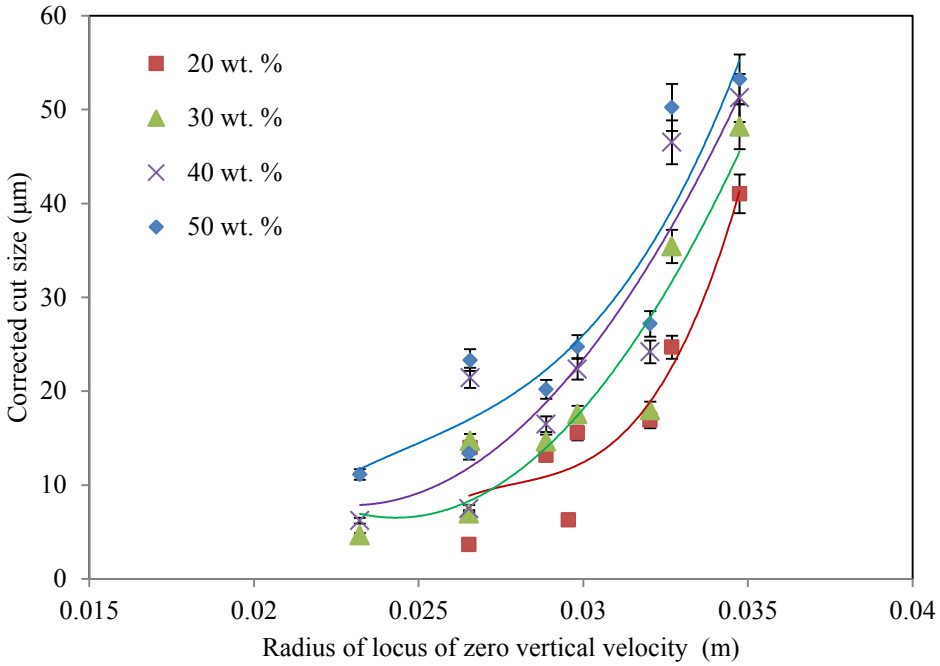

Figure 4-15: Effect of RLZVV on the cut size

The variation in the cut size with regard to the cone ratio for the hydrocyclone treating iron ore was evaluated. The results using the iron ore are presented in Figure 4-16.

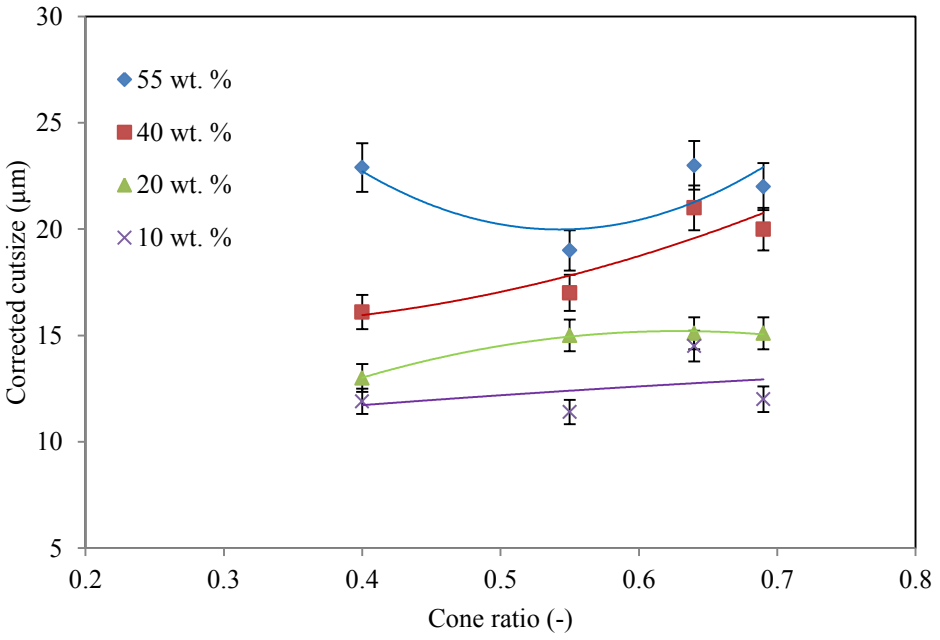

Figure 4-16: Effect of cone ratio and solids concentration on cut size for iron ore

It was observed that the cut size increased with the cone ratio for feed solids concentrations of 10, 20 and 40 wt. %. However, for the tests done at 55 wt. % solids, the cut size decreased and reached a minimum at a cone ratio of approximately 0.55, before increasing again. This indicates that, within the range of conditions investigated, the cone ratio has a similar effect on the corrected cut size when the feed solids concentration is less than 40 wt. %. However, at 50wt. % the behavior is different, and this can be attributed to the fact that, at higher solids concentrations, the slurry viscosity increases, which retards the rotational motion of the slurry (Plitt, 1976). The increase in slurry viscosity moreover results in a decrease in the size of the air core, which results in a coarser cut size.

To evaluate the variation of the cut size at different cone ratios and solid concentrations, 3D surface plots shown in Figures 4-17 and 4-18 were generated. For both UG2 and iron ore, it can be seen that both the cone ratio and the concentration of feed solids affect the cut size. For iron ore, it was observed that the cut size increases with an increase in the cone ratio, until it reaches a peak at a cone ratio of approximately 0.68, before decreasing again. For both ore types, it was observed that, as the solids concentration increases, the cut size coarsens for all cone ratios. This could be due to hindered settling as well as hindered discharge through the spigot, which is caused by the increase in the solids concentration (Asomah, 1996; Fahlstroem, 1963). When the the feed solids concentration increases, the spigot becomes flooded, leading to a coarser cut size. These findings are in conformity with the findings of Asomah (1996), who ran tests on a 10.2 cm cyclone using limestone slurry, which is a slow settling slurry compared to UG2 and iron ore. Similar findings were also observed by Waters et al., (2014).

Within the design space investigated, an analysis of Figure 4-17 illustrates that the cone ratio has a greater impact on the cut size than does the solids concentration for UG2. However, for the iron ore, minor changes in the feeds solids concentration results in more significant changes in the cut size, compared to changes in the cone ratio. This phenomenon could be attributed to the differences in the ore characteristics as well as the cyclones and operating conditions under which the tests were carried out.

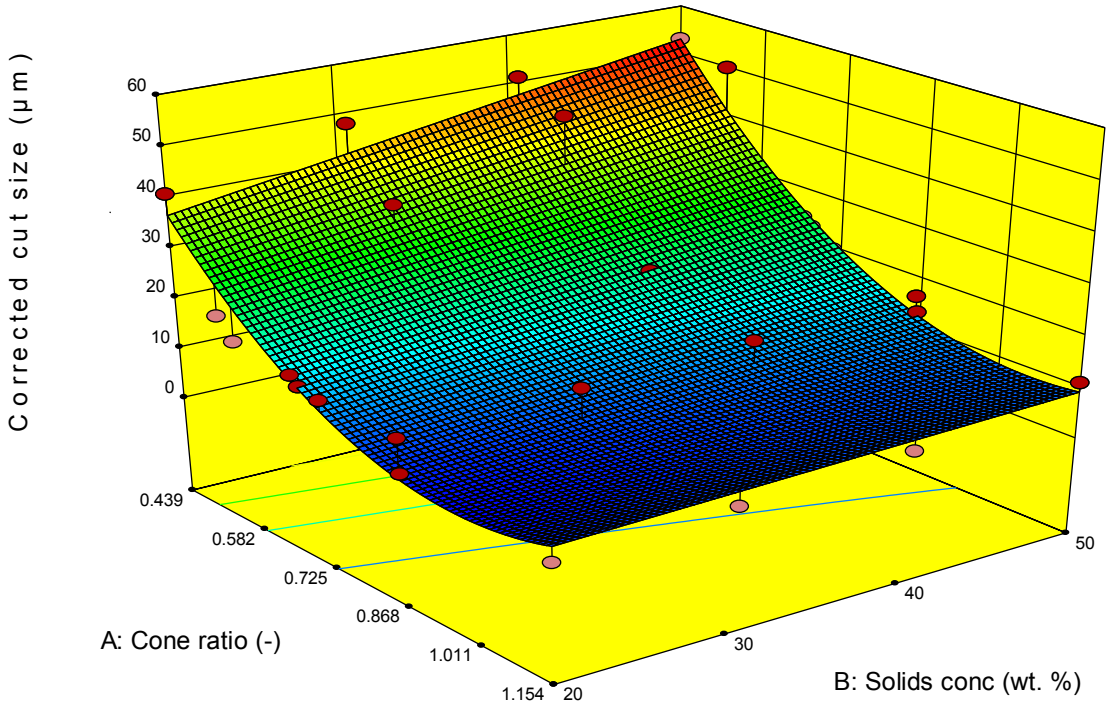

Figure 4-17: 3D surface plot for the cut size as a function of the cone ratio and feed solids concentration for UG2 ore

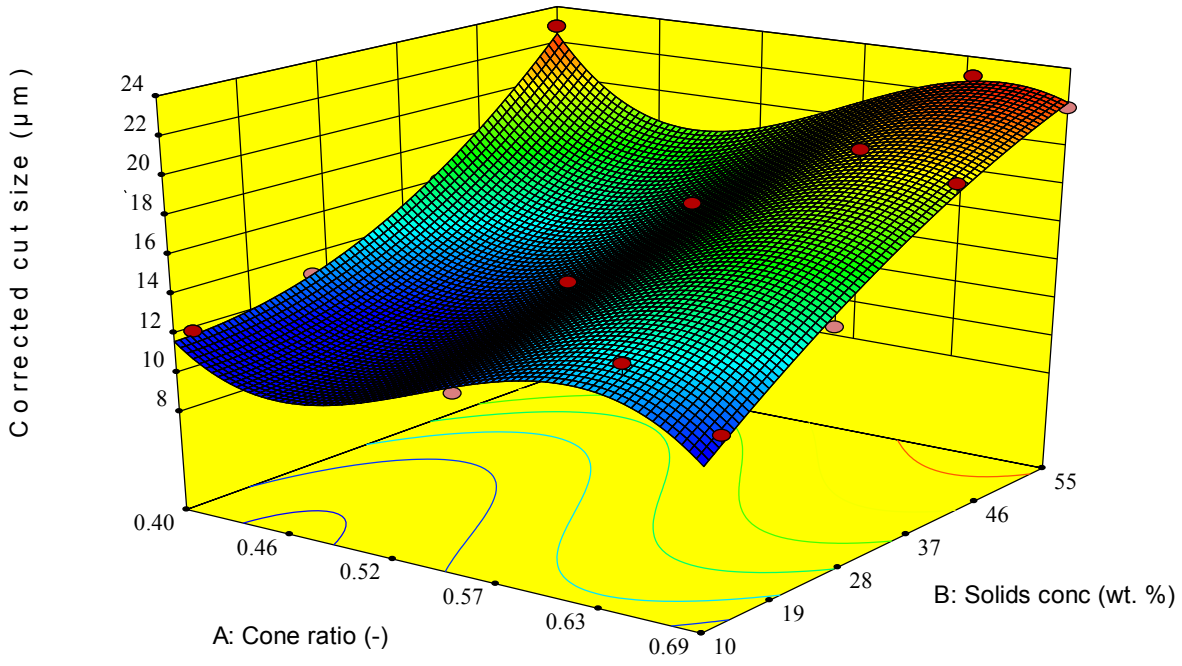

Figure 4-18: 3D surface plot for the cut size as a function of the cone ratio and feed solids concentration for iron ore

4.5.2. Effect of cone ratio on water recovery

The effect of the cyclone cone ratio on the water recovery to the underflow is shown in Figures 4-19 and 4-20 for UG2 ore and iron ore respectively.

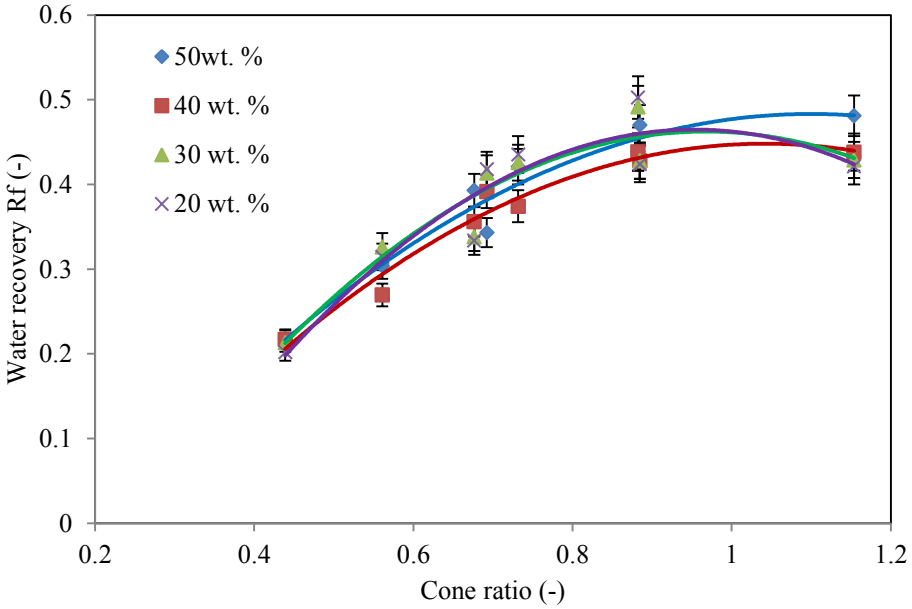

Figure 4-19: Water recovery to underflow for UG2 ore

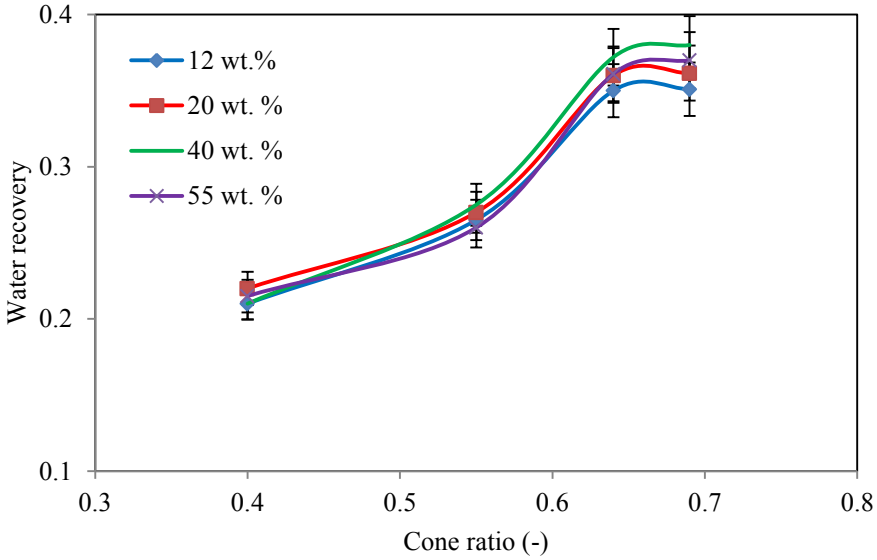

Figure 4-20: Water recovery to underflow for iron ore

For the UG2, increasing the cone ratio resulted in an increase in the amount of water in the feed that was recovered to the underflow. The increase was more pronounced at lower cone ratios and

then almost flattened out at higher cone ratios. It was observed that some of the data points do not lie on the trend line plotted. These outliers could be as a result of experimental errors associated with the test work. The increase in water recovery with cone ratio can be attributed to the fact that, at higher cone ratios, more fluid is pushed to the cyclone periphery and that thus more fluid reports to the cyclone underflow. These results are in accordance with the observations of Kilavuz et al., (2011) and Banerjee et al., (2013).

An analysis of the iron ore graph indicates that the water recovery also increases with an increase in the cone ratio. However, there is no significant difference in water recovery to the underflow between the cone ratios of 0.64 and 0.69: the water recoveries are fairly similar. All water recoveries for the iron ore tests fell within the range of 20% to 40%.

To evaluate the variations in the water recovery, according to different cone ratios and solid concentrations, 3D surface plots were generated (see Figures 4-21 and 4-22). It is observed that, for both UG2 and iron ore, the increase in water recovery is affected by the cone ratio and the feed solids. However, it is also observed that the water recovery is more sensitive to the cone ratio than the feed solids concentration, within the ranges investigated for both the ore types. This is because changing the cone ratio involves altering the vortex or spigot diameter, which in turn affects the slurry flow resistance around these respective ports (Elsayed & Lacor, 2010). This is in agreement with what was observed by Kilavuz et al., (2011) and Banerjee et al., (2013).

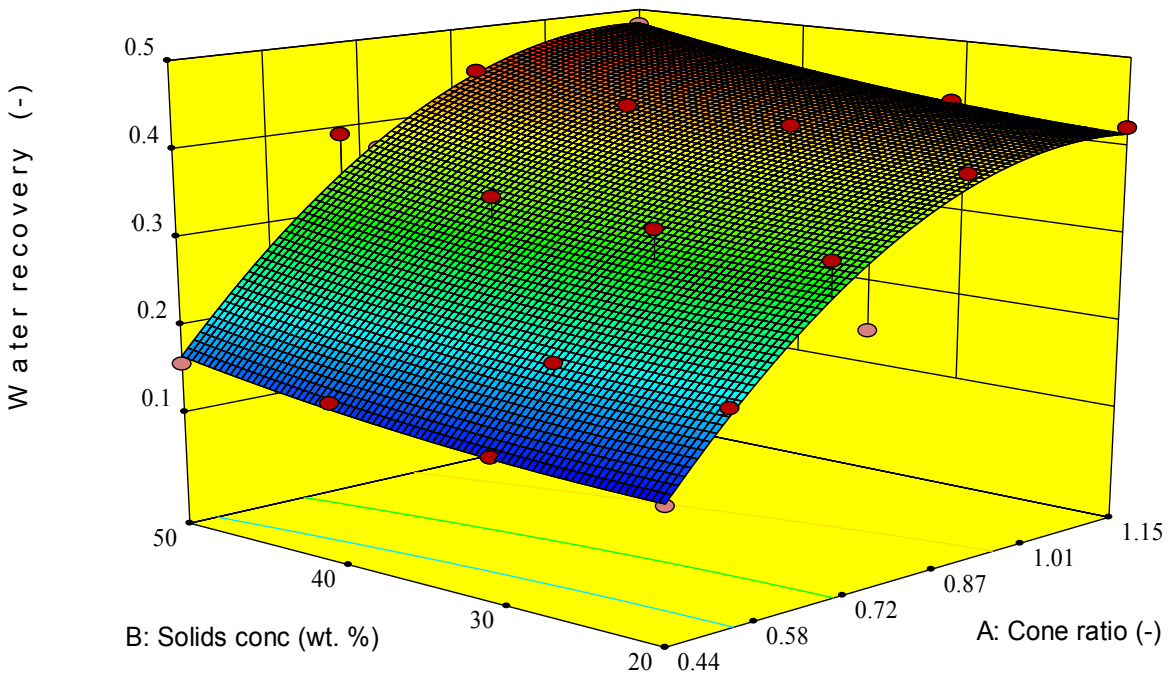

Figure 4-21: 3D surface plot for the water recovery as a function of the cone ratio and feed solids concentration for UG2 ore

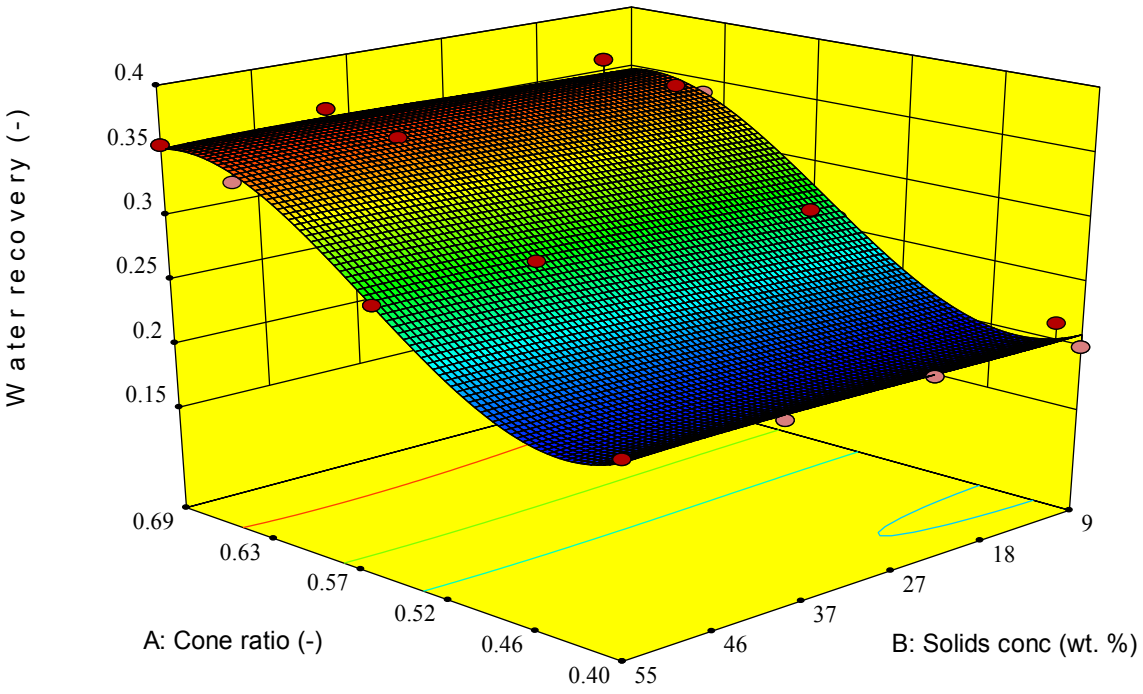

Figure 4-22: 3D surface plot for the water recovery as a function of the cone ratio and feed solids concentration for iron ore

4.5.3. Effect of cone ratio and solids concentration on sharpness of separation

Figures 4-23 and 4-24 illustrate the effect of the cone ratio on the sharpness of separation for UG2 ore and iron ore respectively. With regard to the UG2 ore, it is observed that the sharpness of separation increases with an increase in the cone ratio at all the feed solids concentrations investigated. This means that, as the cone ratio increases, the quantity of misplaced particles in the overflow streams decreases as more fluid reports to the underflow (Majumder et al., 2007) (Kilavuz & Gulsoy, 2011). This phenomenon could be attributed to the fact that, as the cone ratio increases, more fluid reports to the underflow, and thus finer particles report to the overflow, which in turn results in a sharper cut size. The error bars shown are indications of the standard error of the mean about each point, generalised from the tests that were done in triplicate.

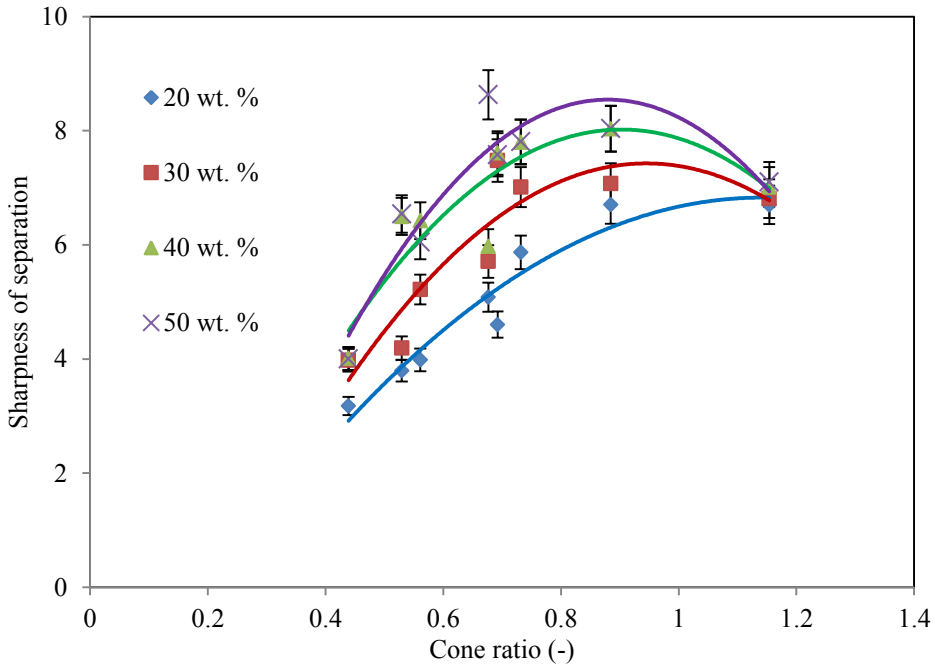

Figure 4-23: Effect of cone ratio on sharpness of separation for UG2 ore

The variation in the sharpness of separation with cone ratio for the hydrocyclone that is treating iron ore is illustrated in Figure 4-24. For tests carried out at 10 and 20 wt. %, it was observed that the sharpness of separation was fairly constant at 3.5 and 4 respectively. However, for the tests carried out at 40 wt. %, the sharpness of separation decreases with an increase in the cyclone cone ratio, while for the tests carried out at 55 wt. %, the sharpness of separation increases with

the cone ratio, before leveling off. The only constant trend is noted for test work carried out at 10 and 20 wt. %. This can be explained by the fact that the size class below 10 microns is significantly high as in the case of iron ore, the fines misplacement increases with cone ratio (10, 20, and 40) wt.%. The same is evident from fish hook nature curves. However, for the 55 wt. % solids case, the fish hook is usually negligible as reported by Narasimha (2010) hence a sharper separation is observed here as well.

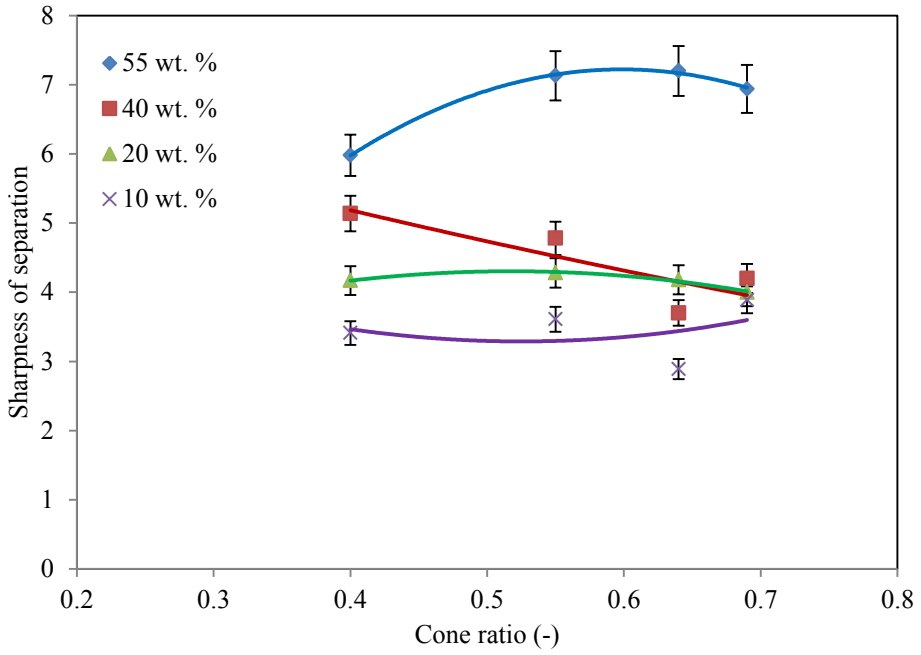

Figure 4-24: Effect of cone ratio on sharpness of separation for iron ore

4.5.4. Effect of cone ratio on volumetric throughput

The effect of the cone ratio on the cyclone volumetric throughput for both the UG2 and iron ore is illustrated in Figure 4-25. With regard to the UG2 ore, it was observed that the throughput increases with cone ratio until it reaches a maximum at cone ratio of approximately 1. However, with regard to the iron ore, the volumetric feed to the cyclone increases with cone ratio, within the range investigated. It was observed in Section 5.4.4, that increasing the spigot diameter led to an increase in volumetric throughput, while an increase in the vortex finder diameter showed a decrease in the volumetric throughput. The volumetric throughput decreases after cone ratio of 1, this is because beyond this cone ratio there is flow restriction within the hydrocyclone at this leads to a decrease in the throughput (Kilavuz & Gulsoy, 2011).

Since the volumetric throughput of the cyclone is also strongly influenced by the feed pressure, the maximum cyclone operating pressure before the onset of roping was plotted against the cone ratio; the results are plotted in Figure 4-26. It is observed that the cyclone operating pressure increases proportionally with the feed volumetric flow rate for both ore types. This is because, as the pressure increases, the force exerted per unit area of the slurry increases too, resulting in an increase in the volumetric flow rate. These findings are in conformity with the observations of Lynch et al., (1975), Hsieh et al., (1991) and Goyal et al., (2010).

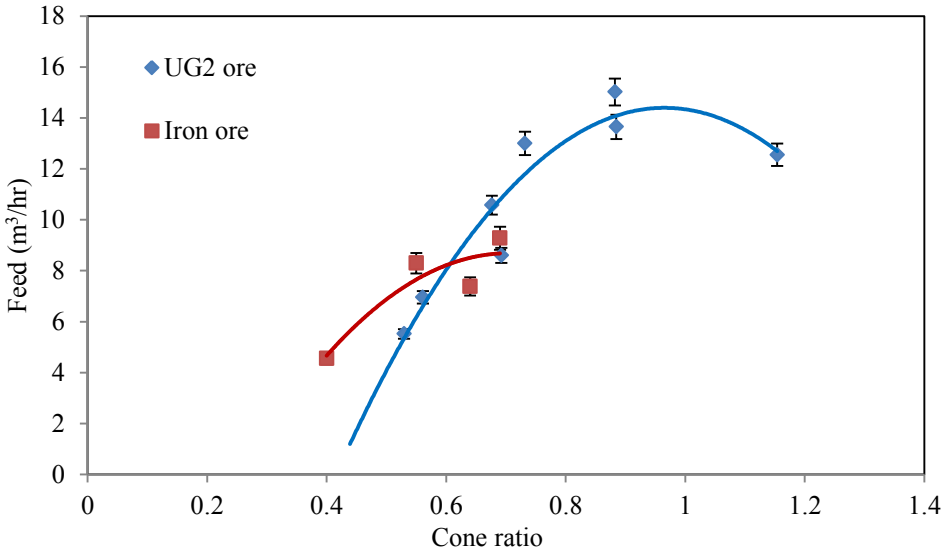

Figure 4-25: Effect of cone ratio on the volumetric feed flow rate

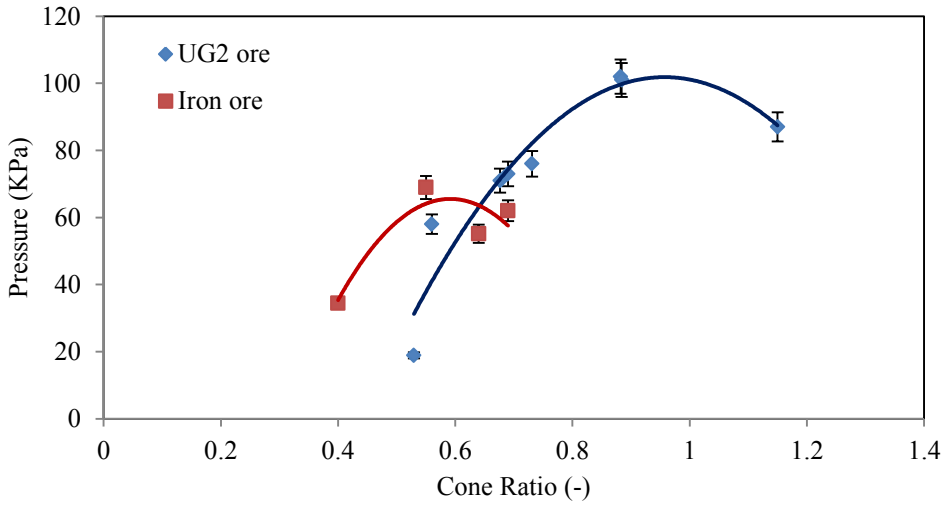

Figure 4-26: Maximum pressure variation with cone ratio

4.6. A performance comparison between the conventional and the flat bottom cyclone

It is common for operations to recommend using flat bottom cyclones for fast settling slurries, such as those used in this test work. In order to assess the differences in performance between the conventional and the flat bottom hydrocyclone, tests were carried out on both types of cyclones at similar cone ratios, feed solids concentrations and operating pressures. Efficiency curves were obtained and the Whitten model was used to obtain the corrected cut size, the efficiency of separation and the water recovery in order to evaluate the performance of these cyclones under the test conditions.

4.6.1. The effect of cyclone type on the corrected cut size

Figure 4-27 illustrates the effect of feed solids concentration on the corrected cut size for the conventional and flat bottom hydrocyclone. In the case of the conventional cyclone, the corrected cut size increases with the feed solids concentration. The corrected cut size follows a similar trend for the flat bottom cyclone. At all the solid concentrations investigated, the flat bottom cyclone has a coarser cut size compared to that of the conventional hydrocyclone.

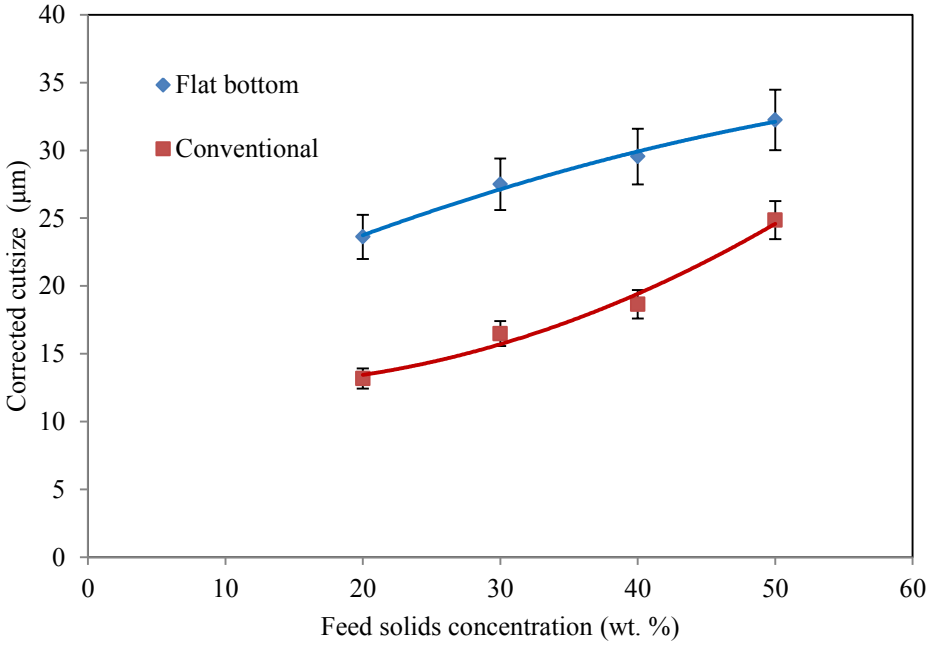

Figure 4-27: Effect of cyclone type on the d50c using UG2 ore at a cone ratio of 0.732

4.6.2. The effect of cyclone type on the sharpness of separation

Figure 4-28 shows the effect of cyclone type on the sharpness of separation, α. For the conditions investigated, the sharpness of separation of the conventional hydrocyclone increases steadily with feed solids concentration, tending to flatten between 20 and 30 wt. % solids concentration. A gradual almost linear increase in the sharpness of separation is observed for the flat bottom cyclone, with an increase in feed solids concentration. At each feed solid concentration, the conventional cyclone had a higher α value than the flat bottom cyclone and this suggests that the conventional cyclone has a sharper separation.

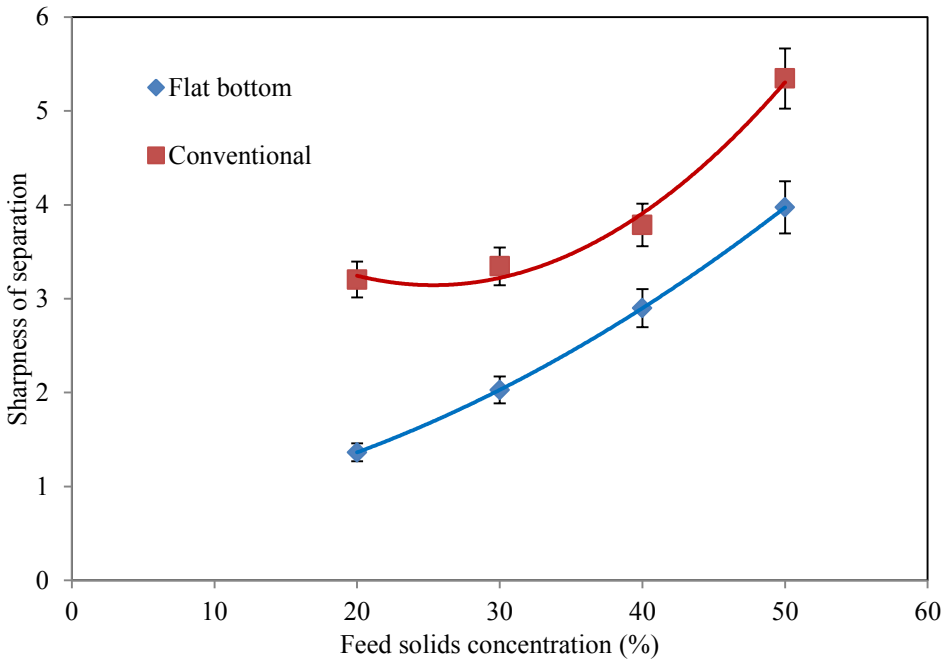

Figure 4-28: Effect of cyclone type on α using UG2 ore at a cone ratio of 0.732

4.6.3. The effect of cyclone type on water recovery to underflow

The effect of the cyclone type on water recovery to the underflow is illustrated in Figure 4-29. The water recovery for the conventional cyclone decreases with an increase in feed solids concentration, while that of the flat bottom cyclone shows a gradual decrease from 0.352 to 0.267 between 20 % and 40 % feed solids concentration, and then a sharp increase above 40 wt.% feed solids concentration. The conventional hydrocyclone has a higher water recovery than the flat bottom cyclone at all solids concentrations, with the exception of 50 wt. % feed solids concentration. This phenomenon of the changeover could be attributed to the fact that as the

solids concentration increases beyond 40 wt. % crowding at the spigot exit is more pronounced in a flat bottom cyclone resulting in higher volume discharges through the spigot.

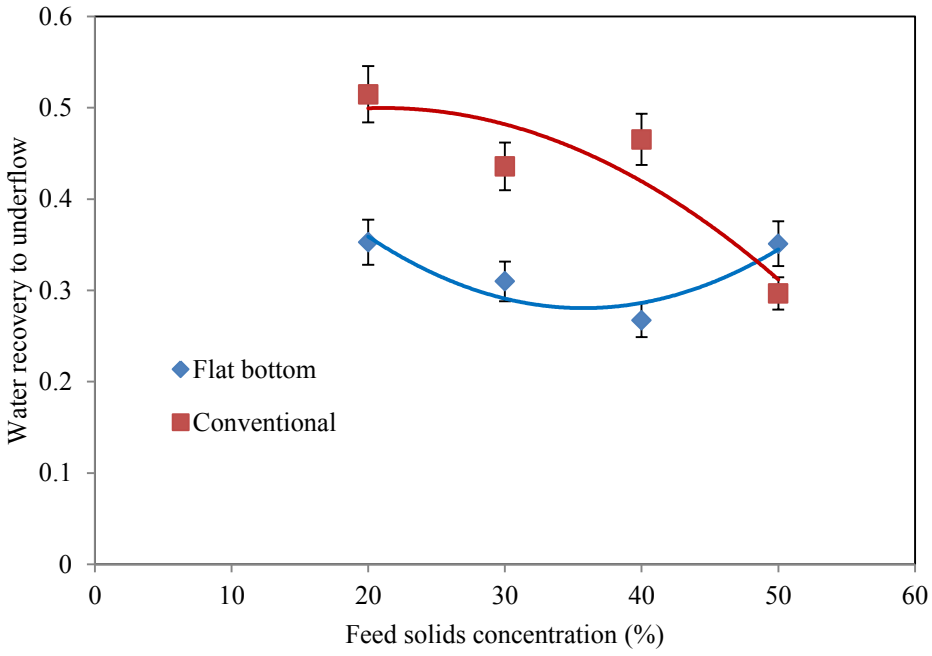

Figure 4-29: Effect of cyclone type on R_f using UG2 ore at a cone ratio of 0.732

4.6.4 Discussion of trends between flat bottom and conventional cyclone

An analysis of the experimental results shows that the flat bottom cyclone gives a coarser cut and a reduced water recovery to the underflow than a conventional hydrocyclone. This trend is in conformity with the findings of Mainza et al., (2005), who used a 600 mm diameter cyclone to process Lonmin UG2 ore.

The function of the conical section in the hydrocyclone is to direct the centrifuged solids towards the central axis of the hydrocyclone. This gives rise to a concentration of solids at the spigot opening and as a result increases the cone angles, which in turn creates coarser cut sizes Mainza et al., (2005) In the flat bottom cyclone, the absence of the conical section creates a "T-piece" at the bottom of the cyclone, which creates eddies, as shown in Figure 4-30. As a result of these eddies, coarse particles tend to report to the overflow stream, thus leading to a coarser cut size. This phenomenon also attributes to the lower α that is noted for the flat bottom cyclone.

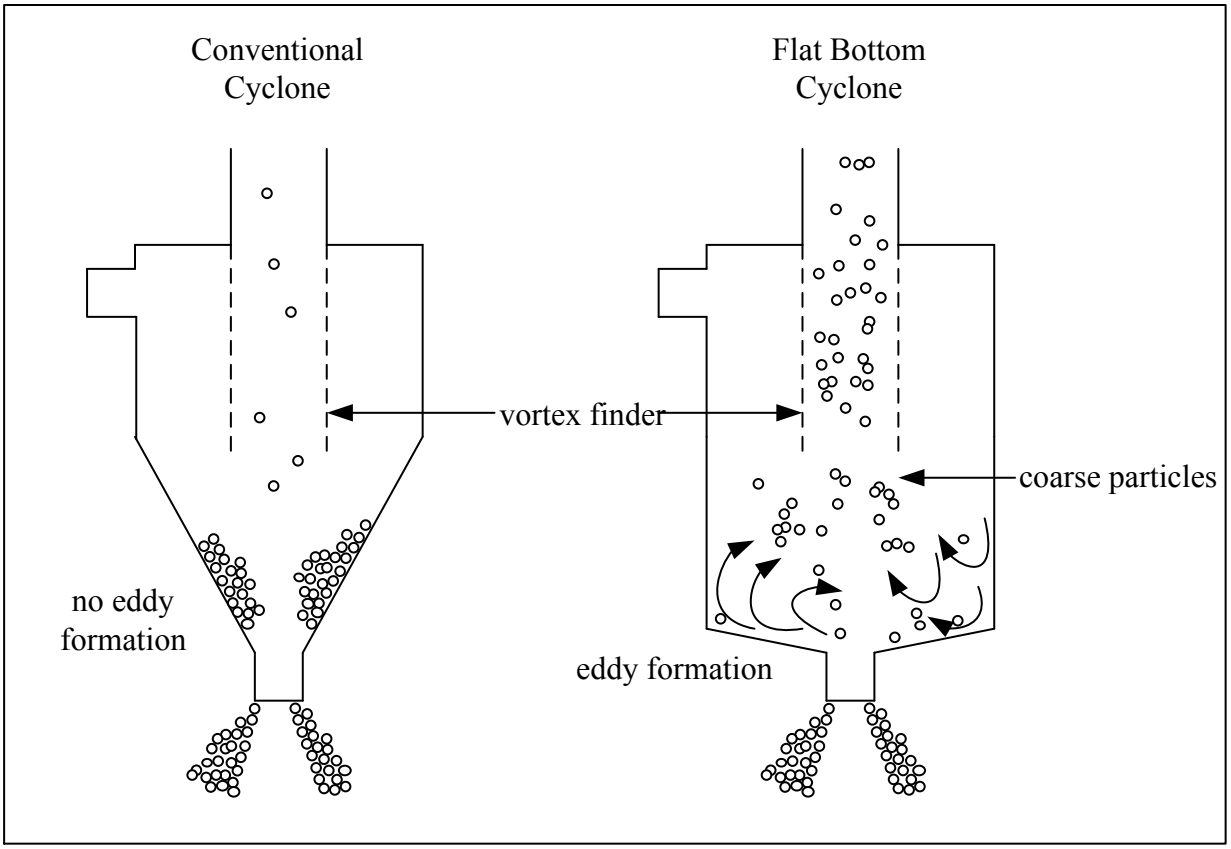

Figure 4-30: Flat bottom vs conventional cyclone classification

4.7. Reproducibility of Experiments

In order to determine the reliability of the measurements taken during the experimental work, repeat tests were performed for some of the conditions. The repeats were conducted on different days than the primary tests. Figure 4-31 illustrates the efficiency curves for 3 tests carried out by using a vortex finder of 34 mm and a spigot diameter of 18 mm, which corresponds to a cone ratio of 0.53 at a feed solids concentration close to 40% for UG2 ore. It is observed from Figure 4-31 that the three partition curves are very similar. Table 4-4 indicates the various responses and their corresponding coefficient of variance. It can be concluded that the observed trends are reproducible with small variations, which are expected for such kind of test work. A similar analysis for iron ore at a cone ratio of 0.64 is presented in Figure 4-32 and Table 4-4. The associated errors observed in all the tests were used to develop the error bars represented in all the graphs presented.

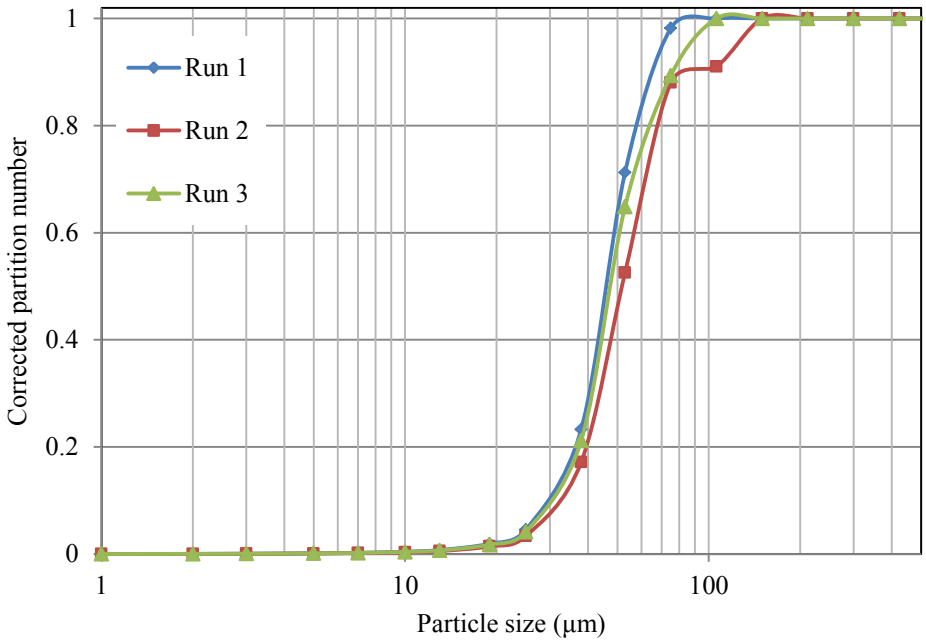

Figure 4-31: Triplicate tests for cone ratio 0.53 close to 40wt. % feed UG2 ore

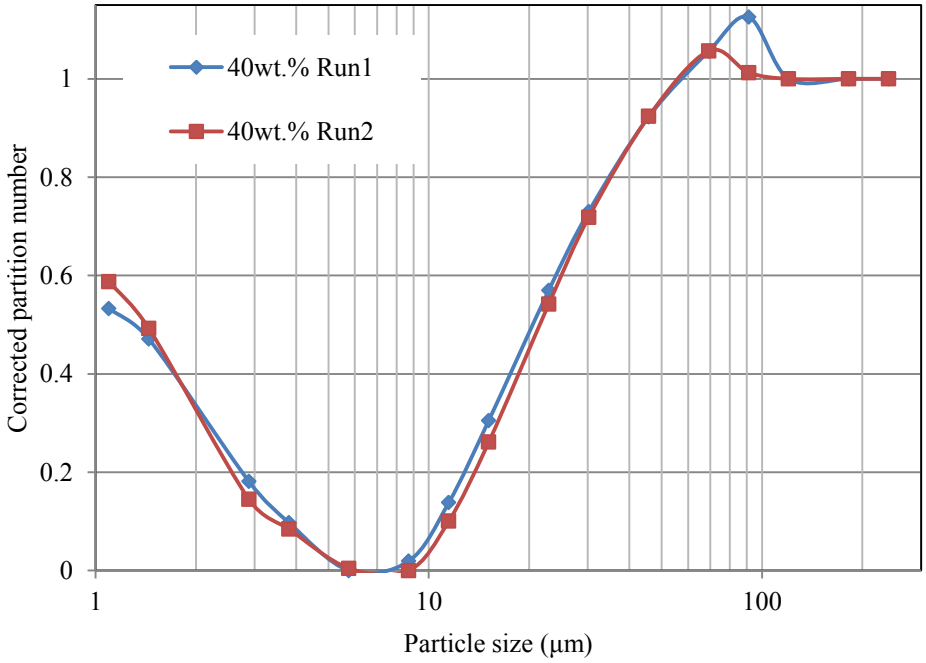

Figure 4-32: Replicate tests for cone ratio 0.64 close to 40wt. % feed iron ore

Table 4-3: Triplicate tests for vortex finder 34 mm, spigot diameter 18 mm corresponding to a cone ratio of 0.53 for UG2 ore

	Run 1	Run 2	Run 3	Coefficient of variance, %
Feed solid %	41	38.8	40.1	2.77
Feed TPH	8.17	8.24	8.91	4.84
Feed solids TPH	3.35	3.20	3.57	5.60
Water recovery Rf	0.181	0.194	0.197	4.46
Mass split to U/F %	87.1	86.4	87.9	0.86
% passing 75 μm O/F	92	94	92	1.25
P80 O/F μm	21	22	21	2.71
D_{50c}	47	49	51	4.08

Table 4-4: Replicate tests for vortex finder 25 mm, spigot diameter 16 mm corresponding to a cone ratio of 0.64 for iron ore

	Run 1	Run 2	Coefficient of variance, %
Feed solid %	35.6	38.8	6.08
Feed TPH	6.84	7.41	5.66
Feed solids TPH	2.4	2.41	0.29
Water recovery Rf	0.262	0.247	4.17
Mass split to U/F %	78.7	75.3	3.12
% passing 75 μm O/F	53	61	9.92
P80 O/F μm	47	51	5.77
D_{50c}	20	21	3.45

CHAPTER 5: RHEOLOGY RESULTS AND DISCUSSION

5.1. Introduction

This chapter presents the results and analyses of the rheology experiments carried out at the UCT analytical laboratory and at the CMR laboratory. A conventional AR 1500EX TA vane rheometer was used for the rheological characterization of the UG2 and iron ore feed and overflow samples at different solids concentrations. Rheological characterizations were also done of the UG2 ore feed at different size classes. The range of solids concentrations investigated was between 0-70 wt. % and 0-60 wt. % for the feed and overflows respectively. Separate rheology tests were performed on -212 µm, -150 µm, -106 µm and -53 µm particle size classes at different solids concentrations to assess the effect of particle size on slurry rheology.

5.2. Rheological characterization of UG2 and iron ore

5.2.1. Characterization of feed and overflow at different solid concentrations

The rheograms obtained from the characterization of the UG2 feed and overflows at different solid concentrations using the AR 1500EX TA vane rheometer are given in Figures 5-1 to 5-4.

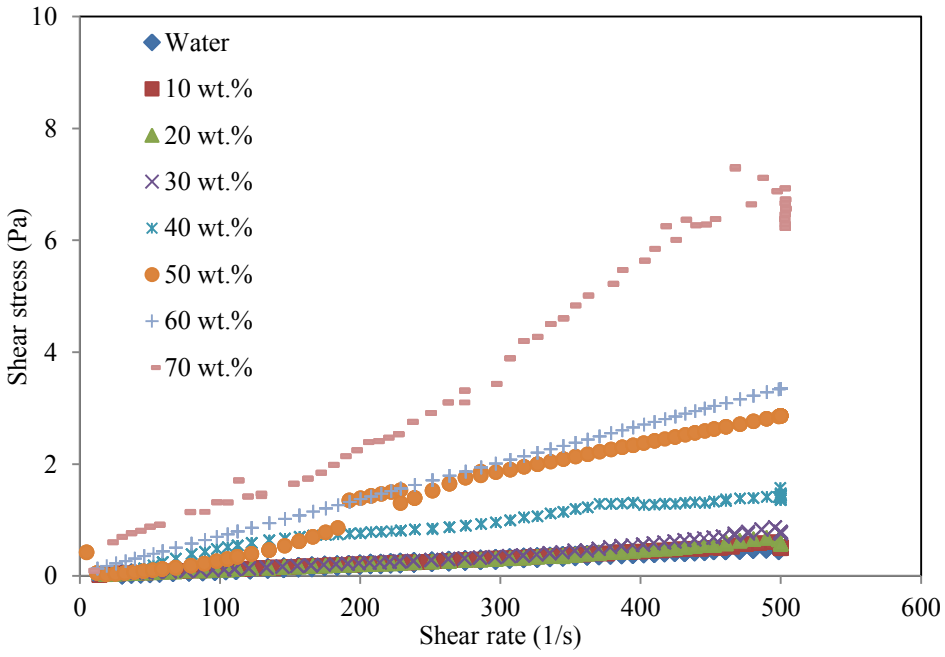

Figure 5-1: Rheograms for UG2 feed at different feed solids concentrations at 25˚C

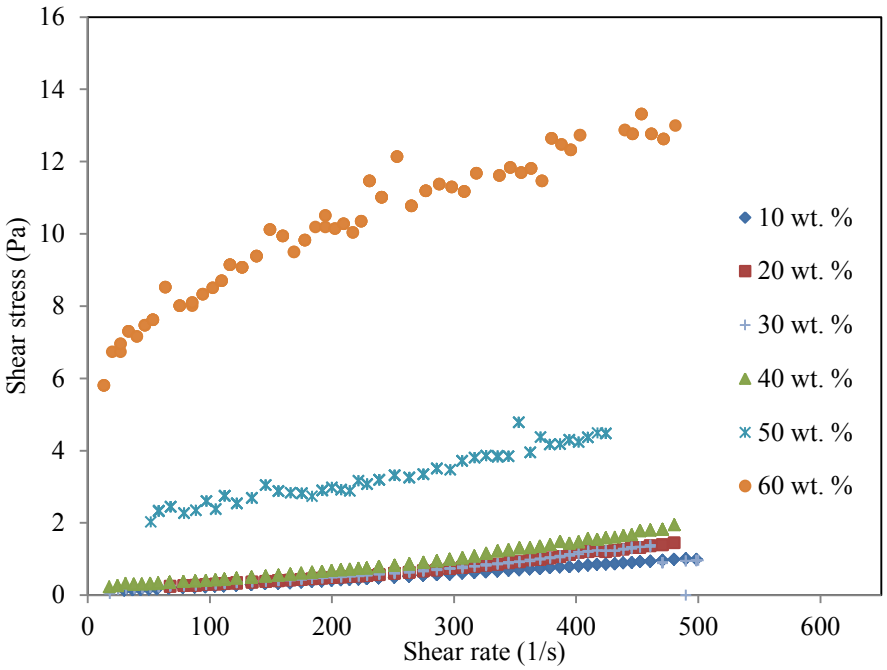

Figure 5-2: Rheograms for UG2 overflow at different feed solids concentrations at 25˚C

The rheograms show a linear relationship between the shear rate and the shear stress. As the solids concentration increases, the shear stress also increases for all scenarios. This phenomenon could be attributed to the fact that, as the solids concentration increases, more energy is required to move the suspension. A similar trend was observed by He et al. (2006), who conducted rheological measurements on limestone slurry -100 µm, using a Bohlin Visco 88 BV rotational viscometer for solids concentrations between 0-78.5 wt. % . A similar trend is noted for the iron ore feed and overflow rheograms; these are presented in Appendix A.

5.2.2. Characterization of UG2 at different size classes

The rheograms for UG2 ore obtained using the AR 1500EX TA vane rheometer for size class -212 µm at different solids concentration are given in Figure 5-3. As the solids concentration increases, the shear stress increases. A gradual increase is noted for solids concentrations between 10 wt. % and 60 wt. %. A large increment in the shear stress is noted for solids concentrations between 60 wt. % and 70 wt. %. This trend is similar to what was noted for rheograms at -150 µm, -106 µm and -53 µm size classes. These rheograms are presented in Appendix A.

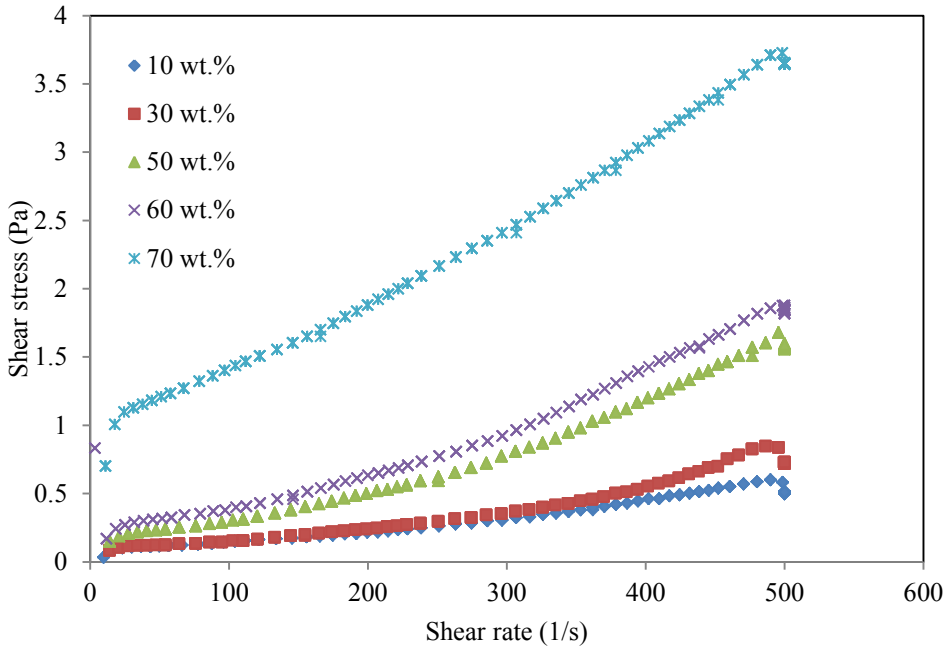

Figure 5-3: Rheogram for UG2 -212 µm size class at different solids concentrations

5.3. Model fitting

5.3.1. Correction of systematic error

The calibration water rheogram obtained from the AR 1500EX TA vane rheometer is shown in Figure 5-4 with the expected theoretical water rheogram at 25 ˚C. It shows a dilatant behavior for water at room temperature, instead of the expected Newtonian behavior. A correction factor had to be applied to the measured rheological data to eliminate this systematic error generated by the rheometer before the rheological models were fitted. The correction to the measured rheological data was obtained by subtracting the theoretical rheogram curve for water at room temperature, which is represented by Equation 5-1.

$$\tau = (1 \times 10^{-3})\dot{\gamma} \qquad \textbf{5- 1}$$

Where τ is the shear stress and $\dot{\gamma}$is the shear rate

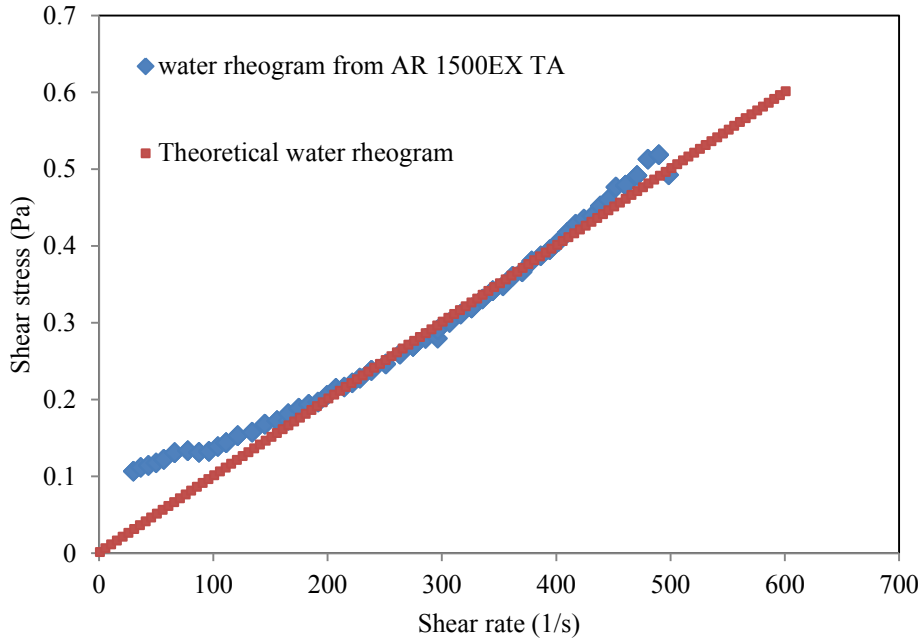

Figure 5-4: Theoretical water rheogram and actual rheogram

For the range of solids concentrations tested, the best fitting curve for the measured water data was a quadratic polynomial. In this regard, the following procedure was applied:

1. The theoretical water rheogram curve represented by Equation 5-1 was subtracted from the best fitting curve, which can be represented by the following generic equation ($a\dot{\gamma}^2 + b\dot{\gamma} + c$). This yielded the correction factor ($\boldsymbol{\tau_c}$) required:
2. Provided that the trend of the measured shear stress (τ_m), for m= 0%, 10%, 20%, 30%, 40%, 50% and 60% solids concentration, does not deviate significantly from the quadratic fit, the measured shear stress values can be corrected by simply subtracting the corresponding correction (τ_c):

$$\tau_n = \tau_m - \tau_c$$

Where τ_n is the corrected shear stress

5.3.2. Fitting of Bingham model to experimental data

The Bingham model was chosen because the experimental data showed a linear trend. Furthermore, the Bingham model contains both a power form and a yield stress parameter as shown in Equation 5-2, which was discussed in Chapter 2:

$$\tau = \eta\dot{\gamma} + \tau_s \qquad \textbf{5-2}$$

Where τ is the shear stress (Pa), η is the viscosity in (Pa.s), $\dot{\gamma}$ is the shear rate (1/s) and τ_s is the yield stress (Pa).

The fitted curves of the Bingham model for the feed sample at the different solids concentrations is given in Figure 5-5. The rheograms exhibit a similar trend to the experimental data. As the solids concentration increases for a specific shear rate, the shear stress increases.

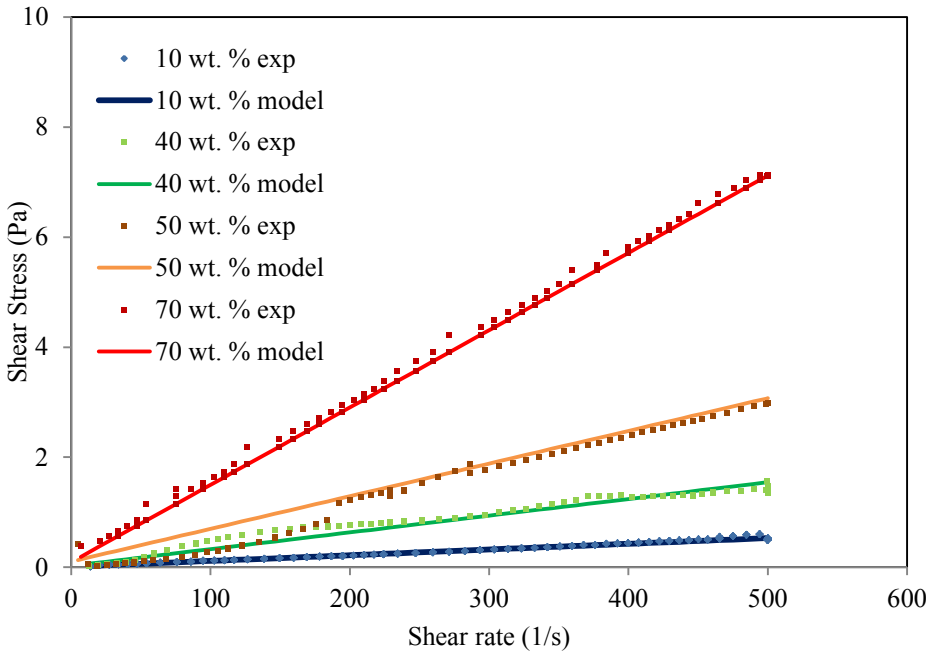

Figure 5-5: Bingham model fit for UG2 feed at different solids concentrations

The Bingham model was also fitted to the -212 µm, -150 µm, -106 µm and -53 µm size class rheograms at the different concentrations. The graphs are presented in Appendix A. For each size class, as the solids concentration increases, the shear stress also increases. Table 5-2 illustrates

the viscosity extracted from the Bingham model for the different size classes of the UG2 ore at different solids concentrations. The R^2 values from the model are also given. It was observed that, at each size class, the viscosity increases with solids concentration. Viscosity values increased with a reduction in the particle size class.

5.3.1.1. Viscosity for feed and overflow

The viscosity at each solids concentration was determined by the gradient of the rheogram. Tables 5-1 and 5-2 illustrate the viscosity for the feed and overflows for the both ore types at the different solids concentrations as well as the coefficient of determination (R^2) for the model fit.

It is noted that the viscosity steadily increases with solids concentration. However, sudden large increments are noted at higher solid concentrations. The reported R^2 values for both the feed and overflow are close to unity, which indicates that the Bingham model is a good fit to the experimental data.

The viscosities for the cyclone feed and overflow at different solids concentrations for both ore types are presented in Figure 5-6. It can be seen that, for both ore types, viscosity increases with solids concentration. At low solids concentrations of up to 30 wt. %, the viscosity values attained are 1 cP, which is close to that of water at room temperature. However, when increasing the solids concentration beyond 30 wt. %, a steady increase in the viscosity is noted until an inflection point appears. This inflection point is indicative of a solid concentration above which the flow characteristics are less predictable and more difficult to control (Becker, et al., 2013). The inflection points for UG2 are noted at approximately 60 wt. % and 50 wt. % for the feed and overflow respectively, while those for iron ore are observed at 60 wt. % and 60 wt. % for the feed and overflow respectively.

Table 5-1: Bingham model viscosities and R^2 values for UG2 ore feed and overflow

Solids Concentration (wt. %)	Viscosity (cP)	R^2 value
Feed		
0	1.002	0.948
10	1.036	0.917
20	1.082	0.969
30	1.398	0.988
40	2.842	0.961
50	4.196	0.984
60	6.592	0.993
70	14.954	0.964
Overflow		
0	1.002	0.989
10	1.317	0.968
20	1.554	0.972
30	1.578	0.954
40	3.205	0.931
50	5.149	0.939
60	22.146	0.941

Table 5-2: Bingham model viscosities and R^2 values for iron ore feed and overflow

Solids Concentration (wt. %)	Viscosity (cP)	R^2 value
Feed		
0	1.002	0.948
10	1.101	0.917
20	1.321	0.969
30	1.417	0.988
40	1.617	0.961
50	2.094	0.984
60	4.571	0.993
70	10.081	0.964
Overflow		
0	1.002	0.986
10	1.081	0.968
20	1.201	0.972
30	1.357	0.954
40	1.456	0.931
50	2.929	0.939
60	5.912	0.941

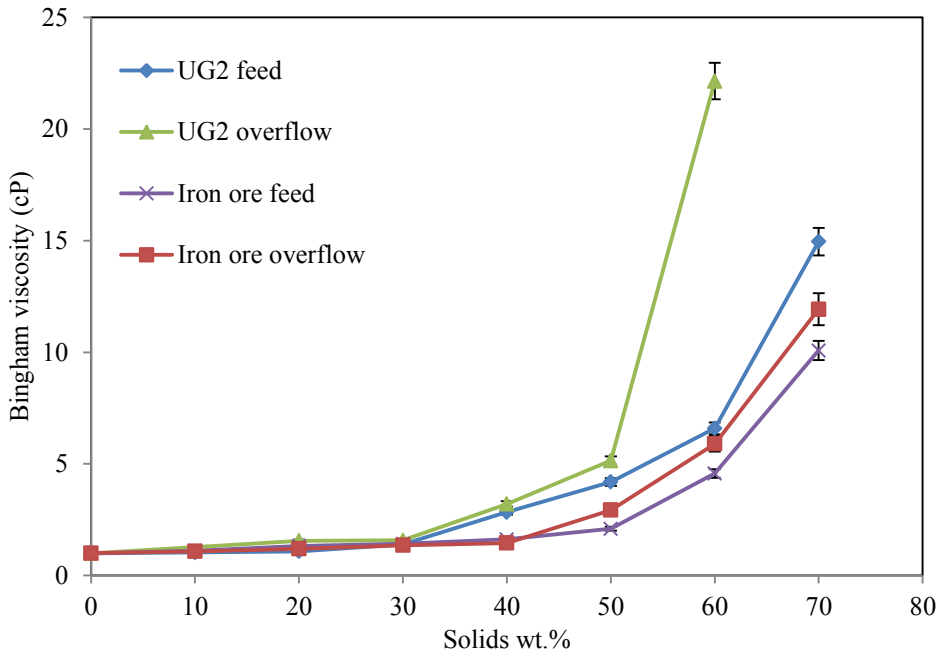

Figure 5-6: Viscosity of UG2 feed and overflow at different solids concentration

For the UG2 ore, the overflow stream point of inflection occurs at a lower solids concentration; as a result, it is said to be a more rheologically complex suspension than the feed stream (Becker, et al., 2013). This difference in behavior could be attributed to a difference in particle size. The overflow stream is finer with a d_{50}=8 µm relative to the feed d_{50}=148 µm. Similar trends were noted by Becker et al., (2013), when they characterized Lonmin UG2 flotation feed as well as the concentrate. The flotation concentrate (d_{50}=7 µm) showed a more complex rheological behavior than the feed (d_{50}=18 µm). This is congruent to the work by Kawatra and Eisele (1988); they observed that, at constant solids concentration, a reduction in particle size resulted in an increase in the slurry viscosity. They attributed this to an increased particle surface area, which results in greater particle interactions within the slurry. A similar observation is made for the iron ore. The overflow viscosity after 40 wt. % is higher than that of the feed. This is also attributed to the particle size difference in the overflow and feed streams.

The iron ore feed has a finer particle size distribution than the UG2 feed, as illustrated in Figure 5-7; however, the UG2 was found to be more rheologically complex. This can be attributed to the shape of the UG2 and iron ore particles. The author hypothesizes that the iron ore particles

are longer and narrower than the UG2 particles, which are more spherical. As a result, the UG2 in its coarser state will be more rheologically complex than the iron ore.

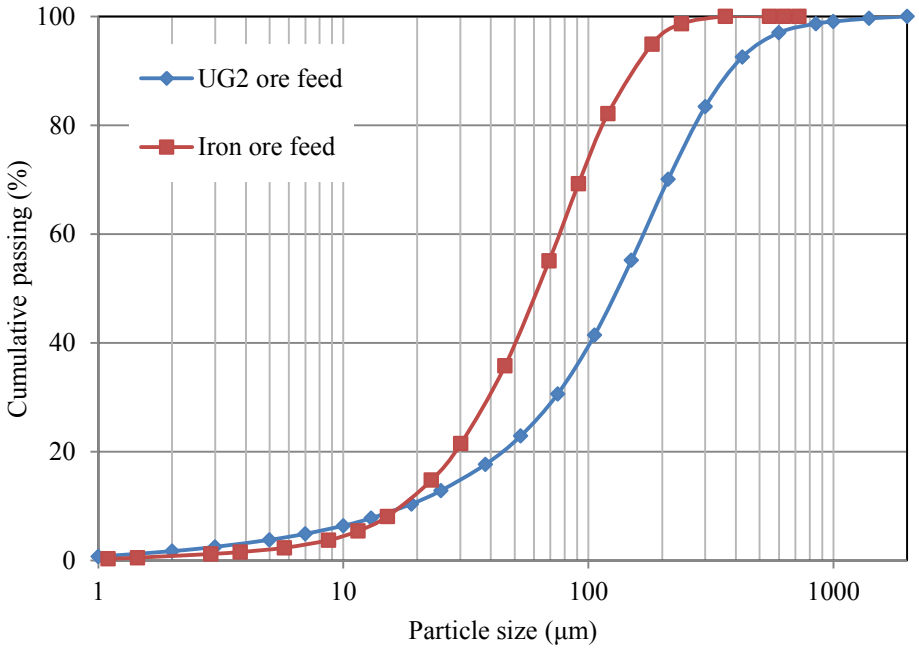

Figure 5-7: Particle size distributions comparison for UG2 and iron ore feed

5.3.1.1. Viscosity for UG2 feed at different particle size classes

In order to support the findings in Section 6.4.1, further rheological characterization of UG2 ore was done for different class sizes at different solids concentrations. Table 5-3 illustrates the viscosities obtained from the Bingham model and the respective R^2 values. The viscosities at the different solids concentration are represented in Figure 5-8. It was observed that, between 10 wt. % and 30 wt. %, the viscosity for all size classes is fairly constant at 1 cP. However, between 30 wt. % and 50 wt. %, the viscosity increases for all size classes. It can be seen that particle size has a significant influence on viscosity. The sub 53 µm particle size has higher viscosity values than the other size classes, tested above 50 wt. % solids concentration. The viscosity values decrease with size and the inflection point shifts from 50 wt. % to 60 wt. % for the other size classes.

Within the range of particle sizes investigated, the smaller size classes seem to be more rheologically complex than the higher size classes. This is because, for the lower size classes, the

point of inflection occurs at lower solids concentration by weight than in the higher size class. This could be attributed to the fact that finer particles are more prone to agglomeration and aggregation than coarse particles (Mingzhao, et al., 2004). A higher surface area in smaller particles leads to a reduction in the free fluid thus increasing the solid concentration (He et al., 2004). However, this contradicts the findings of Clarke (1967), which revealed that slurry viscosity increased with particle size class. He attributed his findings to inertial effects, which resulted in higher energy dissipation.

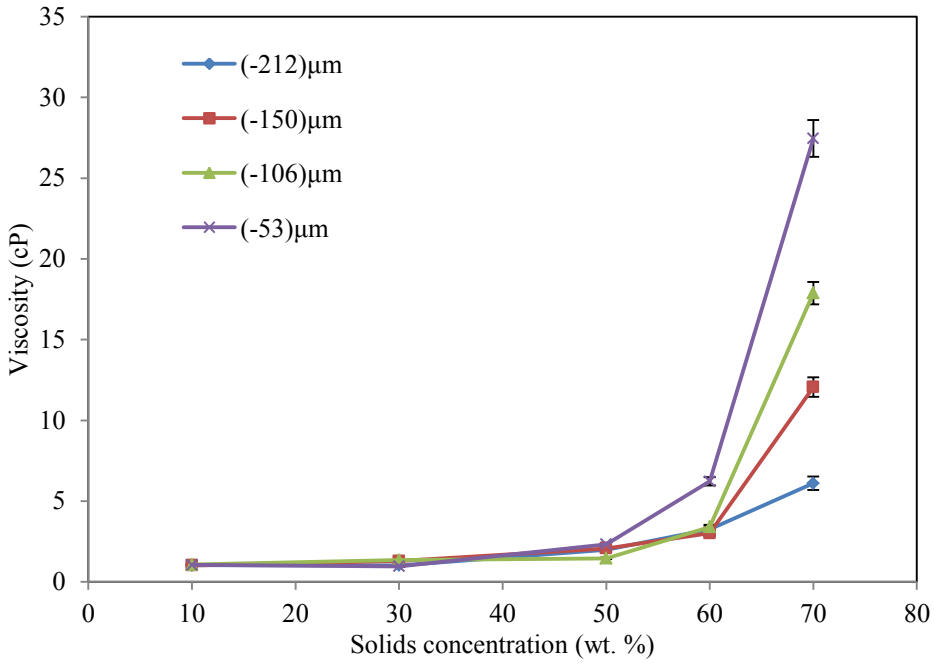

Figure 5-8: Effect of solids concentration on viscosity for different size classes

Table 5-3: Model R2 values and viscosities for UG2 at different size classes

Size class (µm)	Solids concentration (%)	Viscosity (cP)	R^2
-212	10	1.03	0.991
	30	1.02	0.961
	50	2.00	0.977
	60	3.01	0.985
	70	6.11	0.995
-150	10	1.03	0.995
	30	1.29	0.987
	50	1.46	0.993
	60	3.25	0.996
	70	12.06	0.986
-106	10	1.08	0.997
	30	1.35	0.996
	50	2.08	0.986
	60	3.40	0.997
	70	17.88	0.998
-53	10	1.06	0.999
	30	1.48	0.997
	50	2.33	0.991
	60	6.22	0.999
	70	27.46	0.946

5.4. Impact of both solids concentration and particle size class on viscosity

To evaluate the variation of the viscosity at different solids concentrations and particle size classes, a 3D surface plot shown in Figure 5-8 was generated. For the range of feed solids concentrations investigated and the particle size classes, it is observed that at the viscosity is more sensitive at smaller size classes and higher feed solids concentrations by weight.

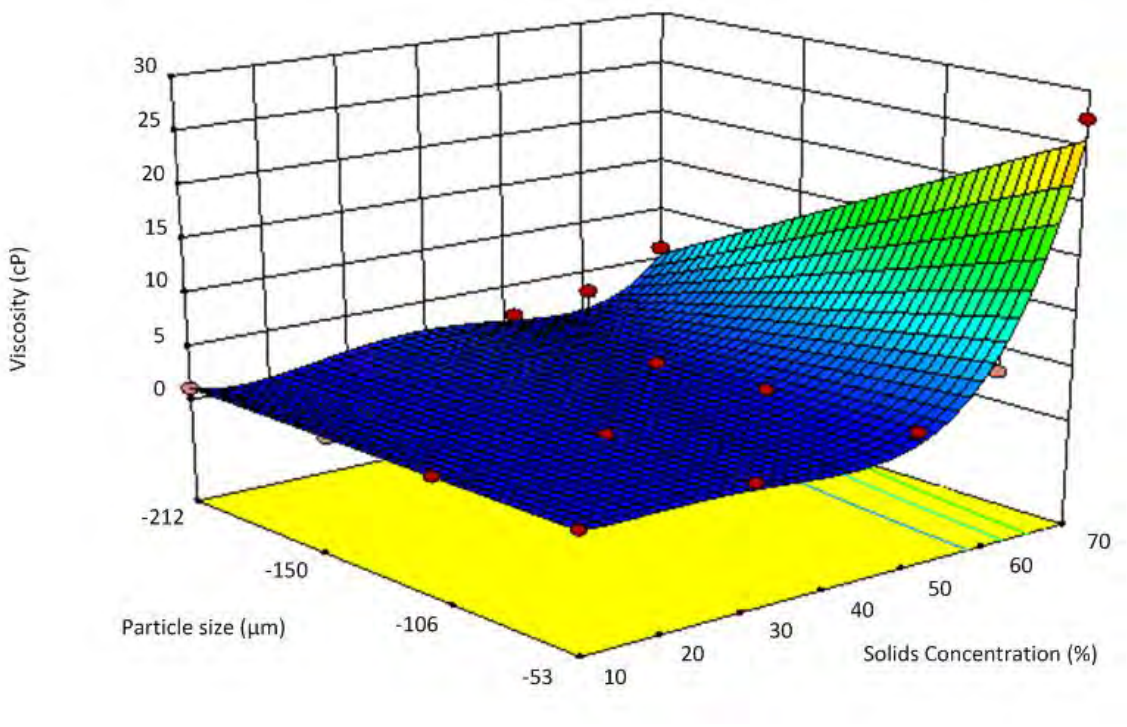

Figure 5-9: 3D surface plot for viscosity as a function of solids concentration and particle size classes for UG2 ore

5.5. Effect of viscosity on hydrocyclone performance

Slurry rheology is known to have an influence on the performance of wet comminution devices like hydrocyclones (Tavares , et al., 2002). This section of the report presents results, which illustrate the effects of rheology for UG2 and iron ore classification at the conditions tested. The error bars shown in these results are indications of the standard error of the mean about each point. For tests that were not done in triplicate the error was generalized from the treatment of the triplicates.

5.5.1. Effect of viscosity on hydrocyclone cut size

The effect of the slurry viscosity for both the UG2 and iron ore on the cut size were assessed (see Figures 5-12 and 5-13). For both ores, it is observed that the cut size increases with viscosity for all the hydrocyclone cone ratios investigated. This is attributed to the fact that, as the viscosity of the fluid increases, rotational motion of the slurry is retarded (Plitt, 1976) because particle interaction is increased; this results in hindered settling and hindered discharge through the spigot, which in turn results in coarser particles being misplaced to the overflow stream, thus

increasing the cut size (Asomah, 1996). These results are in conformity with what was observed by Shi et al., (1999), who did test work on lead and zinc based slurries, as well as by Salopek et al., (1995), who carried out tests using a 25 mm diameter cyclone with fine grinded limestone as the feed media. (Waters, 2012) also observed an increase in cut size with viscosity when he carried out tests on a plat reef and copper based ore using 4 inch Multotec cyclone.

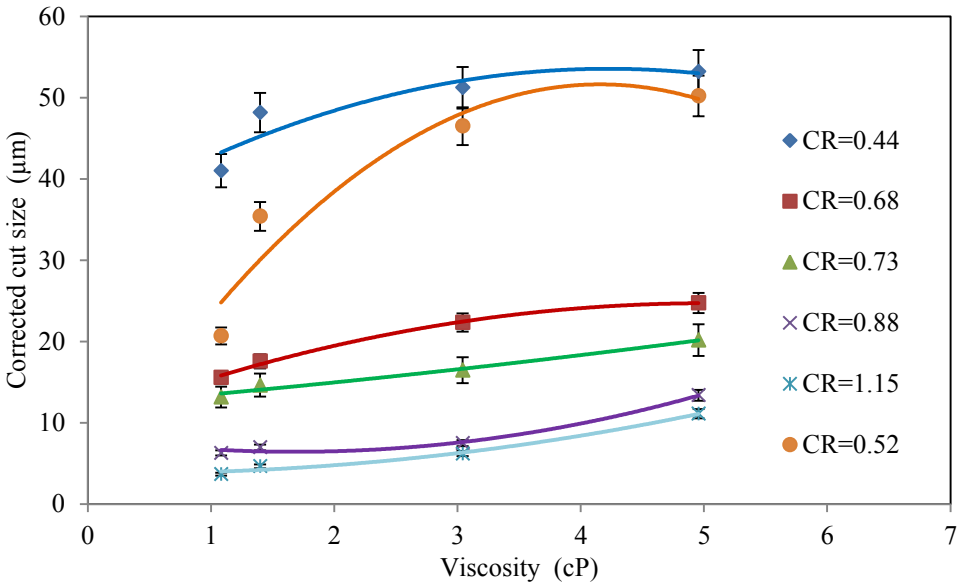

Figure 5-10: Effect of viscosity on the corrected cut size for UG2 ore

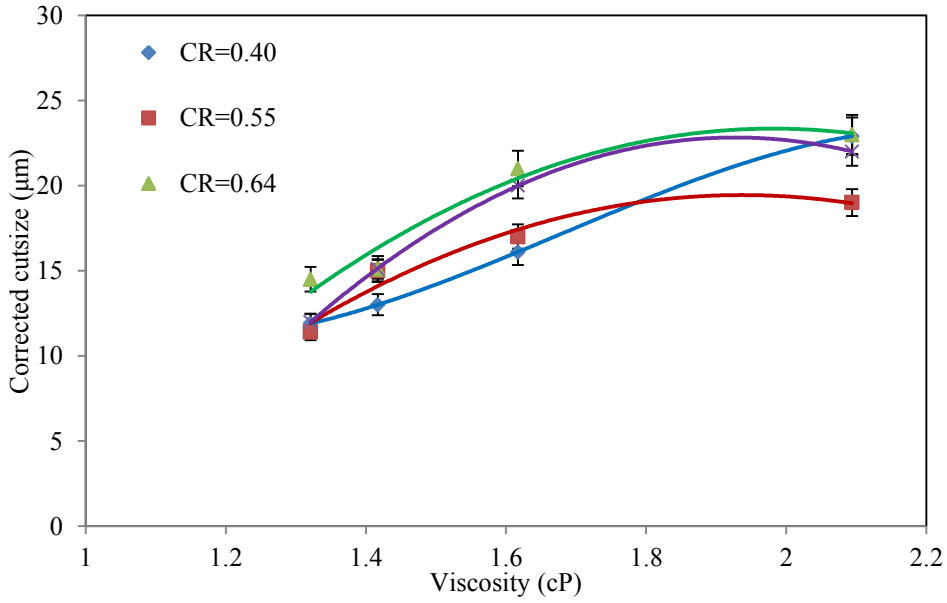

Figure 5-11: Effect of viscosity on the corrected cut size for iron ore

5.5.2. Effect of viscosity on hydrocyclone water recovery

The effect of the slurry viscosity on the water recovery to the underflow is illustrated in Figures 5-12 and 5-13 for UG2 and iron ore respectively. For both ore types, it was observed that the water recovery increased with viscosity for all cone ratios investigated. However, the increase in water recovery is more pronounced for the test work done using UG2 ore. It can be concluded that, for UG2 ore, viscosity has a more significant influence on water recovery to the underflow than it does for iron ore, within the range of experimental conditions investigated. This phenomenon can also be attributed to the same phenomenon, which pertained to the increase in cut size with viscosity. As the slurry viscosity increases, hindered settling and hindered discharge occurs through the spigot. This results in the decrease in the size of the air core, which in turn results in more fluid reporting to the underflow stream, thus increasing the water recovery (Braun, 2004). These results are in agreement with the work that was done by several authors, namely Asomah (1996), Shi et al., (1999), and Waters (2012).

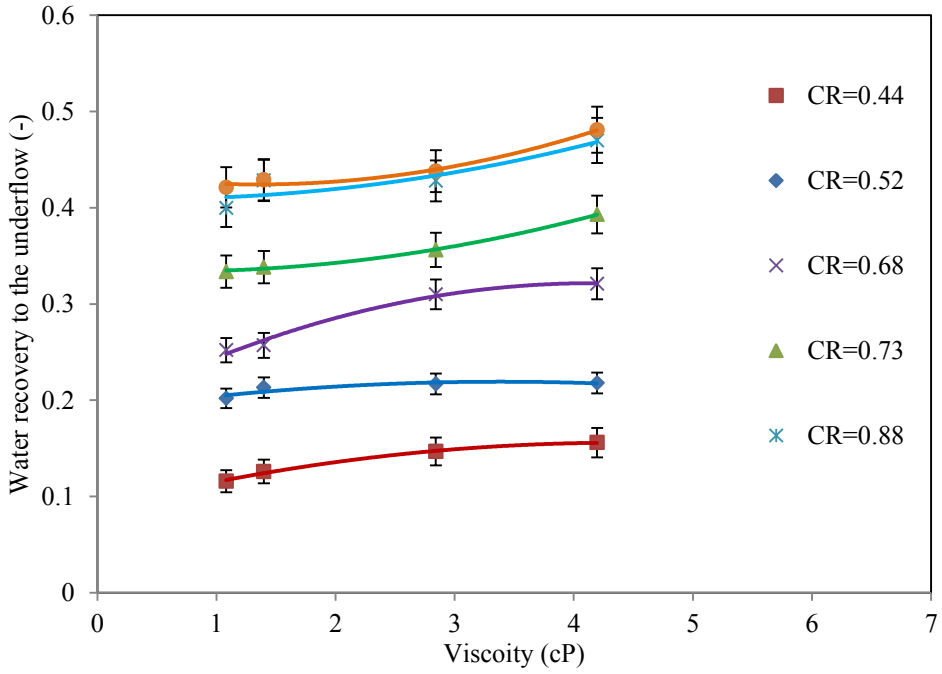

Figure 5-12: Effect of viscosity on water recovery for UG2 ore

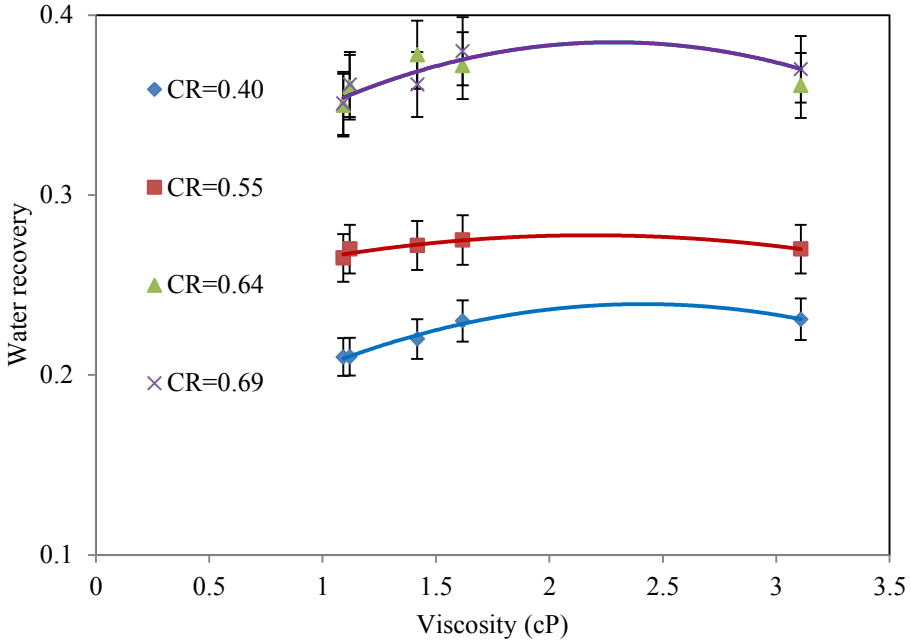

Figure 5-13: Effect of viscosity on water recovery for iron ore

5.5.3. Effect of viscosity on hydrocyclone sharpness of separation

The effect of viscosity of the hydrocyclone sharpness of separation is shown in Figures 5-14 and 5-15 for UG2 and iron ore respectively. For both ore types, it was observed that the sharpness of separation increased with viscosity for the range of conditions investigated. However, the increase in the sharpness of separation with viscosity was more pronounced in the test work done using iron ore. It can be concluded that, within the design space investigated, the viscosity has a greater influence on the sharpness of separation of the iron ore than it does in relation to the UG2 ore. This could have been attributed to the difference in ore properties or the cyclone types and geometries used for the two different ore types. These results are in agreement with the observations of Asomah (1996).Waters (2012) also observed an increase in the sharpness of separation with viscosity on the test he did using plat reef and copper based ores.

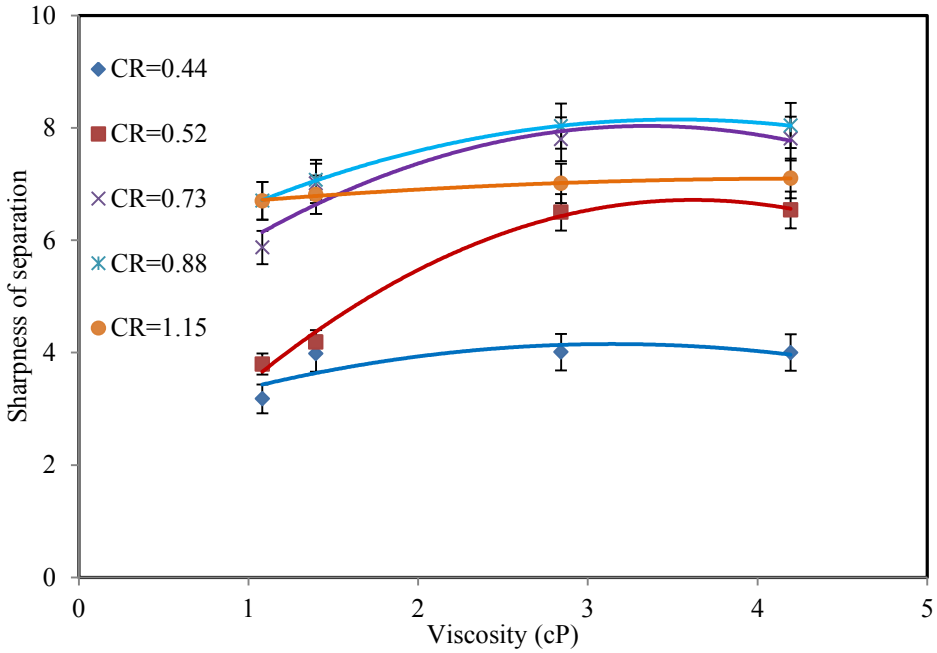

Figure 5-14: Effect of viscosity on sharpness of separation for UG2 ore

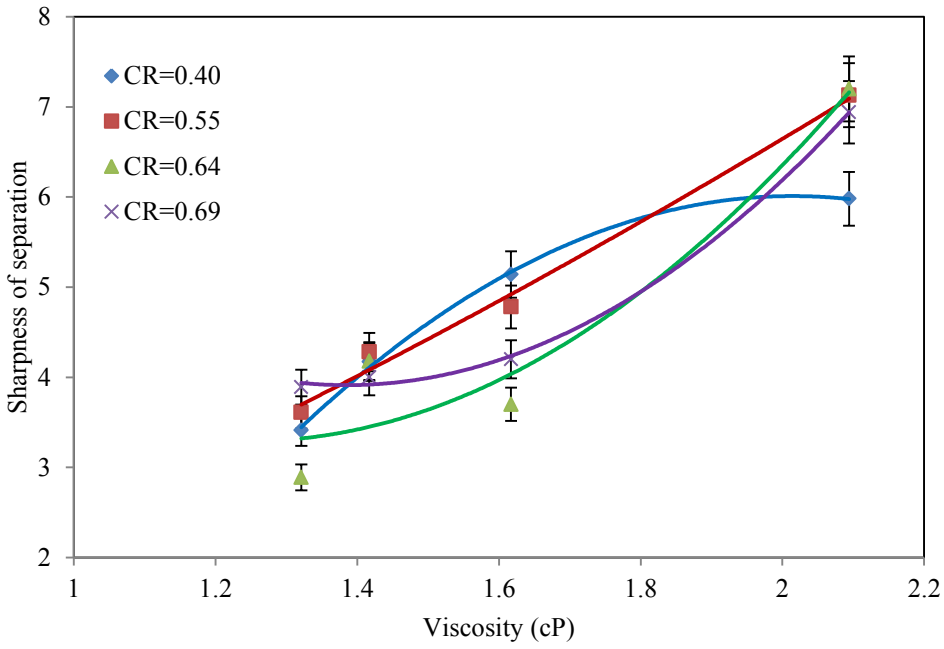

Figure 5-15: Effect of viscosity on sharpness of separation for iron ore

5.6. Reproducibility of rheological experiments

In order to determine the reliability of the measurements taken during the rheology experimental work, all measurements were performed in triplicate. Figure 5-16 illustrates rheograms at 46 wt. % solids for the cyclone feed. The graph shows that the data for Run 1, Run 2 and Run 3 are close together. The corresponding viscosities and R^2 values are presented in Table 5-4. It can be seen from the percentage errors in the calculated viscosities, that the findings are reproducible.

Table 5-4: Triplicate rheological characterization tests for UG2 ore

	Viscosity			
Run Number	**1**	**2**	**3**	**Error (%)**
10 wt. %	1.11	1.21	1.19	4.52
40 wt. %	1.67	1.71	1.65	1.82
60 wt. %	4.57	4.68	4.71	1.58
70 wt. %	10.8	10.7	10.4	1.96

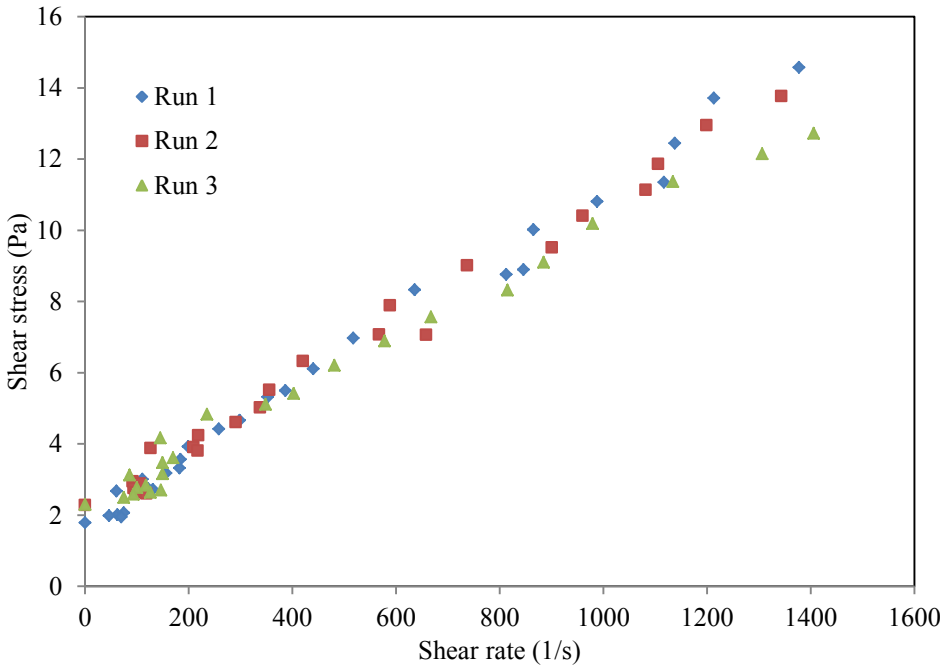

Figure 5-16: Rheograms for 46 wt. % solids for UG2 ore at 24˚C

Table 5-5: Triplicate rheological characterization tests for iron ore

	Viscosity			
Run Number	**1**	**2**	**3**	**Error (%)**
10 wt. %	1.01	1.08	1.1	4.44
20 wt. %	1.32	1.21	1.3	4.59
30 wt. %	1.42	1.44	1.47	1.74
40 wt. %	1.63	1.69	1.67	1.84
50 wt. %	2.09	2.01	2.21	4.79
60 wt. %	4.57	4.68	4.71	1.58
70 wt. %	10.1	10.7	10.4	2.88

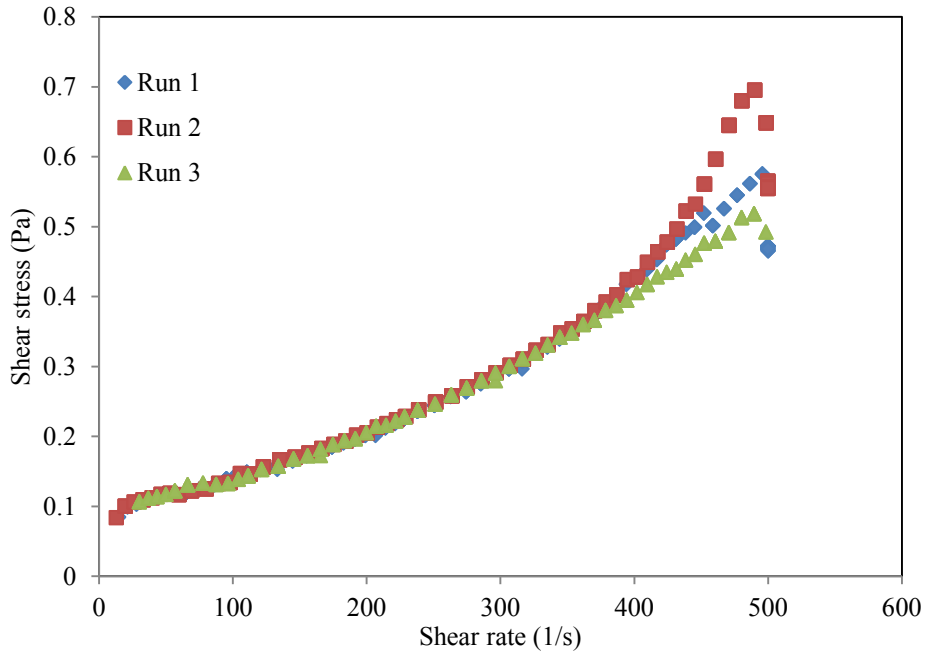

Figure 5-17: Rheograms for 20 wt. % solids for iron ore at 24˚C

CHAPTER 6: COMPARISON OF RESULTS TO A SEMI-MECHANISTIC MODEL

6.1. Introduction

This chapter of the thesis compares the results obtained during the test work to a semi mechanistic hydrocyclone model developed by Narasimha et al., 2014. This was done to determine if the results obtained can be predicted by the model. The model was developed using a dimensionless approach based on both fluid mechanics concepts from Computational Fluid Dynamics (CFD) and a wide range of industrial cyclone performance data (Narasimha et al., 2014). It consists of a set of equations for the water split to underflow (R_f), reduced cut-size (d_{50c}), throughput (Q) and sharpness of the separation (α). The respective equations for these parameters are highlighted in the Chapter 2 of the thesis.

6.2. Volumetric throughput

The cyclone throughput is an important variable as it affects the separation phenomenon Svarovsky, (2000). The variation of the predicted throughput and observed throughput for test work using both UG2 and iron ore is illustrated in Figure 6-1.

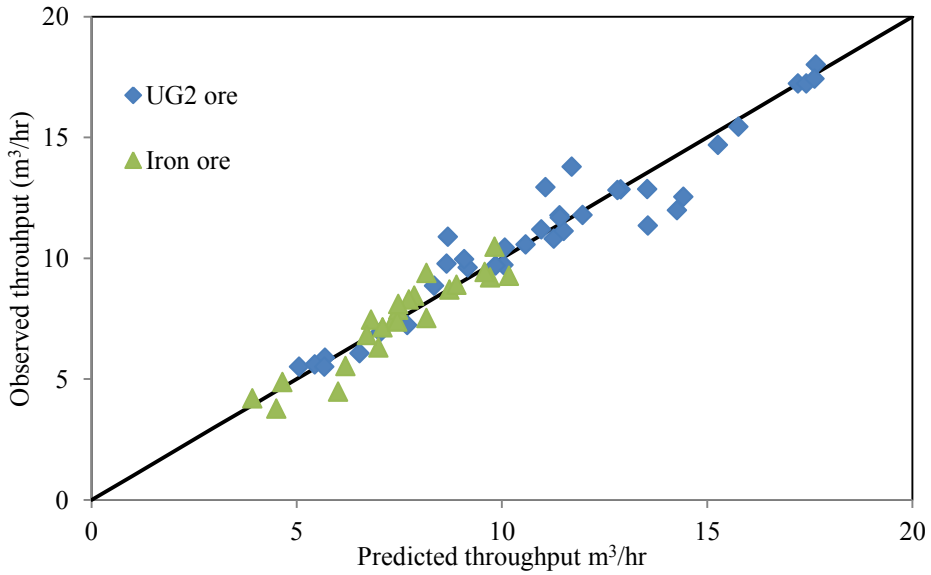

Figure 6-1: Correlation observed and predicted feed throughput

For the range of conditions investigated for the both the UG2 ore and iron ore, it was observed that the model matches the experimental data well. For the UG2 ore the standard error on the capacity was found to be 6.09% and that of iron ore was found to be 8.08%. This deviation is smaller from that which was quoted by the Narasimha et al., 2014 as 9.79% when they validated the model. It can be concluded that the model can predict the capacity of both the UG2 and iron ore for the range of conditions investigated. The model fitting constants are presented in Table 6-1

Table 6-1 : Model constants for Q_f

	k	a	b	c
UG2	0.000418	1.25	0.06	0.45
Iron ore	0.00483	1.25	0.06	0.45

6.3. Water recovery

The water recovery to the hydrocyclone is an important factor which affects the separation efficiency (Mainza, 2006). The variation of the predicted water recovery to the cyclone underflow and observed throughput for test work using both UG2 and iron ore is illustrated in Figure 6-2. For the range of tests investigated, it was observed that the good agreement between the measured and predicted results. The error associated with the UG2 was found to be 22.8% where as that of iron ore was found to be 21.7 %. Both these errors are lower than that observed by Narasimha et al., 2014 of 30 %. This means that the model can predict the results obtained within the design space investigated. The fitting constants are presented in Table 6-2.

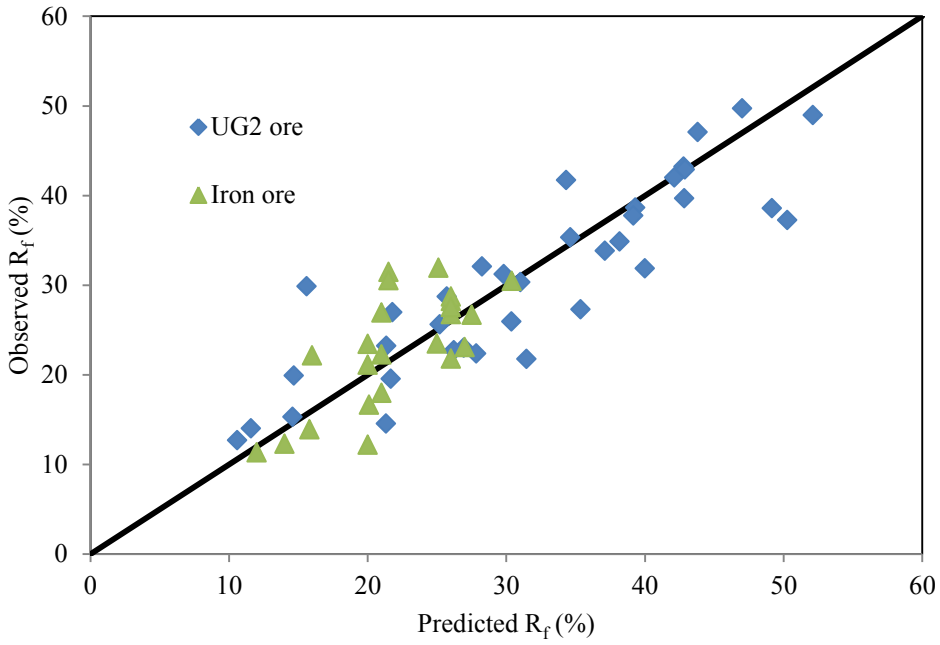

Figure 6-2: Correlation observed and predicted water recovery

Table 6-2: Model constants for R_f

	k	a	b	c
UG2	0.52	-1.068	-2.2062	-0.205
Iron ore	0.0045	-1.068	-2.2062	-0.205

6.4. Corrected cut size

The correlation between the observed and predicted cut size for the UG2 and iron ore is illustrated in Figure 6-3. For the both ore types it was observed that the model did not predict the cut size accurately. For the UG2 ore the associated error was 41 % and for iron ore 43%. This is a significantly larger error compared to that observed by Narasimha et al., 2014 of 19 %. This error could be attributed by the by the fact that there are distinct density difference between the components present in both the UG2 ore and iron. The UG2 consists of silicates with relative density of 2.80 and chromite with a relative density of 4.97 while iron ore consists of silicates as well with iron which has a relative density of 4.19 (Anglo-American (2013); Mainza, 2006). The model assumes an average particle density as this could be potentially the root cause of the discrepancy. Furthermore the model does not account for the fish hook effect and this was observed in the Iron ore test work. The fitting constants for the model are presented in Table 6-3

Table 6-3: Model constants for D_{50c}

	k	a	b	c	d
UG2	4.6-8.91	1.1026	-0.943	-0.71	-0.396
Iron ore	16.1-18.21	1.1026	-0.943	-0.71	-0.396

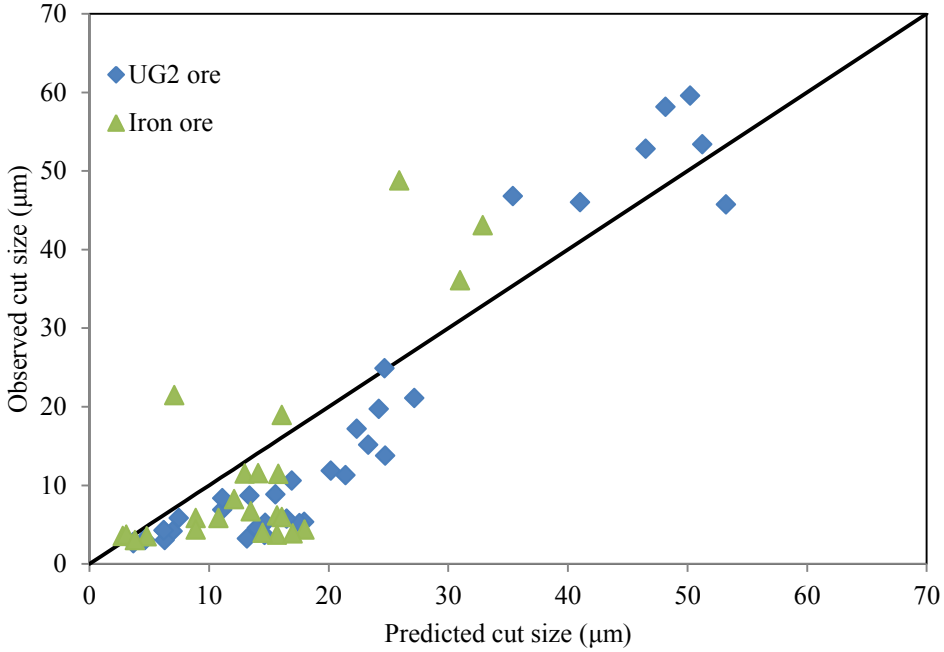

Figure 6-3: Correlation observed and predicted cut size

6.5. Sharpness of separation

The correlation between the observed and predicted alpha for the UG2 and iron ore is illustrated in Figure 6-4. It was observed that there was a scatter for both the UG2 and iron ore within the range of conditions investigated. The error associated with each was 21 % and 23 % for the UG2 and iron ore respectively. These standard errors are comparable to what was also observed by Narasimha et al., (2014). Who got a standard error of 23.4 % which is a significant decrease from that observed by in the model by Asomah (1996) of 41.5 %. The authors of the model acknowledged that more work still needs to be done on the model to decrease the standard error. The fitting constants were found to be between the ranges of (12-21) and (7.8-9.2) for UG2 and iron ore respectively.

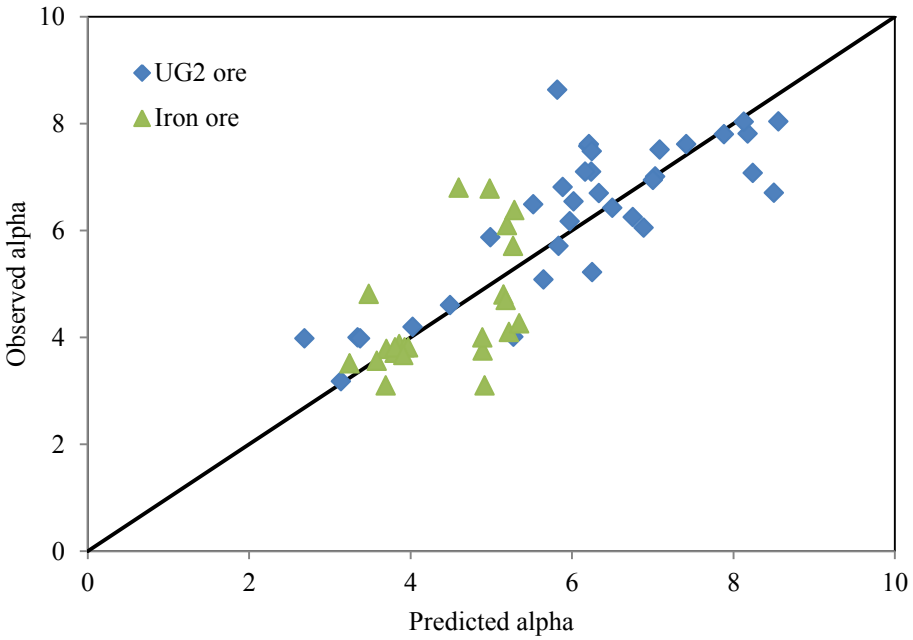

Figure 6-4: Correlation observed and predicted sharpness of separation

6.6. Viscosity

It is important to consider the slurry rheology to understand the separation mechanism within the hydrocyclone (He and Laskowski, 1994; Narasimha et al., 2007; Shi, 1994). The semi mechanistic model used takes in to account the equation that describes the viscosity as a function of solids concentration. It does not take into account any fine fraction of viscosity of slurries and it assumes a Newtonian behavior for all shear rates for a given system. Figure 6-5 illustrates the predicted and measured viscosity for the UG2 and iron within the design space investigated. It was seen that the model predicted the viscosity accurately for both the UG2 and iron ore, the respective standard errors where 11.5 % for UG2 ore and 6.2 % for iron ore. The standard error observed by the authors of the model was to be 23%. It can be concluded that the iron ore viscosity can be predicted more accurately than the UG2 ore within the design space investigated. This could be attributed to the difference in the particle characteristics within the two ores.

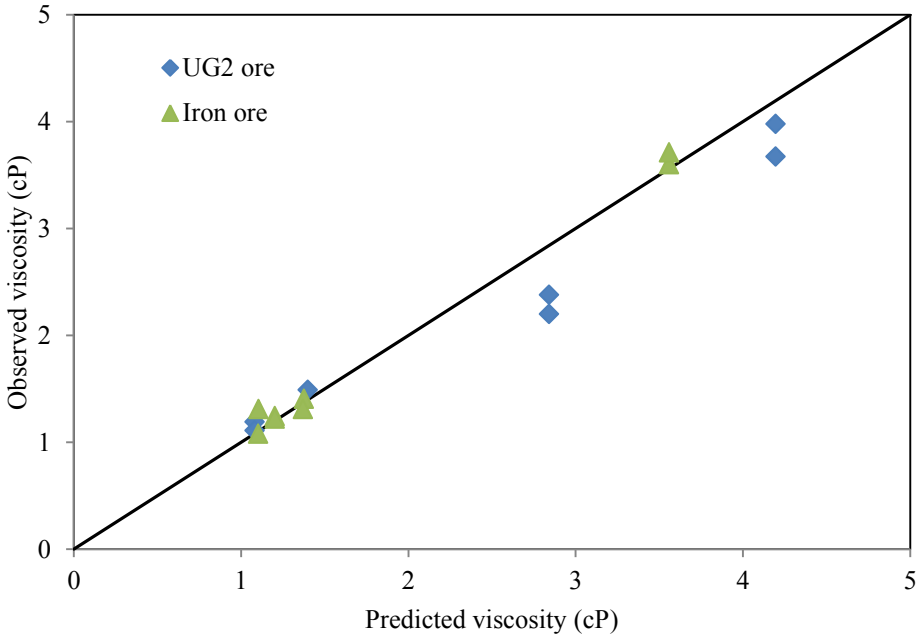

Figure 6-5: Correlation observed and predicted viscosity

6.7. Summary

The semi mechanistic model developed by Narasimha et al., 2014 showed a good fit for the volumetric throughput, water recovery and viscosity. The associated errors were comparable to the standard errors observed by the developers. However, the cut size, sharpness of separation model fit results showed higher standard errors than those observed by the authors of the model. It can be concluded that the semi mechanistic model can predict the volumetric throughput, viscosity and water recovery to the underflow fairly accurately for both ore types.

CHAPTER 7: CONCLUSIONS AND RECOMMENDATIONS

This chapter summarizes the main observations from the test work performed to assess the performance of the hydrocyclone at various cone ratios on both UG2 and iron ore. The main conclusions from the work are stated and recommendations to be considered for future work are given.

7.1. Key observations

The following observations were made from the hydrocyclone test work:

7.1.1. Water only tests

1. Water recovery to the hydrocyclone underflow increased as the spigot diameter increased. This is because as the spigot diameter increases, resistance to the flow of material near and through this port decreases, allowing for more water to report to the underflow stream.
2. Water recovery to the hydrocyclone underflow decreased with an increasing vortex finder diameter. This is because the resistance of the fluid flow around and through the spigot is increased and this results in more fluid exiting through the overflow port, thus decreasing amount reporting to the underflow.
3. Irrespective of the spigot to vortex finder combination used, the water recovery to the underflow increased with increasing cone ratio. At the lowest cone ratio investigated, viz. 0.3, the water recovery was 0.0325 and at the highest cone ratio of 0.73, the water recovery was found to be 0.339.

7.1.2. Test carried out on UG2 in a conventional cyclone

1. Increasing the vortex finder diameter at a constant spigot diameter resulted in a decrease in the water recovery to the underflow. However, increasing the spigot diameter while keeping a constant vortex finder led to an increase in the water recovery. The highest water recovery achieved was 0.49 at a vortex finder diameter of 0.026 m and a spigot diameter of 0.030 m, while the lowest water recovery of 0.18 was attained at a vortex finder diameter of 0.041 m and a spigot diameter of 0.018 m.

2. Increasing in the vortex finder diameter at the same spigot diameter resulted in coarsening of the cut size. Increasing the spigot diameter for the same vortex finder diameter resulted in a finer cut size. The highest cut size achieved was 53 μm at a vortex finder diameter of 0.042 m and a spigot diameter of 0.018 m, while the lowest cut size of 12 μm was achieved at a vortex finder diameter of 0.026 m and a spigot diameter of 0.030 m.
3. At the range of vortex finder diameters investigated, it was observed that sharpness of separation decreased slightly with an increase in the vortex finder diameter for spigot diameters of 30 and 23 mm. However at a spigot diameter of 18 mm the sharpness of separation increases slightly then declines.

7.1.3. Comparison of performance between conventional and flat bottom cyclone

1. The conventional cyclone had higher water recoveries between solids concentrations of 20% and 40%. However at 50% solids concentration, the flat bottom hydrocyclone had a higher water recovery.
2. The flat bottom was found to have a coarser cut size than the conventional cyclone under similar operating conditions and the same cone ratio. This is attributed to the absence of the conical section in the flat bottom cyclone resulting in the formation of eddies which leads to the displacement of coarser particles to the overflow.
3. At all the conditions investigated the conventional cyclone had a sharper separation than the flat bottom cyclone. This is also attributed to the absence of the conical section in the flat bottom cyclone.

7.1.4. Influence of cone ratio on separation performance

1. The water recovery to the underflow increased with increasing cone ratio for both the UG2 and iron ore. This is because decreasing the vortex finder reduces the amount of material that can leave the hydrocyclone via the overflow, thus forcing more of the fluid to the underflow; the same logic applies to increasing the size of the spigot.
2. For the UG2 ore, it was observed that the cut size decreased with an increase in the cone ratio. This can be explained by the equilibrium orbit theory which suggests that as the cone ratio increases, the LZVV decreases, causing the cut size to decrease. For iron ore, it

was observed that the cut size increased with an increase in the cone ratio, until it reached a peak at a cone ratio of approximately 0.68, before decreasing again. The cone ratios investigated range from 0.4 to 0.69. This indicates that the vortex finder or spigot has a significant contribution for cone ratios higher than 0.68.

3. It was observed for both ore types that the sharpness of separation increased with cone ratio. For the UG2 ore the sharpness of separation increased from cone ratio 0.4 till 0.88.
4. Increasing the cone ratio for both ore types led to an increase in the cyclone throughput. This is because as the cone ratio increases the spigot share of the ratio increases and this decreases the flow resistance within the cyclone allowing more throughput.

7.1.5. Influence of viscosity on separation performance

1. The UG2 ore viscosity inflection point occurred at a lower solids concentration than the iron ore for both the overflow and feed streams. This is because the UG2 ore is more rheologically complex than the iron ore.
2. A coarser feed size distribution shifted the viscosity inflection point to a higher solids concentration. This is because particle interaction is minimized in coarser particles.
3. Increasing the solids concentration (and viscosity) resulted in an increase in the water recovery to the underflow for both ore types. However, this was more pronounced for UG2 ore. The range of solid concentrations investigated was between 10 % and 55 % and 20 % and 50 % for iron ore and UG2 ore respectively
4. For both the UG2 ore and iron ore, an increase in the viscosity led to an increase in the cut size. This is because as the viscosity increased the rotational motion the slurry became retarded as a result of the increased particle interaction and this causes hindered settling and discharge through the spigot increasing the cut size.
5. The sharpness of separation tends to be higher at higher viscosities.

7.1.6. Comparison of results to a semi-mechanistic model

1. A good fit between the measured and model predicted values for the volumetric throughput, water recovery and viscosity was observed. The associated standard errors where comparable to those observed by the authors who developed the model. However there was scatter in the corrected cut size and sharpness of separation between the

measured and predicted values. This is because the model assumes an average density of particles which is not the case for the ore types investigated. Secondly the model does not take into account the fish hook phenomenon and this was observed on test work carried out using iron ore. Lastly the authors acknowledged that scatter in the alpha model results was observed during the development and detailed that it needs further refinement.

7.2. Conclusions

In addressing the hypotheses for this thesis, the following conclusions were drawn:

- For both UG2 and iron ore, the performance of the hydrocyclone can be altered by a change in the cone ratio. For UG2 ore increasing the cone ratio resulted in a decrease in the cut size while an increase in cone ratio led to an increase in the cut size for iron ore. It can be concluded that the equilibrium orbit theory which suggests as the cone ratio increases, the R_{LZVV} decreases, causing the cut size to decrease can be applied to the UG2 ore but not to the iron ore. Furthermore, increasing the cone ratio led to an increase in water recovery, sharpness of separation and throughput for both ore types.
- Even though the viscosity increases with increasing solid concentration, it only becomes a problem in the cyclones when the solid concentration is close to the inflection point, where the flow characteristics are less predictable and difficult to control. It was observed that within the conditions investigated an increase in viscosity led to an increase in the cut size, water recovery and a sharper separation.
- For the same solid concentrations and operating conditions, a flat bottom cyclone classifying UG2 gave a coarser cut size and reduced water recovery, thus producing a denser underflow. This is because the in a flat bottom cyclone, the absence of the conical section creates a ‘T-piece’ and the bottom of the cyclone which generates eddies within the cyclone which result in coarse particles reporting to the overflow stream.

7.3. Recommendations for future work

For future work on the assessment of the effects of cone ratio, feed solids concentration and viscosity on hydrocyclone performance, the author proposes the following:

- At the various cone ratios and solid concentrations investigated, the pressure should be kept constant. This is because the inlet pressure affects the centrifugal force, which

initiates separation. Thus comparing different cone ratios and solid concentrations operated at a similar pressure will be a better proxy.

- Scanning electroscope microscope (SEM) images of the ores used should be generated. This will be able to determine the shapes of the particles and confirm the hypothesis that, despite the iron ore being finer, the UG2 ore is more rheologically complex, because the UG2 particles are spherical in shape, whereas the iron ore particles are narrow and rectangular.
- In order to assess the cyclone performance in greater detail, it is recommended to generate flow field and turbulence field information. Furthermore, an elegant approach such as CFD or flow visualization techniques should be used to analyse the flow reversal pattern within the cyclones.
- Using a coarser ore will enable the use of screens during particle size distribution analysis, thus allowing different size classes to be obtained, which can be assayed for the different minerals. This will help in evaluating the effect of cone ratio on the individual deportment of silicates, and chromite (UG2 ore) and silicates and iron (iron ore) to the underflow and overflow streams of the hydrocyclone.
- The author recommends that further tests should be carried out for an iron ore beyond the cone ratio of 0.69. This was not done in this work because the facility where these experiments were carried out did not have the vortex finder and spigot diameters to facilitate this test work.

8. REFERENCES

Agar, G. E. & Herbst, J. A., 1966. The effect of fluid viscosity on cyclone classification. *Transactions of AIME,* Volume 235, pp. 145-149.

Asomah, I., 1996. *Improved Models of Hydrocyclones,* Queensland: University of Queensland.

Asomah, I. & Napier-Munn, T. J., 1996. An empirical model of hydrocylones incorporating angle of inclination. *Minerals Engineering,* 10(3), pp. 339-347.

Banerjee, C., Suresh, Majumder & Verma, 2013. Effect of Variables on Water Split Behavior in hydrocyclones. *International Journal of Scientific Research,* 2(4), pp. 9-16.

Barnes , H. A., Hutton, J. F. & Walters, K., 1998. *An Introduction to Rheology.* 3 ed. London: Elsevier.

Becker, M. et al., 2013. A rheological investigation of the behaviour of two Southern African platinum ores. *Minerals Engineering,* Volume 49, pp. 92-97.

Bradley, D., 1958. Flow patterns in the hydraulic cyclone and their interpretation in terms of performance. *Trans.Inst.Chem.Eng,* pp. 99-123.

Bradley, D., 1965. *The Hydrocyclone.* London: Pergamon Press.

Braun, T., 2004. Influence of feed solids concentration on the performance of hydrocyclones. *Chemical Engineering Technology,* Issue 13, pp. 15-20.

Bretney, E., 1891. USA Patent. *453105*.

Brujin, D., 1951. Ethanol separation from organic process streams in the chemical industry. *Delft: Tu Delft.*

Castro, O., 1990. *An investigation of pulp rheology effects and their applications to the dimensionless type hydrocyclone models,* Queensland: The University of Queensland.

Chaponda, B., 2011. *Effect of operating variables on IsaMillTM performance using Platinum bearing Ores. MSc. Thesis,* Cape Town: University of Cape town.

Cilliers, J. J. & Hinde, A. L., 1991. An improved hydrocyclone model for backfill preparation. *Minerals Engineering,* 4(11), pp. 683-693.

Cilliers, J. R., 1994. *Modelling and fault diagnosis of backfill hydrocyclones,* Cape Town: University of Cape Town.

Clarke, B., 1967. Rheology of coarse settling suspensions. *Transt Institute of Chemical Engineering,* Volume 45, pp. 251-256.

Concha, F., Barrientos, A., Montero, J. & Sampaio, R., 1996. Air core and roping in hydrocyclones. *International Journal of Mineral processing,* Volume 45, pp. 743-749.

Criner, H. E., 1950. Hydrocyclone classification theory. *Rev.Industrial Mining,* Issue 4, p. 449.

Dahlstrom, D. A., 1954. Fundamentals and applications of the liquid cyclone. *Chemical Engineering Progress, Sympossium series,* Issue 15, p. 50.

Driessen, M. G., 1951. Theories of Separation. *Minerals Engineering ,* pp. 550-563.

Dyakowski, T., 1995. Process tomography applied to multi-phase flow measurement. *Science and Technology,* Volume 7, pp. 343-353.

Elsayed, K. & Lacor, C., 2010. The Effect of Vortex Finder Diameter on Cyclone Separator Performance and Flow Field. *European Conference on Computational Fluid Dynamics,* pp. 17-23.

Fahlstroem, P., 1963. *Studies of a hydrocyclone as a classifier.* Canees, Mineral processing congress.

Feng, D. & Aldrich, C., 1999. Effect of particle size on flotation performance of complex sulphide ores. *Minerals Engineering, 12(7): 721 - 731.*

Fuerstenau , M. C. & Han, K. N., 2003. *Principles of Mineral Processing.* 1st ed. Littleton Colarado: Society for Mining , Metallurgy , and exploration , Inc.

Fuerstenau, D. W., De, A. & Kapur, P. C., 2004. Linear and nonlinear particle breakage processes in comminution systems. *International Journal of Mineral Processing, 74: 317 - 327.*

Fuerstenau, M. C. & Han, N. K., 2003. *Principles of Mineral Processing.* 1st ed. Colarado: SME.

Goyal, A., Papiya, R. & Banerjee, P. K., 2010. Effect of air core on flow rate and split in hydrocyclones. *Mineral Processing Technology,* p. 124–131.

He , Y. B. & Laskowski, J. S., 1994. *12th International Coal preparation.* Cracow, s.n.

He, M. & Forssberg, E., 2007. Influence of slurry rheology on stirred media milling of quartzite. *International Journal of Mineral Processing,,* pp. 84: 240 - 251.

Hesham, M. & Batsh, E., 2013. Improving cyclone performance by proper selection of the exit pipe. *Applied Mathematical Modelling,* Volume 37, pp. 5286-5303.

Hoffman, H. A., 1962. Coverting Gravity-Flotation plant to All-Flotation. *Minerals Benefication,* pp. 121-138.

Horsley, R. R. & Allen, D. W., 1987. *The effect of yield stress on hydrocyclone performance in the mining industry.* Oxford , International conference on hydrocyclones.

Hotta, Y. & Yoshioka, N., 1955. Liquid cyclone as a hydraulic classifiers. *Chemical engineering,* Issue 19, pp. 632-640.

Hsieh, K. T. & Rajamani, K., 1991. Phenomenological model of the hydrocyclone based on the physics of fluid flow. *American Institute of Chemical Engineers,* Volume 37, pp. 735-746.

Irannajad, M., 2009. *Validation of proposed methods.* Tehran, Mining and Metallurgical Engineering.

Kawatra, S. K., Bakshi, A. k. & Rusesky, M. T., 1996. The effect of slurry viscosity on hydrocyclone classification. *International Journal of Mineral Processing ,* Volume 48, pp. 39-50.

Kelsall, D. F., 1952. A study of the motion of solid particles in a hydraulic cyclone. *Transactions of the Institution of Chemical Engineers ,* 30(1), pp. 87-107.

Kilavuz, F. S. & Gulsoy, O. Y., 2011. The effect of con ratio on the separation efficiency of small diameter hydrocyclones. *International Journal of Mineral Processing ,* Volume 98, pp. 163-167.

King, R., 1982. Flotation of fine particles. In: *Principles of flotation.* Johannesburg: South African Institute of Mining and Metallurgy, pp. 215-225.

King, R. P., 2001. *Modeling and simulation of mineral processing systems.* Oxford: Butterworth-Heinemann.

Klimpel, R., 1997. *Instructional module on introduction to the principles of size reduction of particles by mechanical means.* 1st ed. Florida: NSF Engineering Center for Particle Science and Technology.

Lilge , E. O., 1962. Hydrocyclone fundamentals. *Institution of mining and Metallurgy,* pp. 285-335.

Lusinga, D., Angombe, J. & Mainza, A. N., 2009. Assessing the effects of the cone force ratio on the performance of hydrocyclones. *The Journal of The Southern African Institute of Mining and Metallurgy,* Volume 109, pp. 239-244.

Lynch, A. J. & Rao, T. C., 1968. Studies on the operating characteristics of hydrocyclone classifier. *Mining and metallurgical engineering,* Volume 6, pp. 106-114.

Lynch, A. J., Rao, T. C. & Bailey, C. W., 1975. The influence of design and operating variables on the capacity of hydrocyclone classifiers. *International Journal Mineral Processing,* Volume 2, pp. 29-37.

Lynch, A. J. & Rowland , C. A., 2005. *The History of Grinding.* Colarado: Society for Mining ,Metallurgy and Exploration. Inc, (SME).

Magwai, M. K. & Bosman, J., 2008. The effect of cyclone geometry and operating conditions on spigot capacity of dense medium cyclones. *International Journal of Mineral Processing,* Volume 86, pp. 94-103.

Mainza, A. N., 2006. *Contribution to the understanding of the three product cyclone on the classification of a dual density platinum ore,* Cape Town: University of Cape town.

Mainza, A. N., Powell, M. S. & Knopjes, B., 2005. A comparison of different cyclones in addressing challenges in the classification of the dual density UG2 platinum ore. *The Journal of The South African Institute of Mining and Metallurgy,* Volume 106, pp. 341-348.

Mainza, A., Powell, M. S. & Knopjes, B., 2004. Differential classification of dense material in a three product cyclone. *Minerals Engineering,* pp. 537-579.

Majumder, A. K., Shah, H., Shukla, P. & Barnwal, J. P., 2007. Effect of operating variables on shape of fish hookcurves in cyclones. *Minerals Engineering,* 2(20), pp. 204-206.

Mangesana, N., 2011. *Developing a methodology for characterising in-situ viscosity profiles in tumbling mills,* Cape Town : University of Cape Town (MSc Thesis).

Marthinussen, S. A., 2011. *The effect of fluid viscosity on hydrocylone performance,* Bergen: University of Bergen.

Mingzhao, H., 2005. *Slurry rheology of limestone and its effects on wet ultra fine grinding,* s.l.: Lulea University of Technology.

Mingzhao, H., Yanmin, W. & Forssberg, E., 2004. Slurry rheology in wet ultrafine grinding of industrial minerals. *Powder Technology,* Volume 147, pp. 94-112.

Muster, T. H. & Prestidge, C. A., 1995. Rheological investigations of sulphide mineral slurries. *Minerals Engineering,* 8(1), pp. 1541-1555.

Nageswararao, K., 2000. Reduced efficiency curves of industrial hydrocyclones-an analysis for plant practice. *Minerals Engineering,* 5(12), pp. 517-544.

Nageswararao, K., Wiseman, D. M. & Napier-Munn, T. J., 2004. Two empirical hydrocyclonemodels revisted. *Minerals Engineering,* Volume 17, pp. 671-687.

Napier-Munn, T. J., 1980. Particle segregation in hydrocyclones. *SME,* pp. 689-701.

Napier-Munn, T. J., Morell, S., Morrison, R. D. & Kojovic, T., 2005. *Mineral Comminution Circuits: Their Operation and Optimisation.* Brisbane: : Julius Kruttschnitt Mineral Research Centre.

Napier-Munn, T. J., Morrell, S. & Morrison, R. D., 2005. *Mineral Comminution Circuits.* 1st ed. Queensland: JKMRC.

Narasimha, 2010. *A phenomenological model of the hydrocyclone,* s.l.: s.n.

Narasimha, M., Brennan, M. S. & Holtham, P. N., 2007. A review of CFD modelling for performance predictions of hydrocyclones. *Minerals Engineering,* pp. 109-125.

Narasimha, M., Mainza, A. N. & Holtham, P. N., 2012. *Multi-component modelling concept for hydrocyclone classifier.* New Delhi, IMPC.

Narasimha, M. et al., 2014. A semi-mechanistic model of hydrocyclones-Developed from industrial data and inputs from CFD. *International Journal of Mineral Processing,* Issue 133, pp. 1-12.

Obeng, D. P. & Morrell, S., 2003. The JK three-product cyclone performance and potential applications. *International Journal of Mineral Processing,* Volume 69, pp. 129-142.

Paterson, A. J. C., 2004. High density slurry and paste tailings, transport systems. *The South African Institute of Mining and Metallurgy, 159 - 166.*

Periccleous, K. A., Rhodes, N. & Cutting, G. W., 1984. *A mathematical model for predicting the flow field in a hydrocyclone classifier.* s.l., s.n.

Plitt, L. R., 1976. A mathematical model of the hydrocyclone classifier. *Cim Bulletin,* pp. 114-123.

Rietema, K., 1960. The performance and design of hydrocyclones as a classifier. *Chemical engineering science,* Issue 15, pp. 298-302.

Salopek, P., 1995. *Rheological properties of aqueous solutions.* Chicago, s.n.

Schmidt, M. P. & Turner, P. A., 1993. *Flat bottom or horizontal cyclones-which is right for you ?*. s.l., World mining equipment.

Shah, H., Majumder, A. K. & Barnwal, J. P., 2006. Development of watersplit model for a 76 mm hydrocyclone. *Minerals Engineering,* Volume 19, pp. 102-104.

Shi, F., 1994. *Slurry rheology and its effects on grinding,* Queensland: Julius Kruttschnitt Mineral Research Centre.

Shi, F. et al., 2009. Comparison of energy efficiency between ball mills and stirred mills in coarse grinding. *Minerals Engineering, 22: 673 - 680.*

Shi, F. N. & Napier-Munn, T. J., 1996. A model for slurry rheology. *Minerals Engineering,* pp. 481-492.

Shi, F. N., Napier-Munn, T. J. & Asomah, I. K., 2010. Rheological effects in grinding and classification. *Mineral Processing and extractive Metallurgy,* 20(1), pp. 123-131.

Smith, M. R. & Gochin, R., 1984. Classifiers Part 1: An introduction to theory and practice.. *Mining Magazine,* pp. 27-39.

Svarovsky, L., 2000. *Solid-Liquid Separation.* 4th ed. Oxford: Butterworth-Heinemann.

Tarr, D. T., 1985. Hydrocyclones. In: N. L. Weiss, ed. *Mineral Processing Handbook.* New York: SME , pp. 3D-10-3D-45.

Tarr, D. T., 1998. Hydrocyclones. *SME,* Volume 4.

Tavares , L. M., Souza, L. G., Lima, J. B. & Possa, M. V., 2002. Modelling classification in small-diameterhydrocyclones under variable rheological conditions. *Minerals Engineering,* Volume 15, pp. 613-622.

Tongsiri, S., 2007. *The simulation of hydrocyclone network for separating yeast and calcium in ethanol production,* Bangkok: University of North Bangkok .

Trawinski, H. F., 1969. *Practical aspects of the design and industrial applications of the hydrocyclone,* Loughbough: Loughbough University.

Waters, J., 2012. *The influence of slurry viscosity on hydrocylone performance,* Cape Town: University of Cape Town.

Waters, J., Mainza, A. & Indresan, 2014. *A rheological comparison of concentrator slurry streams.* Cape Town , IMPC.

Wills, B., 1997. *Mineral Processing Technology.* London: Butterworth-Heinemann.

Wills, B. A. & Napier-Munn, T. J., 2006. *Mineral Processing Technology.* 7th ed. Queensland: Elsevier Science and Technology Books.

APPENDIX: A

Partition Curves UG2 ore

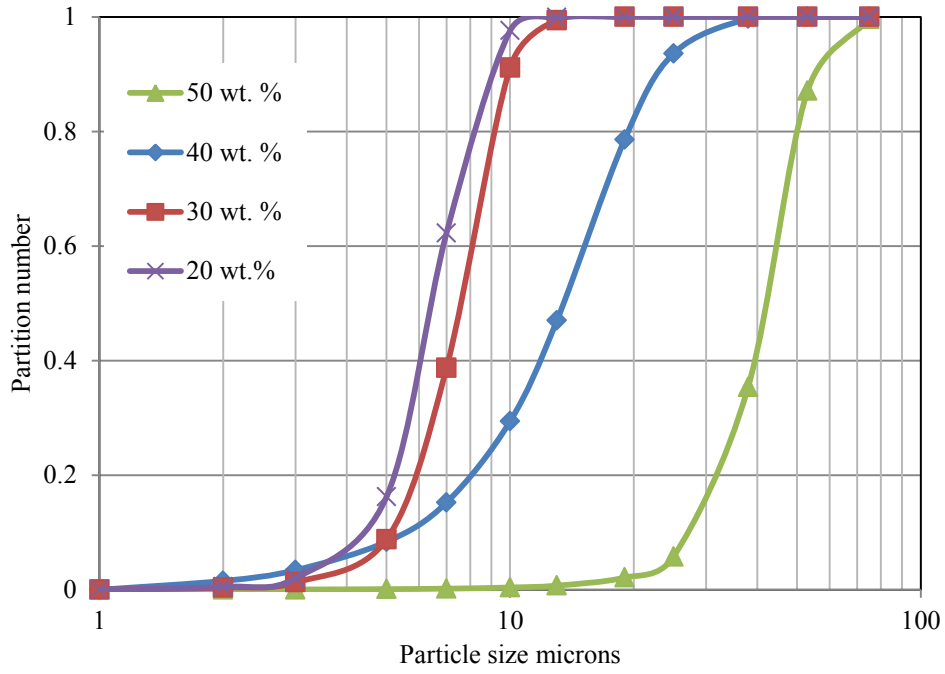

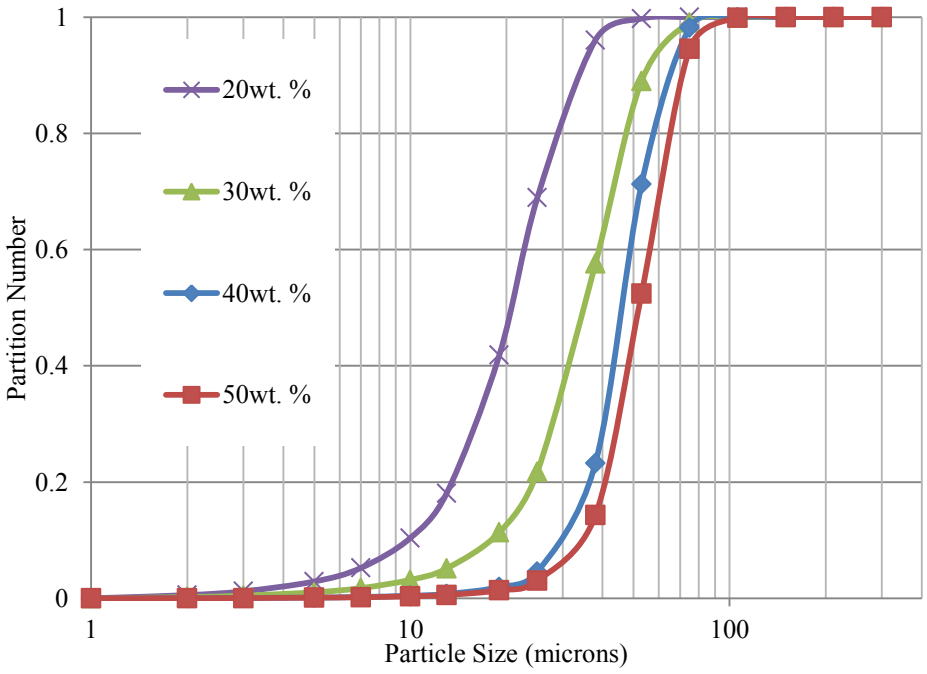

Partition Curves iron ore

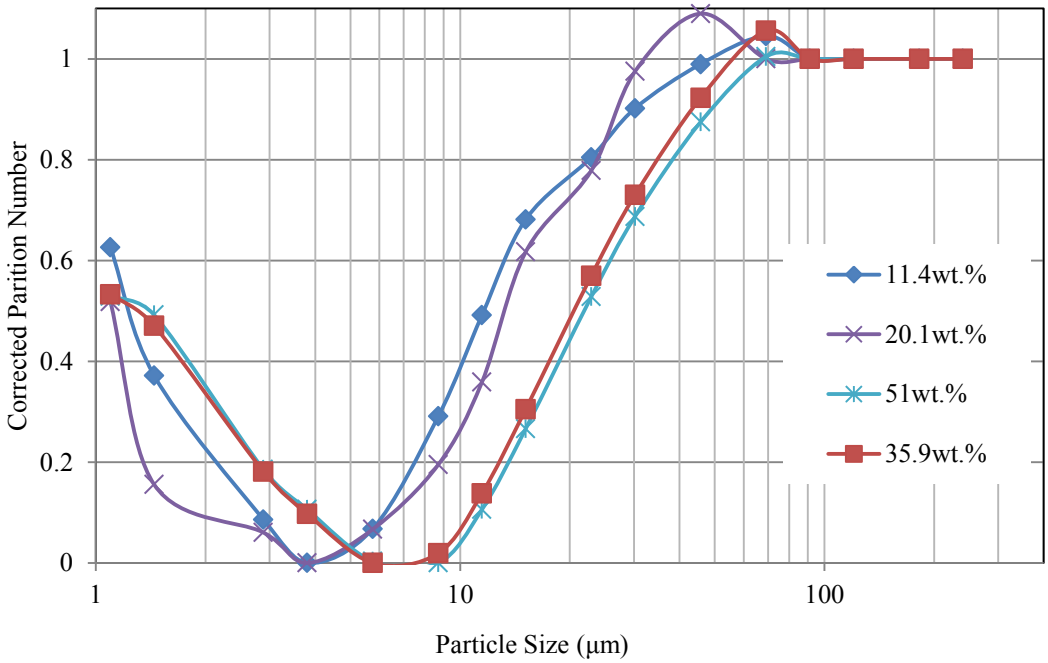

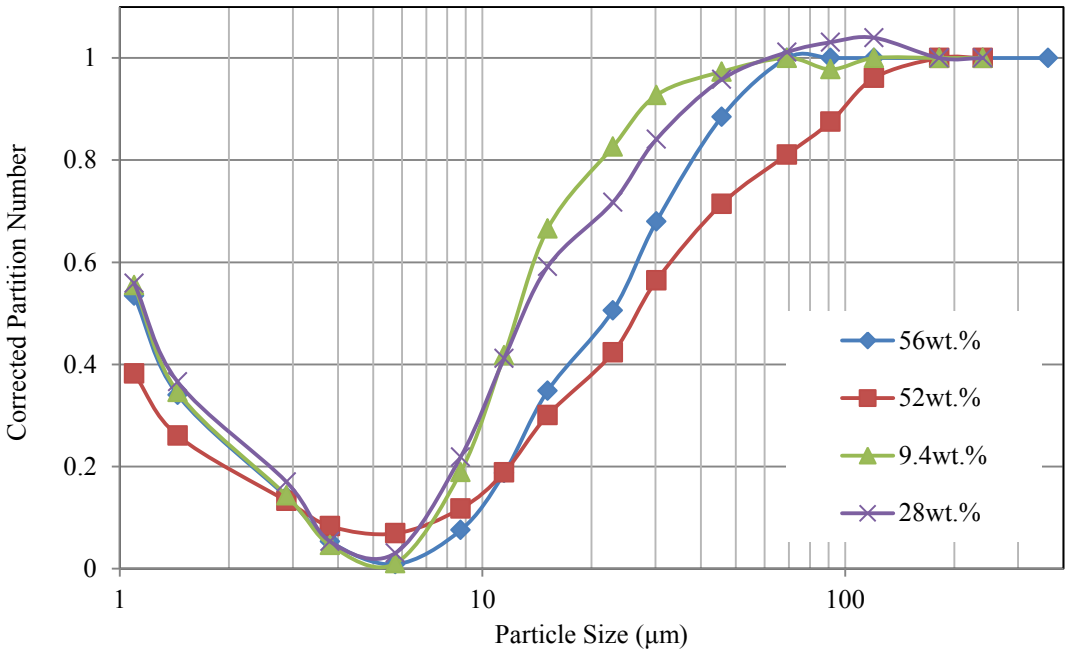

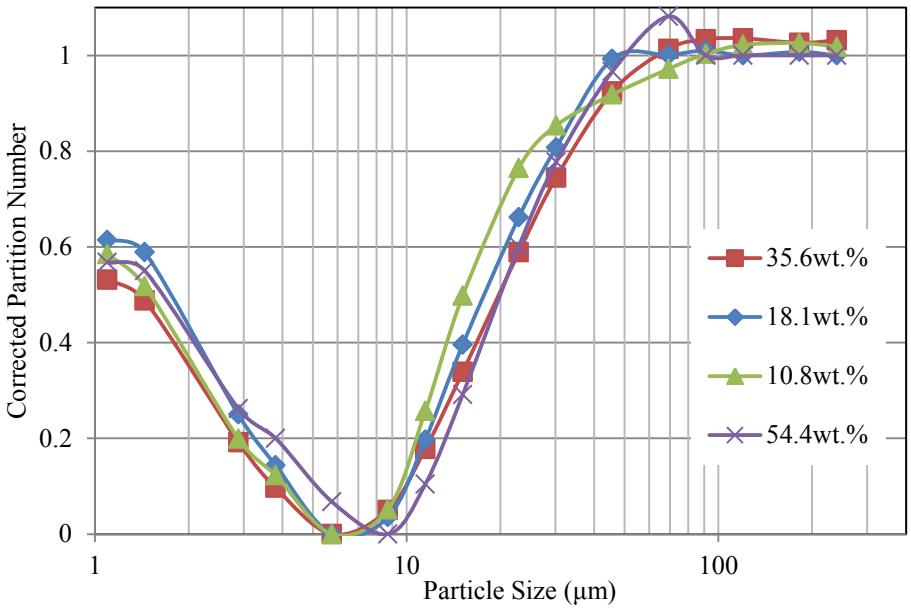

Rheograms for iron ore

Feed:

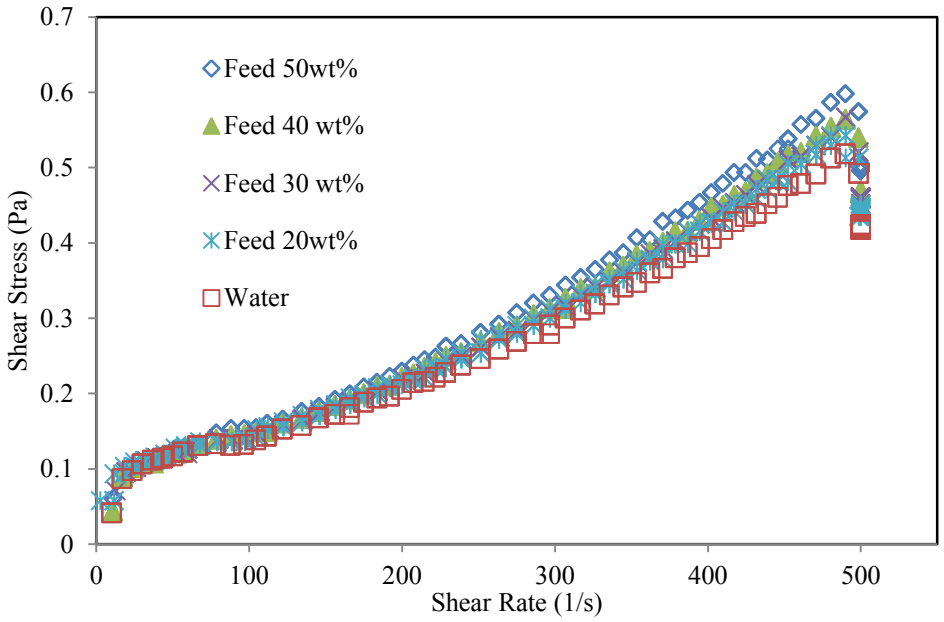

Bingham Model Fit:

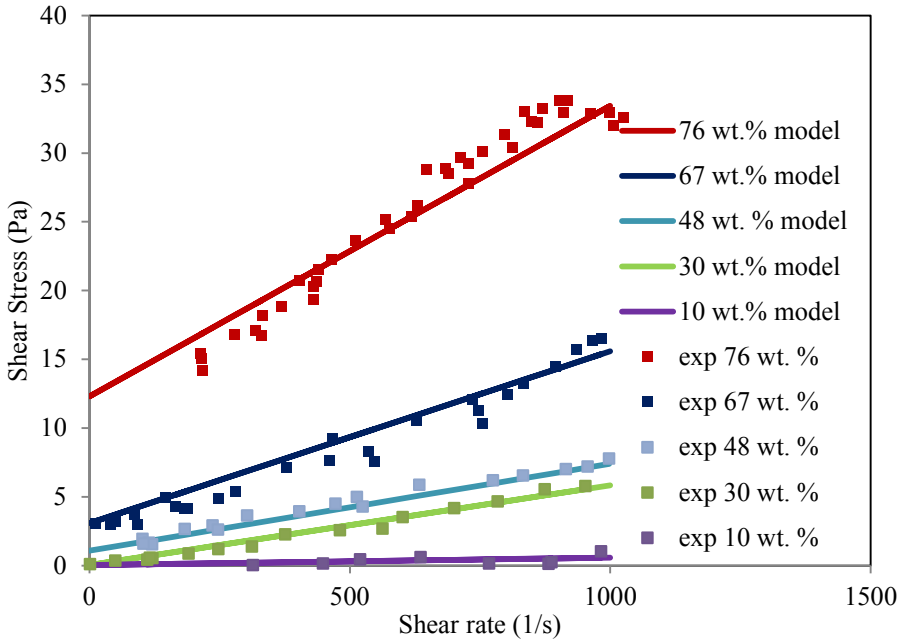

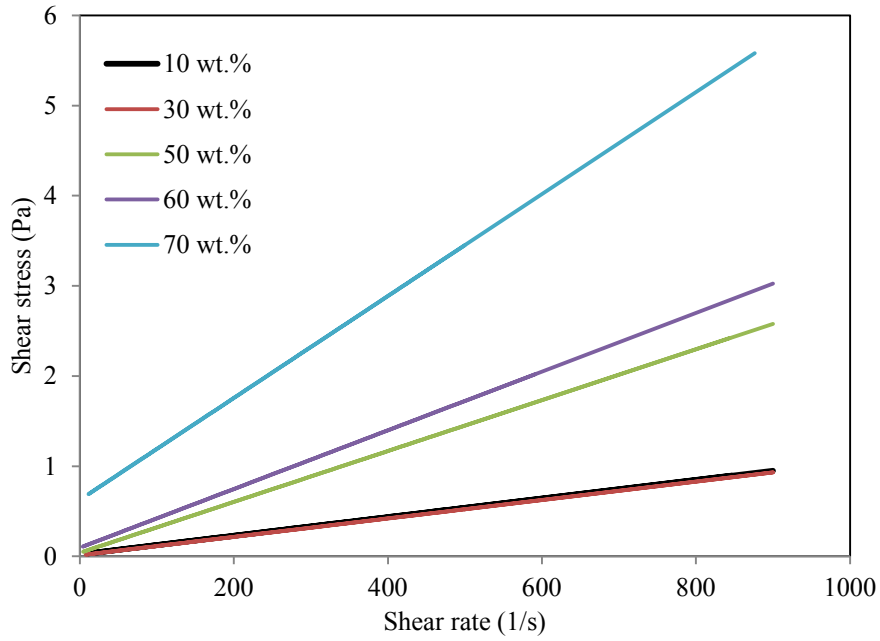

UG2 by size

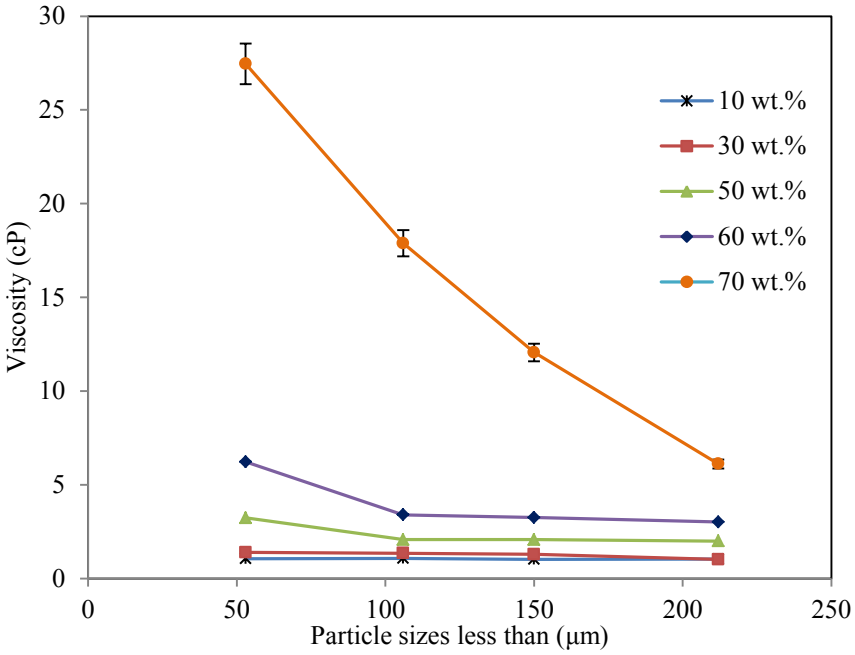
Viscosity (cP)
Particle sizes less than (µm)
10 wt.%
30 wt.%
50 wt.%
60 wt.%
70 wt.%

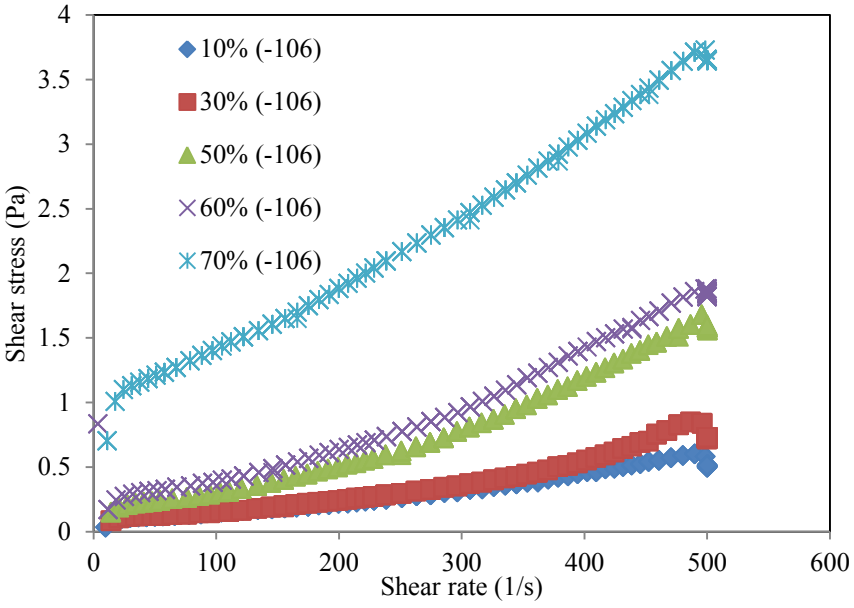
Shear stress (Pa)
Shear rate (1/s)
10% (-106)
30% (-106)
50% (-106)
60% (-106)
70% (-106)

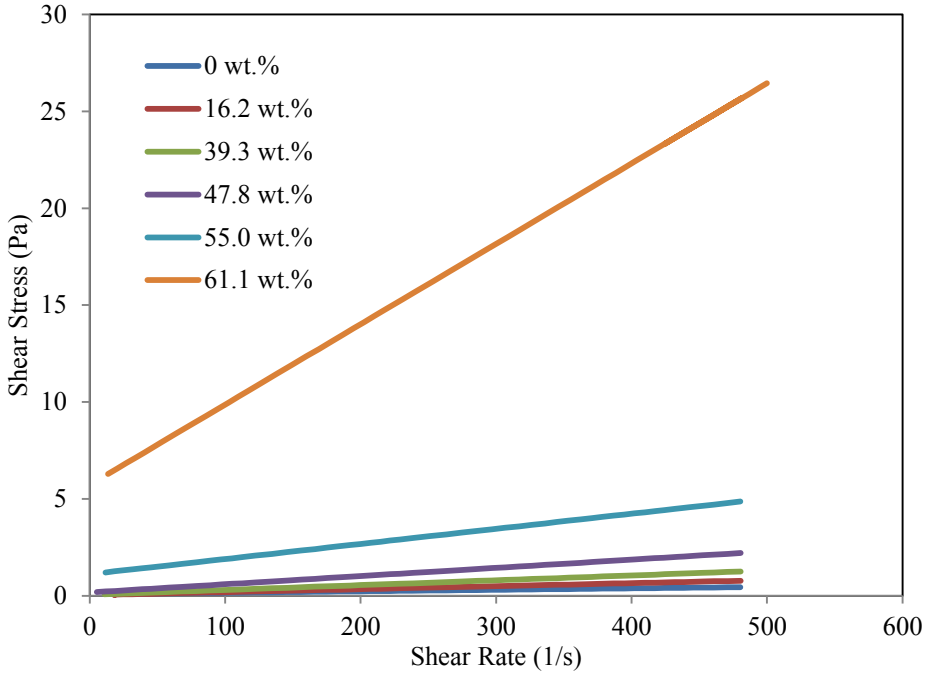
Shear Stress (Pa)
Shear Rate (1/s)
0 wt.%
16.2 wt.%
39.3 wt.%
47.8 wt.%
55.0 wt.%
61.1 wt.%
0
5
10
15
20
25
30
0
100
200
300
400
500
600

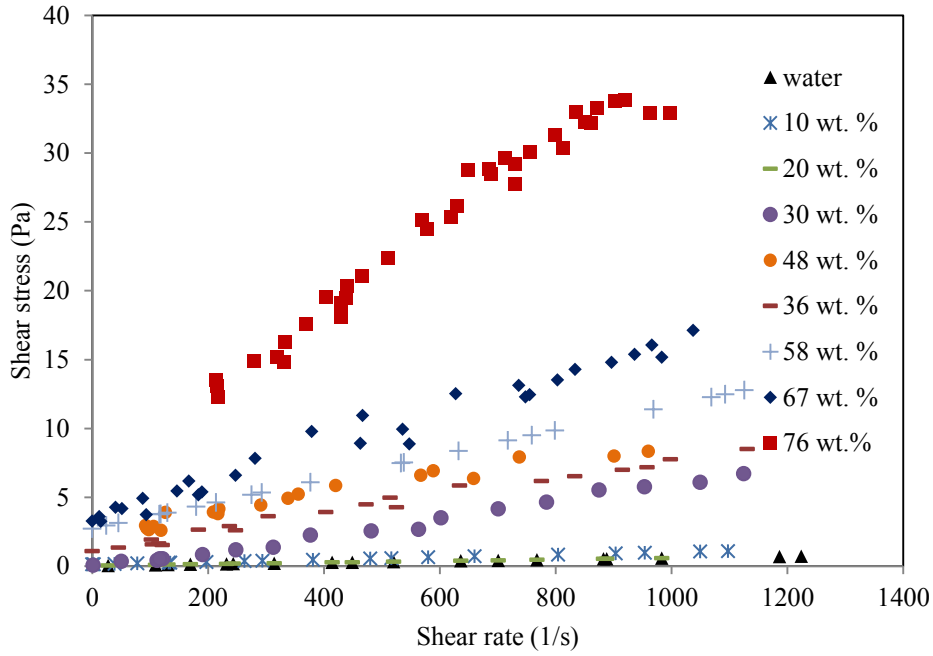
Shear stress (Pa)
Shear rate (1/s)
water
10 wt. %
20 wt. %
30 wt. %
48 wt. %
36 wt. %
58 wt. %
67 wt. %
76 wt.%
0
5
10
15
20
25
30
35
40
0
200
400
600
800
1000
1200
1400

Summarized data for UG2 ore

Run Number	Capacity Q_f (m^3/hr.)	Pressure (KPa)	Feed solids wt. %	Inlet Diameter (mm)	Vortex finder diameter (mm)	Spigot diameter (mm)	Cone ratio (-)	d50c (µm)	Rf (-)	α (-)
1	5.92	21.00	48.70	12.00	41.00	18.00	0.44	4.00	0.22	4.00
2	8.88	35.00	38.90	12.00	41.00	18.00	0.44	4.01	0.22	4.01
3	12.27	51.00	28.70	12.00	41.00	18.00	0.44	3.98	0.21	3.98
4	12.87	51.00	20.78	12.00	41.00	18.00	0.44	3.18	0.11	3.18
5	3.57	15.00	45.00	12.00	34.00	18.00	0.53	6.54	0.16	6.54
6	4.30	18.90	36.90	12.00	34.00	18.00	0.53	6.49	0.15	6.49
7	9.67	58.00	27.80	12.00	34.00	18.00	0.53	4.20	0.15	4.20
8	10.20	58.00	16.13	12.00	34.00	18.00	0.53	3.79	0.12	3.79
9	9.53	40.00	49.13	12.00	41.00	23.00	0.56	6.05	0.30	6.05
10	13.38	58.00	36.10	12.00	41.00	23.00	0.56	6.42	0.27	6.42
11	13.25	53.00	24.50	12.00	41.00	23.00	0.56	5.22	0.26	5.22
12	13.39	52.00	19.25	12.00	41.00	23.00	0.56	3.98	0.31	3.98
13	6.90	40.00	47.70	12.00	34.00	23.00	0.68	8.63	0.39	8.63
14	10.81	70.00	37.40	12.00	34.00	23.00	0.68	6.17	0.35	6.17
15	11.41	71.00	28.43	12.00	34.00	23.00	0.68	5.71	0.30	5.71
16	11.97	71.00	18.42	12.00	34.00	23.00	0.68	5.08	0.35	5.08
17	3.07	23.00	44.56	12.00	26.00	18.00	0.69	7.58	0.34	7.58
18	3.16	23.00	38.10	12.00	26.00	18.00	0.69	7.61	0.39	7.61
19	8.05	87.00	26.50	12.00	26.00	18.00	0.69	7.48	0.21	7.48
20	8.04	84.00	21.50	12.00	26.00	18.00	0.69	4.60	0.28	4.60
21	12.42	56.00	50.00	12.00	41.00	30.00	0.73	7.81	0.37	7.81
22	13.44	56.00	34.80	12.00	41.00	30.00	0.73	7.80	0.31	7.80
23	17.69	75.00	24.30	12.00	41.00	30.00	0.73	7.01	0.26	7.01
24	18.25	76.00	20.00	12.00	41.00	30.00	0.73	5.87	0.25	5.87

Summarized data for UG2 ore continued

Run Number	Capacity Q_f (m^3/hr.)	Pressure (KPa)	Feed solids wt. %	Inlet Diameter (mm)	Vortex finder diameter (mm)	Spigot diameter (mm)	Cone ratio (-)	d50c (µm)	Rf (-)	α (-)
25	14.95	110.50	45.00	12.00	34.00	30.00	0.88	7.61	0.38	7.61
26	14.92	102.00	33.70	12.00	34.00	30.00	0.88	7.51	0.28	7.51
27	15.76	102.00	22.70	12.00	34.00	30.00	0.88	6.94	0.49	6.94
28	11.06	60.01	13.60	12.00	34.00	30.00	0.88	6.25	0.50	6.25
29	8.65	107.00	46.30	12.00	26.00	23.00	0.88	8.04	0.47	8.04
30	8.68	101.00	37.30	12.00	26.00	23.00	0.88	8.03	0.43	8.03
31	9.08	101.00	28.00	12.00	26.00	23.00	0.88	7.08	0.43	7.08
32	9.54	101.00	17.10	12.00	26.00	23.00	0.88	6.70	0.40	6.70
33	7.42	85.00	49.10	12.00	26.00	30.00	1.15	7.10	0.52	7.10
34	8.08	87.00	34.90	12.00	26.00	30.00	1.15	7.10	0.44	7.10
35	8.51	88.00	25.60	12.00	26.00	30.00	1.15	6.81	0.43	6.81
36	9.14	94.00	20.40	12.00	26.00	30.00	1.15	6.70	0.42	6.70
37	10.20	58.00	16.13	12.00	34.00	18.00	0.53	3.79	0.12	3.79
38	3.07	23.00	44.56	12.00	26.00	18.00	0.69	7.58	0.34	7.58
39	8.88	35.00	38.90	12.00	41.00	18.00	0.44	4.01	0.22	4.01
40	12.27	51.00	28.70	12.00	41.00	18.00	0.44	3.98	0.21	3.98
41	12.87	51.00	20.78	12.00	41.00	18.00	0.44	3.18	0.11	3.18
42	15.19	101.00	31.70	12.00	34.00	30.00	0.88	7.91	0.26	7.25
43	8.05	107.00	48.30	12.00	26.00	23.00	0.88	9.04	0.47	8.04
44	9.10	96.00	20.40	12.00	26.00	30.00	1.15	6.70	0.42	6.70
45	13.25	54.00	21.50	12.00	41.00	23.00	0.56	4.22	0.25	5.52
46	9.14	94.00	20.40	12.00	26.00	30.00	1.15	6.70	0.42	6.70
47	3.27	23.00	47.56	12.00	26.00	18.00	0.69	8.58	0.34	7.18

Summarized data for iron ore

Run Number	Capacity Q_f (m^3/hr)	Pressure (KPa)	Feed solids wt. %	Inlet Diameter (mm)	Vortex finder diameter (mm)	Spigot diameter (mm)	Cone ratio (-)	d50c (µm)	Rf (-)	α (-)
1	4.208	27.58	55.9	12	40	16	0.4	32.9	0.215	6.1
2	3.784	27.58	52.7	12	40	16	0.4	31	0.215	6.38
3	4.88	27.58	42.6	12	40	16	0.4	16.1	0.210	5.71
4	7.465	103.43	28.35	12	40	16	0.4	13	0.200	4.8
5	7.499	103.43	9.43	12	40	16	0.4	8.9	0.201	3.75
6	5.543	103.43	42.6	12	40	16	0.4	7.1	0.200	6.8
7	7.139	103.43	14.63	12	40	16	0.4	12.1	0.140	4
8	8.455	103.43	28.4	12	40	16	0.4	14.1	0.158	4.7
9	7.525	103.43	9.43	12	40	16	0.4	10.8	0.120	3.1
10	4.489	103.43	28.23	12	40	16	0.4	15.8	0.210	4.1
11	9.39	103.43	22.33	12	40	16	0.4	13.5	0.200	4.26
12	6.315	103.43	56.31	12	40	16	0.4	25.9	0.210	6.78
13	6.824	103.43	22.8	12	40	22	0.55	15.7	0.260	3.87
14	8.295	103.43	24.55	12	40	22	0.55	16.1	0.275	3.81
15	9.205	103.43	13.56	12	40	22	0.55	8.9	0.260	3.78
16	10.48	103.43	8.49	12	40	22	0.55	15.7	0.250	3.1
17	9.43	103.43	19.06	12	40	22	0.55	14.5	0.260	3.81
18	7.874	103.43	11.4	12	25	16	0.64	2.8	0.160	3.71
19	7.385	103.43	12.25	12	25	16	0.64	3.1	0.270	3.81
20	8.11	103.43	11.25	12	25	16	0.64	4.8	0.260	3.67
21	9.276	103.43	23.6	12	32	22	0.69	18	0.251	3.56
22	8.707	103.43	18.26	12	32	22	0.69	17	0.304	4.81
23	8.91	103.43	10.89	12	32	22	0.69	3.8	0.260	3.51

Summarized data for iron ore continued

Run Number	Capacity Q_f (m^3/hr)	Pressure (KPa)	Feed solids wt. %	Inlet Diameter (mm)	Vortex finder diameter (mm)	Spigot diameter (mm)	Cone ratio (-)	d50c (µm)	Rf (-)	α (-)
24	7.81	103.43	14.1	12	25	16	0.64	13.1	0.35	3.70
25	6.91	10.3.43	53.4	12	25	16	0.64	24.7	0.37	4.80
26	7.18	103.43	50.1	12	25	16	0.64	26.1	0.37	6.71
27	9.91	103.43	20.1	12	32	22	0.69	6.9	0.32	3.51
28	4.489	103.43	28.2	12	40	16	0.4	12.5	0.32	6.10
29	4.208	27.58	55.9	12	40	16	0.4	32.9	0.22	6.10
30	3.784	27.58	52.7	12	40	16	0.4	31.0	0.22	6.38
31	4.88	27.58	42.6	12	40	16	0.4	16.1	0.21	5.71
32	7.465	103.43	28.4	12	40	16	0.4	13.0	0.20	4.80
33	7.499	103.43	9.4	12	40	16	0.4	8.4	0.20	3.75
34	5.543	103.43	42.6	12	40	16	0.4	7.3	0.20	6.80
35	10.48	103.43	8.5	12	40	22	0.55	16.1	0.25	3.10
36	9.43	103.43	20.1	12	40	22	0.55	15.7	0.26	3.81
37	7.874	103.43	12.5	12	25	16	0.64	2.9	0.16	3.71
38	7.385	103.43	11.3	12	25	16	0.64	3.9	0.27	3.81
39	7.139	103.43	14.1	12	40	16	0.4	15.1	0.33	4.00
40	8.455	103.43	30.1	12	40	16	0.4	13.0	0.30	4.70
41	7.525	103.43	10.1	12	40	16	0.4	11.1	0.33	3.10
42	4.489	103.43	30.1	12	40	16	0.4	13.0	0.40	4.10